8-2018

Geologic Mapping of the Northern Third of the Six Mile 7.5-Minute Quadrangle, South Carolina, USA

Victoria Beth Sellers
Clemson University, vseller@g.clemson.edu

GEOLOGIC MAPPING OF THE NORTHERN THIRD OF THE SIX MILE 7.5-MINUTE QUADRANGLE, SOUTH CAROLINA, USA

A Thesis
Presented to
the Graduate School of
Clemson University

In Partial Fulfillment
of the Requirements for the Degree
Master of Science
Hydrogeology

---

by
Victoria Beth Sellers
August 2018

Accepted by:
James Castle, Committee Chair
Scott Brame
John Garihan
Stephen Moysey

ABSTRACT

Mapping of Six Mile quadrangle in the current study was restricted to the northern third and included comparison with lithologies mapped by Garihan (2005) in Sunset quadrangle. Following Garihan's naming convention, six lithologic units were identified in Six Mile quadrangle: Walhalla hornblende gneiss, Table Rock gneiss, Tallulah Falls gneiss, Tallulah Falls schist, ultramafic rocks, and Quaternary alluvium. A major objective of this study was differentiating Table Rock gneiss from Tallulah Falls gneiss, undifferentiated previously within the study area. Age of rock units ranges from Early to Middle Cambrian (Tallulah Falls schist and gneiss; Hatcher, 2002) to Middle to Late Ordovician (Table Rock gneiss; Garihan, 2005). Age of Walhalla hornblende gneiss and ultramafic rocks is unknown.

Walhalla hornblende gneiss ranges from a white to gray to black, hornblende gneiss with foliation defined by aligned bands of hornblende and quartz-feldspar, to a fine- to medium-crystalline amphibolite dominated by hornblende. Amphibolite is defined in this work as having greater than fifty percent hornblende. Epidote is interfoliated locally with hornblende. Walhalla hornblende gneiss dominates the western portion of the study area as well as antiformal exposures in the central portion.

Table Rock gneiss is a leucocratic, fine- to medium-crystalline biotite gneiss that appears in stringers in the western part of the study area as well as in antiformal exposures in the central part. As mapped, Table Rock gneiss is surrounded by Walhalla hornblende gneiss. In this study, Walhalla hornblende gneiss and Table Rock gneiss are inferred to comprise the Walhalla nappe (Walhalla thrust sheet preferred usage).

Two of the three units of the Tallulah Falls Formation (Lower to Middle Cambrian; (Hatcher, 2002) occur in the study area: Tallulah Falls gneiss and Tallulah Falls schist. Tallulah Falls gneiss is a gray to black, medium- to coarse-crystalline, schistose, muscovite-biotite-porphyroclastic feldspathic gneiss. Tallulah Falls gneiss is found within synformal exposures in the central and eastern portions of the study area.

Tallulah Falls schist is a tan to red to purple to black, muscovite schist, ±garnet, sillimanite, biotite. Black, medium- to coarse-crystalline amphibolite is found within the unit and commonly as float. Tallulah Falls schist is commonly crenulated (wavelength= microscopic-2cm), with axial plane cleavage forming lineations on pavement exposures of schist. Tallulah Falls schist overlies Tallulah Falls gneiss and is found in the central and eastern portions of the study area. In this investigation, Tallulah Falls schist and Tallulah Falls gneiss are interpreted to be within the Six Mile thrust sheet. Amphibolite is also found as pods and float within Tallulah Falls schist and gneiss.

Two exposures of ultramafic rock were found in the study area. These ultramafic occurrences are 0.5-1.0m in size and include a green, schistose tremolite-clinochlore pod, and a white, talc-containing weathered hillslope exposure. Quartz-, feldspar-, and mica-rich, coarse-crystalline pegmatite is ubiquitous through the study area, but was not found at a mappable scale. Pegmatite was found concordant and discordant with rocks of the Six Mile thrust sheet and Walhalla thrust sheet. Quaternary alluvium was found in major and minor drainages in the study area and consisted of gray to tan to brown, silt to cobbles.

The Seneca fault, mapped by Garihan (2005) in Sunset quadrangle north of Six Mile quadrangle, is not visible in outcrop within the study area. However, location of the Seneca fault was interpreted within approximately 50m by mapping the transition from Walhalla hornblende gneiss and Table Rock gneiss of the Walhalla thrust sheet to Tallulah Falls gneiss and schist of the Six Mile thrust sheet. Ultramafic rocks occur within 500m of the interpreted Seneca fault.

DEDICATION

This thesis is dedicated to the doctors, pharmacists, nurse practitioners, nurses, and patient care technicians of Greenville Memorial Hospital. Without them, this work would not have been possible.

ACKNOWLEDGMENTS

I would like to thank and acknowledge my committee, including Scott Brame, James Castle, Jack Garihan, and Stephen Moysey, for thesis editing, field support, and proper encouragement.

I would like to thank my family and friends for encouraging me through this thesis work.

I would like to thank Backstreets Bar and Grill in Clemson, SC for allowing me space to write.

I would also like to thank the Clemson University Geologic Mapping group, including Matthew Beren and Dalton McCaffrey for accompanying me to the field numerous times and for their inquiries regarding Six Mile geology. I would like to thank Matthew Seigler for use of his photomicrographs in this investigation.

I would also like to thank the people of the Six Mile quadrangle for allowing me to access their land; without their cooperation, this investigation would not have been possible.

TABLE OF CONTENTS

Page

LIST OF FIGURES

Figure Page

List of Figures (Continued)

Page

List of Figures (Continued)

Page

List of Figures (Continued)

Page

List of Figures (Continued)

Page

LIST OF TABLES

Table Page

CHAPTER 1. INTRODUCTION

Inner Piedmont Overview

The Inner Piedmont belt lies between the Kings Mountain belt and Brevard belt (Overstreet and Bell, 1965). According to Hatcher (2002), the Inner Piedmont extends 700km from North Carolina to Alabama and is about 100km wide. The Inner Piedmont is thought to have Laurentian provenance, but has interesting structural style, kinematics, and migmatitic nature (Hatcher, 2002).

Inner Piedmont Lithologies

Overstreet and Bell (1965) described the Inner Piedmont belt as having plutonic schists and gneisses with gabbroic and granitic concordant and discordant intrusions. Lithologies identified by Overstreet and Bell (1965) included biotite schist, quartzite, hornblende gneiss, marble, biotite gneiss, migmatite, biotite granite gneiss, and muscovite pegmatite.

Core rocks of the Inner Piedmont were described during initial mapping by Griffin (1967) to be a petrologic assemblage of mica schist, biotite gneiss, granitoid gneiss, amphibolite, and minor metagabbro. Sillimanite is a principal accessory mineral within the metamorphic core. Biotite gneiss and biotite schists are commonly found together. Porphyroclastic biotite gneiss with plagioclase and microcline augen occurs locally (Griffin, 1971). Granitoid gneiss occurs as medium-crystalline concordant bodies containing microcline. Griffin noted widespread amphibole and amphibolite gneiss that possibly originated from a metagabbro. Metamorphic flank rocks of the Inner Piedmont include amphibole gneiss, amphibolite, granitoid gneiss, feldspathic quartzite, biotite gneiss, and biotite schist (Griffin, 1971). Within the amphibolite, Griffin (1971) stated

that hornblende is the predominant mineral with actinolite occurring in the northwest. Altered ultramafic bodies appear in the northwest flank of the Inner Piedmont. Most ultramafic bodies are composed of chlorite and magnesium-rich amphiboles such as cummingtonite and anthophyllite (Griffin, 1971).

Inner Piedmont Stratigraphy

The Tallulah Falls Formation comprises three units: a lower greywacke-schist-amphibolite member, an aluminous schist member, and an upper greywacke-schist-amphibolite member (Hatcher, 2002). The Tallulah Falls Formation ranges in age from Neoproterozoic to Lower Ordovician, and is interpreted as having been deposited on basement mid-ocean-ridge basalts (MORB) (Hatcher, 2002). Edelman and others (1987) stated that stratigraphy in the Inner Piedmont allochthons resembles the Tallulah Falls Formation of the Blue Ridge, thus suggesting that the Blue Ridge and Inner Piedmont possess stratigraphic continuity. Garihan (2005) applied the informal terms Tallulah Falls gneiss (TF) and Tallulah Falls schist (TFs) to the lower greywacke-schist-amphibolite unit (TF) and the aluminous schist (TFs) units of the Tallulah Falls Formation, respectively.

The Chauga River Formation, a metasiltstone, was deposited above the Tallulah Falls upper greywacke-schist-amphibolite unit with subsequent partial removal by uplift-related erosion (Hatcher, 2002). Mid-ocean ridge basalts (MORB) were thought to have been extruded onto the sea floor (Middle Ordovician) and then overlain by sand (Hatcher, 2002). The basalts and overlying sand were later metamorphosed to Poor Mountain amphibolite and quartzite (Hatcher, 2002). Poor Mountain amphibolite is described as

laminated to massive overlain by quartzite-felsic tuff and marble of the Poor Mountain Formation (Hatcher, 2002).

Inner Piedmont Magmatism

Hatcher (2002) noted that most Inner Piedmont granitoids are likely the product of collisional or post-collisional crustal thickening, instead of subduction-related magmatic arc formation. Inner Piedmont granitoids are isotopically intermediate between western Blue Ridge and Carolina terrane granitoids (Hatcher, 2002).

U-Pb zircon ages support Middle Ordovician ages for several western Piedmont granitoids (Bream, 2002). The Tallulah Falls-Ashe Formation (referred to as the Tallulah Falls Formation by Hatcher (2002), Bream (2002), and Garihan (2005)) was intruded by Middle Ordovician granitoids such the Whiteside Granite (466 Ma), Dyartsville pluton (~460 Ma), and Upper Ordovician (450 Ma; Ranson, et al., 1999) Caesars Head biotite augen gneiss (obsolete naming convention, mapped as Table Rock gneiss by Garihan (2005)) and by this investigation. Table Rock gneiss is included in this granitoid group, as it is Middle (Garihan, 2005) to Late Ordovician in age (Bream, 2002).

Inner Piedmont Structural Features

Nelson (1988) stated that the western Inner Piedmont is dominated by a series of thrust sheets, which they named the Chauga-Walhalla thrust complex, Six Mile thrust sheet, Laurens thrust sheet, and Paris Mountain thrust sheet. Hatcher (2002) mapped the Seneca thrust fault, at the base of the Six Mile thrust sheet, as the Sugarloaf Mountain thrust farther north in the Brushy Mountains of North Carolina. The thrust sheets strike NE-SW and contain evidence for polyphase deformation later complexly overprinted by brittle faulting in the western Inner Piedmont (Garihan, 2012).

The Seneca fault has been mapped in Table Rock quadrangle (Garihan and Ranson, 2001a), Cleveland quadrangle (Garihan, 2007), Sunset quadrangle (Garihan, 2005), and Standingstone quadrangle (Garihan and Ranson, 2007) (Figure 1.1). Regional aspects of this extensive ductile fault in the western Inner Piedmont have been summarized by Garihan (2001). The Seneca fault in Table Rock quadrangle places Tallulah Falls Formation schist, gneiss, and amphibolite and Poor Mountain amphibolite over Poor Mountain Formation metagabbro and amphibolite and Table Rock gneiss (Garihan and Ranson, 2001b). The Seneca fault in Cleveland quadrangle places Tallulah Falls Formation gneiss and schist and Poor Mountain Formation amphibolite, schist, and gneiss over Table Rock gneiss (Garihan, 2007). The Seneca fault in Standingstone quadrangle places Poor Mountain and Tallulah Falls Formations over Walhalla thrust sheet Table Rock gneiss (Garihan and Ranson, 2007). The Seneca fault in Sunset quadrangle places Tallulah Falls gneiss and schist over Poor Mountain amphibolite and Table Rock gneiss (Garihan, 2005).

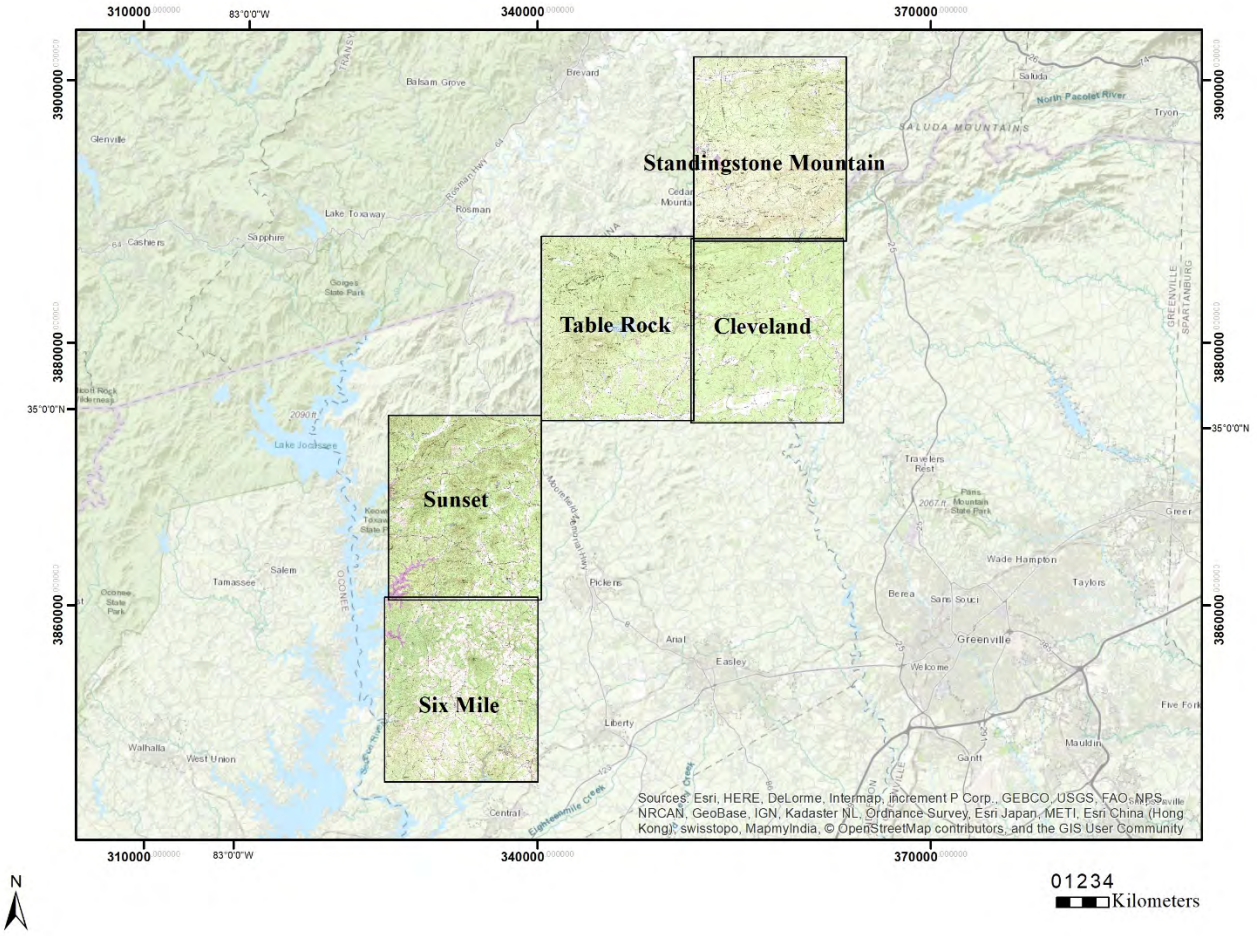

Figure 1.1: Quadrangles in areas of interest in northwestern South Carolina in which the Seneca fault has been mapped.

According to Bream (2002), “Inner Piedmont migmatization, upper amphibolite grade mineral assemblages, and penetrative deformation are likely related to Neoacadian and early Alleghanian orogenesis.” Nelson (1988) showed truncation of the Six Mile (Seneca) fault by Upper Ordovician to Lower Silurian Caesars Head Granite (~435 Ma), thus giving a minimum age of movement.

U-Pb zircon ages of the Chauga-Walhalla thrust sheet and the Six Mile thrust sheet indicate ~385 and 391 to 365 Ma thermal events related to Neoacadian and early Alleghenian orogenesis (Bream, 2002). The Alto allochthon is thought to be an outlying klippe of the Six Mile thrust sheet truncated by the Brevard zone with units similar to the Tallulah Falls Formation (Hopson and Hatcher, 1988). A minimum age of thrust sheet emplacement can therefore be determined to be 335-360 Ma (Hopson and Hatcher, 1988).

Griffin (1974) noted that schistosity and gneissosity are often parallel to compositional layering in the Inner Piedmont. The dominant foliation in the Inner Piedmont is S_2 associated with the metamorphic peak (Hatcher, 2002). Lineations in the Inner Piedmont include mineral lineations, crenulations, fold hinges, and intersections of foliations.). Griffin (1974) stated that conical folding predominates in the area. Griffin (1971) noted that recumbent/reclined folds occur with the Inner Piedmont core (area represented by Six Mile thrust sheet). Recumbent folds predominate in the northwestern flank and plunge gently northeast, with the northwestern portion of the core possessing more recumbent than reclined folds (Griffin, 1971). Griffin (1974) found that southeast-plunging folds were more prominent in Six Mile thrust sheet rocks than in Walhalla

nappe rocks. Griffin (1974) attributed this to fold elongation in the direction of tectonic transport. Hatcher (1978) noted that folding in the Inner Piedmont is polyphase deformed with fabric dominated by post-thermal maximum flowage (F_2) folds that are westward verging. Merschat et al. (2005) added that the Piedmont thrusts are predominantly Type-F, in that they are plastic, fold-derived thrusts with penetrative fabrics that evolved below the brittle-ductile transition.

F_1 folds in the Inner Piedmont are rarely visible, tight- to isoclinal-flow folds (Merschat et al., 2005). F_2 tight- to isoclinal formed contemporaneously with S_2 foliation and L_2 mineral lineation. F_2 axial surfaces typically have shallow dips, with axial planes mimicking L_2 mineral lineations. S_2 foliation has a gentle to moderate dip in the Inner Piedmont (Merschat et al., 2005). L_2 is the most common lineation and is a mineral stretching foliation with variable NE-SW, N-S, and NW-SE trends (Merschat et al., 2005). F_3 folds are inclined, closed to open, and trend NW-SE. F_3 folds formed from refolded F_2 folds, creating a local, axial planar S_3 foliation.

Regional Mapping Overview

Six Mile 7.5-minute Quadrangle is in northwestern South Carolina within the Piedmont physiographic province. Six Mile quadrangle is constrained between 82.875° W and 82.75°W and 34.875°N and 34.75°N (Figure 1.2). Water bodies in Six Mile quadrangle include Lake Keowee to the west and Twelvemile Creek to the east.

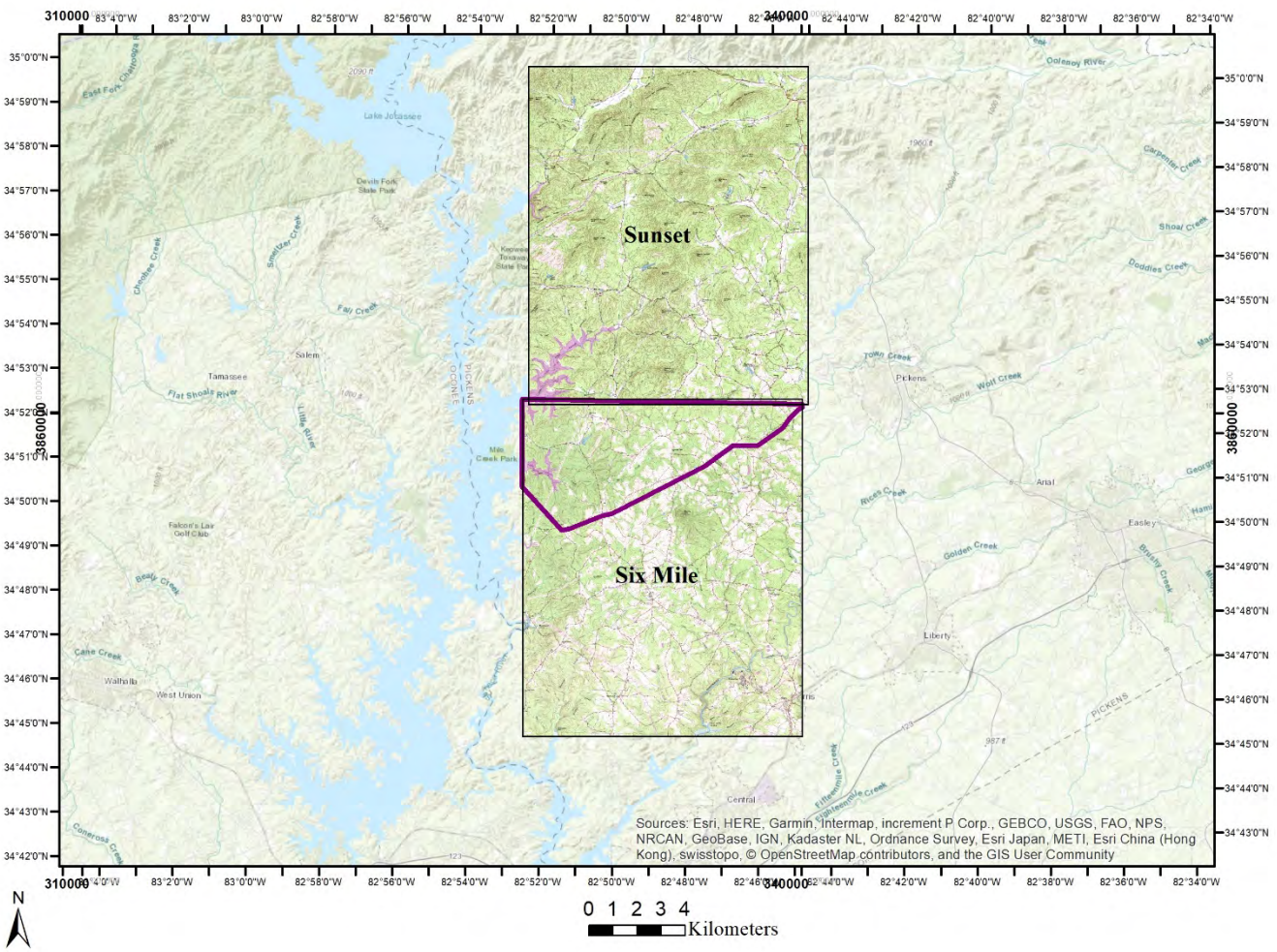

Figure 1.2: Sunset quadrangle (upper) and Six Mile quadrangle (lower) in relation to major towns in northwestern SC with study area outline.

Six Mile quadrangle was initially mapped by Griffin (1967), and the map was published by the South Carolina Development Board's Division of Geology. Lithologies that Griffin mapped in the quadrangle include hornblende gneiss, biotite gneiss, mica schist, and quartzite. Griffin separated areas of hornblende gneiss in the western portion of the quadrangle from biotite gneiss in the eastern portion of the quadrangle by a gradational contact. Griffin (1967) noted the presence of sillimanite in the eastern portion of the quadrangle, which he attributed to an increase in metamorphic grade. Mica schist in the quadrangle was noted to contain biotite and muscovite with sillimanite and is synformally exposed in the central portion of the quadrangle. Griffin noted the presence of biotite gneiss in the west-central and eastern portions of Six Mile quadrangle. Griffin (1967) noted common NE-SW trending foliations.

Garihan (2005) mapped Sunset quadrangle, located directly north of Six Mile quadrangle, and the map was published by the South Carolina Geological Survey. Middle to Upper Ordovician Table Rock gneiss and Poor Mountain amphibolite of the Walhalla thrust sheet occur along the southern boundary of Sunset quadrangle (Garihan, 2005), and NE-SW striking, small (100m-4km in length) ultramafic bodies are present along the southern boundary. Nine Times ultramafic body contains 60% clinoamphibole and 40% chlorite (Gober and Ranson, 2005). Table Rock gneiss and Poor Mountain amphibolite are overlain by rocks of the Six Mile Thrust Sheet, including Tallulah Falls gneiss and schist, and the two thrust sheets are separated by the Seneca fault (Garihan, 2005) (Figure 1.3).

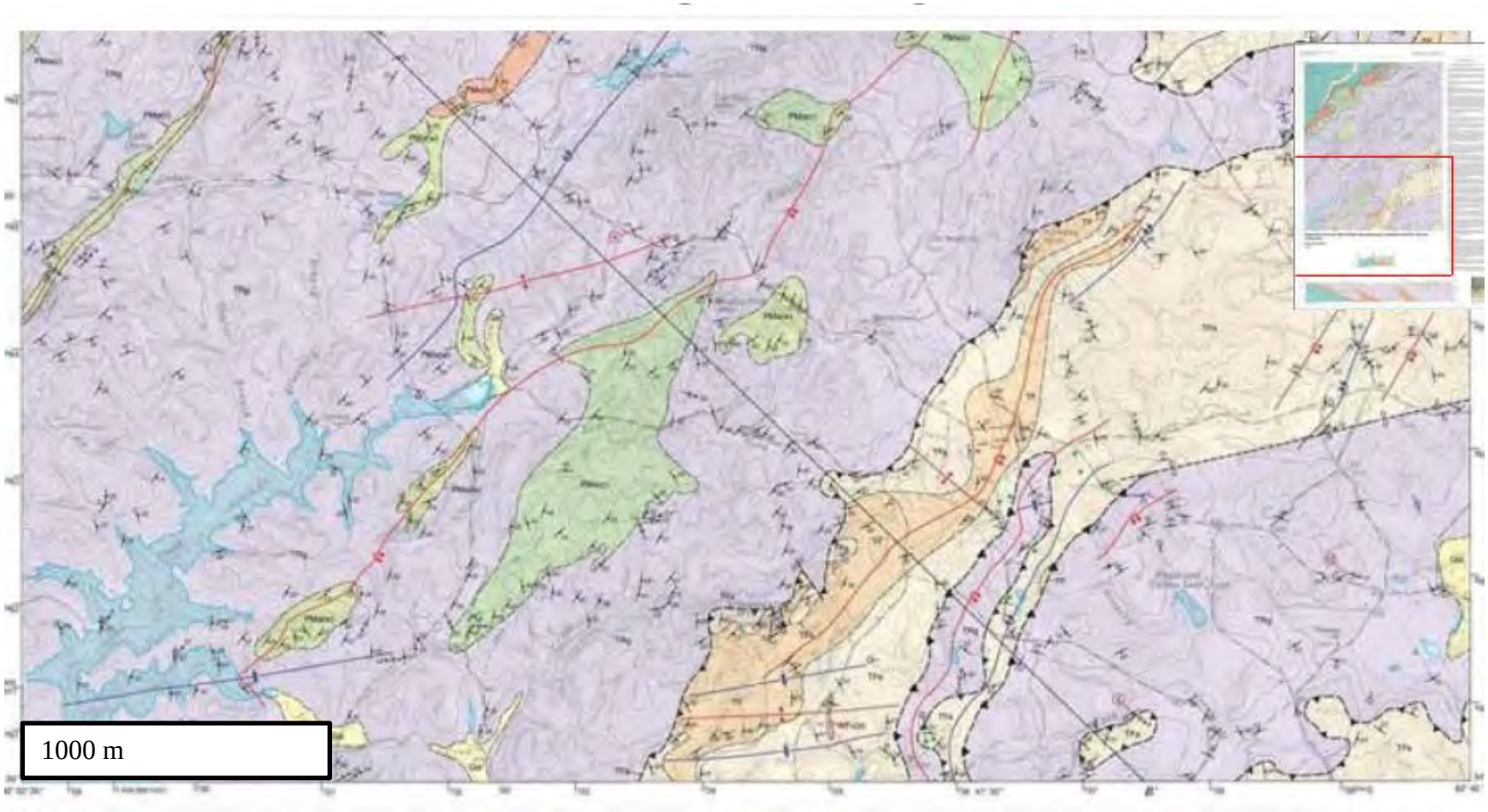

Figure 1.3: Garihan's map of the southern Sunset quadrangle showing expansive Table Rock gneiss (purple) with stringers of Poor Mountain amphibolite (green) of the Walhalla nappe. Tallulah Falls gneiss (orange) and Tallulah Falls schist (cream) are units in the overlying Six Mile thrust sheet.

Objectives

Advances in understanding lithology and structure of the Inner Piedmont by researchers such as Griffin, Hatcher, Bream, Horton, and Garihan have necessitated updated geological interpretations for quadrangles in the northwestern part of South Carolina. Six Mile quadrangle has not been examined since 1967. After Sunset quadrangle was mapped in 2005, edge matching was needed to ensure geologic continuity from Sunset quadrangle to Six Mile quadrangle to the south. One purpose of this study is to update Griffin's 1967 geologic map and to edge match it with more recently mapped Sunset quad. These results will then be used more confidently for others to carry the geologic mapping further south into the quad.

The first objective of the research within the study area is to re-delineate lithologic contacts mapped by Griffin (1967). Griffin's map did not differentiate biotite gneisses of Six Mile quadrangle. From previous research (Garihan, 2005), two biotite gneiss units are known to be present in Sunset quadrangle to the north: Table Rock gneiss and Tallulah Falls gneiss. Because these gneiss units are interpreted as members of different thrust sheets (Garihan, 2005), identification and differentiation are critical to determining location within the Inner Piedmont thrust stack. The original biotite gneiss description will be compared with the descriptions in this study.

The second objective of the research is to determine position of the Seneca fault. Griffin's 1967 Geologic Map of Six Mile quadrangle does not contain the Seneca fault or any other tectonic features relating to imbricate thrust sheets. While Griffin's map

contains synclinal folding of mica schist in the central portion of the map, he did not place this folding in a larger structural context.

The third objective of the research is to produce deliverables that can be used to continue research in Six Mile quadrangle. The first deliverable is a geologic map of the northern third of Six Mile quadrangle. The map shows lithologic contacts and structural features such as faults and folds as well as spatial orientation of foliation using strike and dip. The second set of deliverables are two geologic cross sections of lithologic contacts and structural features and how those are projected with regards to elevation. The third deliverable is a comprehensive lithologic description of units mapped in Six Mile quadrangle with color, crystal size, and mineralogical percentage. The geologic map (1:24000), cross-sections, and comprehensive lithologic description of mapping units are part of this thesis.

CHAPTER 2. METHODS

Field Methods

Garihan accompanied Sellers and Brame on an east-west transect of the southern portion of Sunset quadrangle in July 2014 to associate field samples with lithologic units from the Sunset quadrangle for reference to use in the northern part of Six Mile quadrangle. Lithologies in the study area were identified using guidance provided by Garihan during this outing.

Geologic field mapping of Six Mile quadrangle began in July 2014 with a highway traverse of the entire quadrangle. Major county roads were driven with waypoints created at outcrops. Observations and measurements, including strikes, dips, lithologic descriptions and sketches, were recorded in a field book. Waypoints were given a “SM” designation for Six Mile with associated number, for example SM75. GPS location data with associated lithology were later uploaded to ArcGIS, geographic information systems software in the UTM 17N coordinate system. GPS point data were added to topography and aerial photography layers to assist in further mapping and interpretation. 617 outcrop locations with associated lithologies were recorded in a Garmin GPS unit from the entire Six Mile quadrangle between July 2014-August 2015.

After initial quadrangle-wide road traversal, the mapping area was constrained from the entire Six Mile quadrangle to the northern third of the quadrangle. Boundaries of the study area were set in this investigation to be the northern latitude of Six Mile quadrangle (34°52’ 30” N), western and eastern latitude boundaries of the quadrangle (82° 52’ 30” W and 82 45’ 00” W) and Highway 183 and Gap Hill Rd. as the southern

boundary (Figure 2.1). Creeks in the study area were traversed on foot, with traversals ending in August 2015. 567 waypoints with identified lithologies were taken at locations in the study area (Figure 2.2). 12 additional waypoints were taken in both Sunset (n=9) and Six Mile (n=3) quadrangles during a field check in June 2017.

One hundred three strikes and dips of foliation were measured with a Brunton compass from 103 outcrops in the study area. Samples found within the study area were used to create lithologic descriptions of the units. Approximately three hundred samples were gathered from the study area and are currently stored in Brackett 333A for future reference.

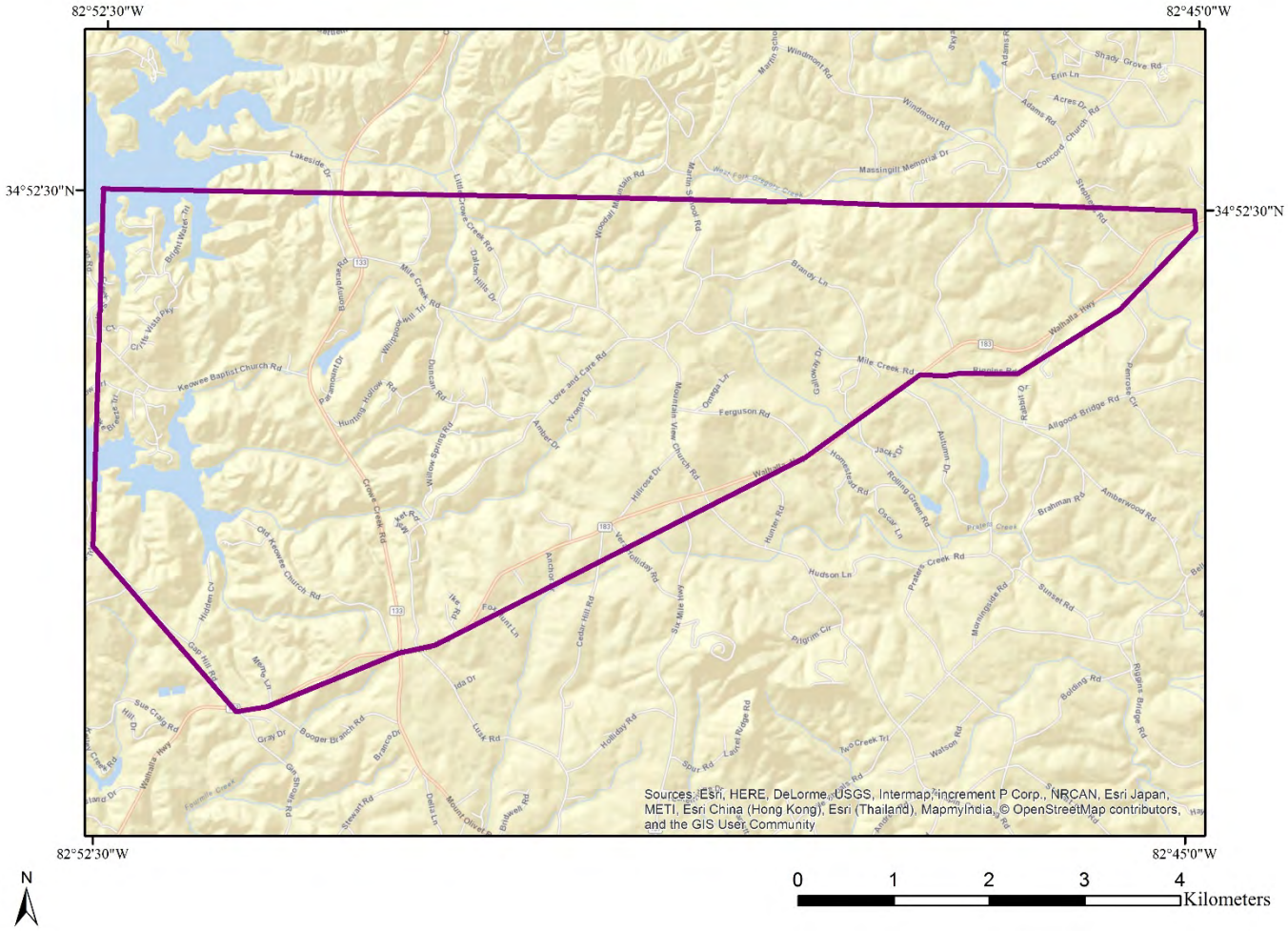

Figure 2.1: Roads in the study area.

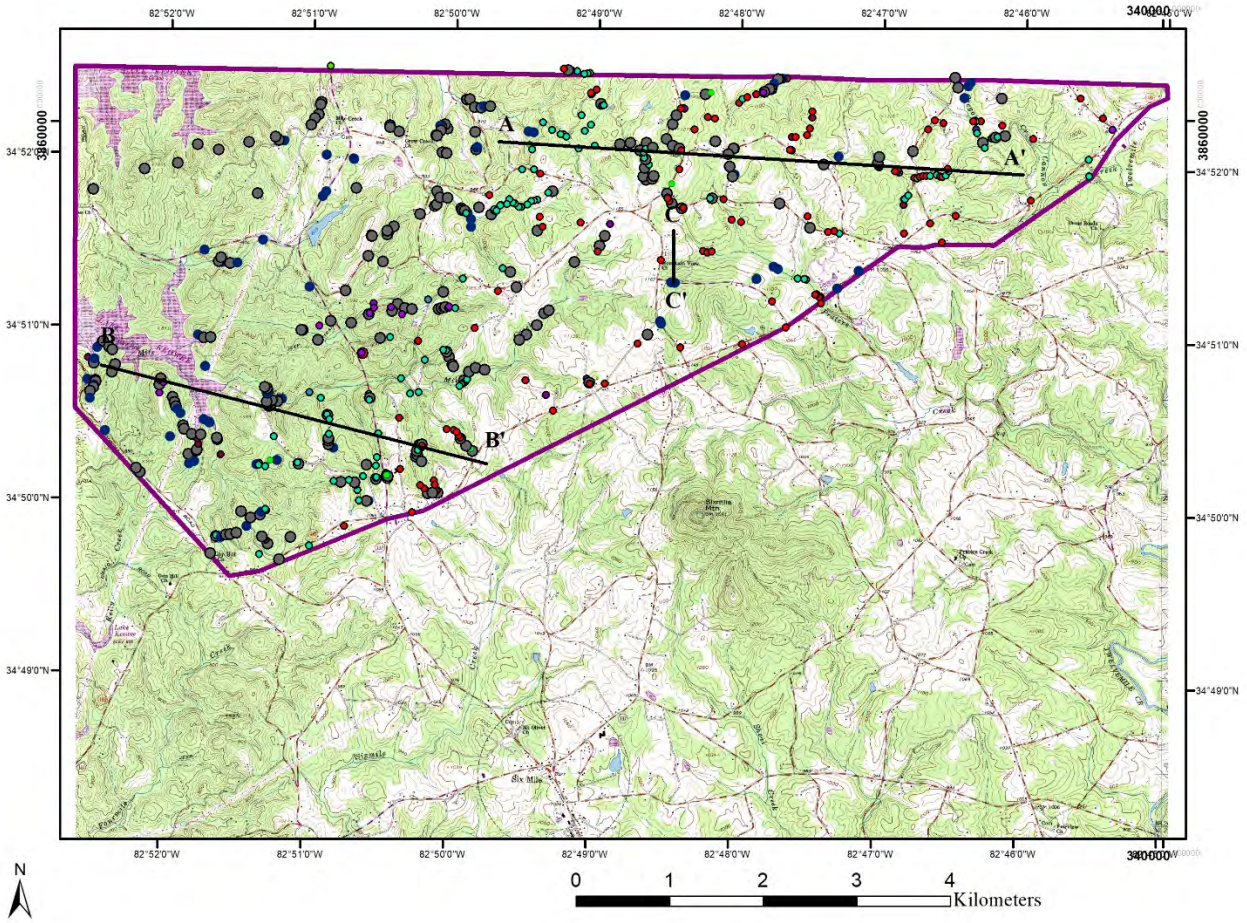

Figure 2.2: Map of waypoints in study area. Study area in regional context in Figure 1.2. Locations of cross sections A-A' and B-B' are shown.

Lithologic Analysis

Lithologic modal analysis was derived from approximately 10 hand samples from each unit that represented dominant lithologic properties of each unit. Each hand sample was examined with a hand lens and mineral percentages estimated to ±10%. Thin sections of ten samples, each from a different location, were prepared by National Petrographic Service and examined using a petrographic microscope for mineralogy and microtectonic structures.

Two samples were analyzed by x-ray diffraction. Preparation included mortaring the bulk rock sample, utilizing a 103-micron sieve to ensure particle size uniformity, and then loading the sample into a Rigaku Miniflex600 x-ray diffractometer. Data were loaded into PDXL software, software created for the x-ray diffractometer, for peak analysis and mineral identification. Mineral identity suggestions were listed by PDXL and eliminated or added by the user depending upon geologic suitability for the study area. Schist in this investigation is defined as medium-crystalline, with average diameter ranging from 1 to 10mm (Davis and Reynolds, 1996; Fossen, 2010). Gneisses in this investigation are composed of medium- to coarse-crystalline minerals and are be defined by compositional banding ranging from centimeter-decimeter in size (Davis and Reynolds, 1996; Fossen, 2010).

Structural Analysis

Structural analysis involved adding strikes and dips of foliation measured in outcrops to stereographic software (Stereonet; Allmendinger, 2011) to determine mean vector of poles to planes. Cross-section lines were constructed in ArcGIS across the study area, converted to points with elevation and distance, and plotted using Microsoft Excel.

The plot was imported to Adobe Illustrator where the final cross-sections were constructed with contacts and symbols added.

CHAPTER 3. RESULTS

Lithologic Description of Units

Units identified in the study area are: Quaternary alluvium (Qal), Table Rock gneiss (TRg), Walhalla hornblende gneiss (Whg), Tallulah Falls gneiss (TF), Tallulah Falls schist (TFs, previously abbreviated TFa by Garihan 2005), and ultramafic rocks (Figure 3.1; Table 3.1).

Quaternary alluvium

Quaternary alluvium was found in major and minor creeks in the study area and consists of gray to tan to brown, silt- to cobble-sized, alluvium.

Table Rock gneiss

Table Rock gneiss is a leucocratic, fine- to medium-crystalline (1-5mm), biotite gneiss predominantly in the western part of the northern third of the study area proximal to Lake Keowee. Easily accessible outcrops occur near the intersection of Highway 133 and Bonnybrae Rd (Figure 3.2), as well as Keowee Baptist Church Rd. and within 50m east of the intersection of Ferguson Rd. and Mountain View Church Rd (Figure 3.3). Two thin sections from hand samples of Table Rock gneiss were examined using a petrographic microscope. A thin section from SM110 indicates microcline with tartan twinning (50%), quartz (30%), plagioclase (10%) and biotite (10%) (Figure 3.4-Figure 3.5). A thin section from SM162 indicates a high leucocratic mineral content of 50%

quartz and 40% plagioclase with 5% biotite and 5% opaques (Figure 3.6). Quartz exhibited undulose extinction in SM162 (Figure 3.7).

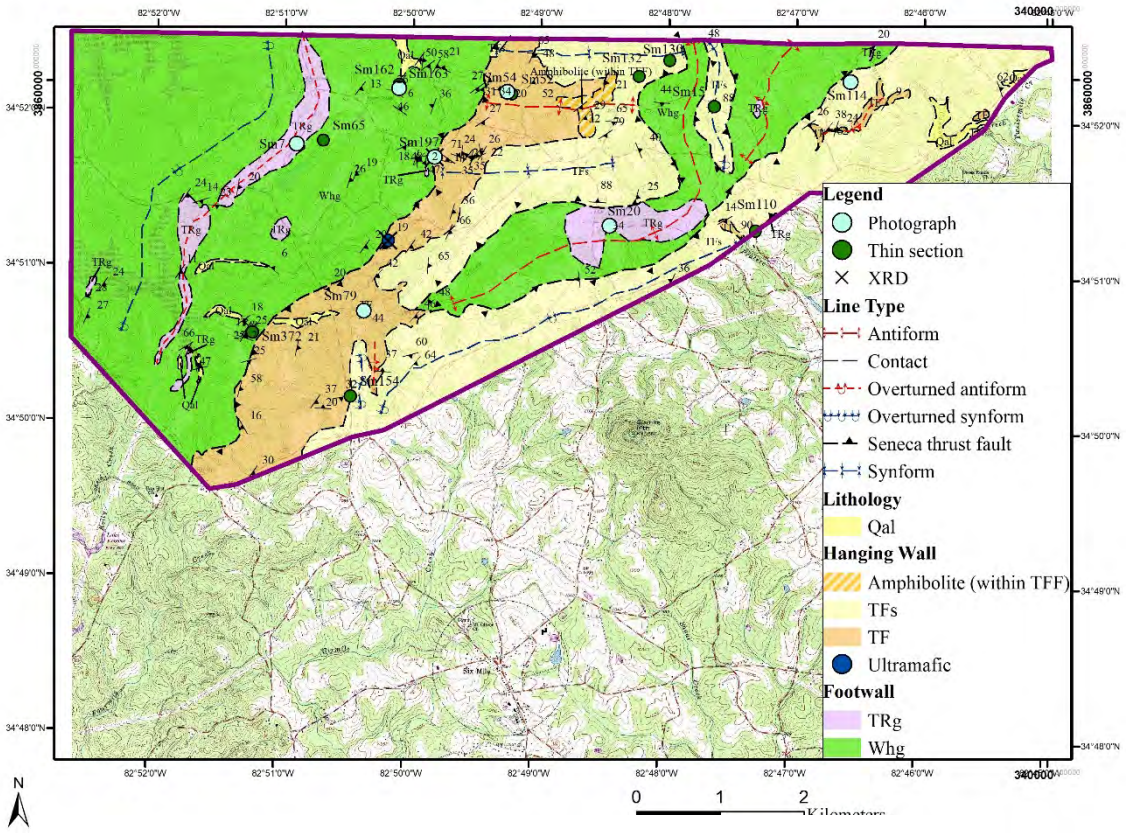

Figure 3.1: Map showing reference locations of lithology in the study area. Photographs (Figure 3.3-Figure 3.27) refer to this map.

Figure 3.2: Outcrop of Table Rock gneiss along Highway 133 at waypoint SM07. (See Figure 3.1 for locations). View approximately to the northwest.

Figure 3.3: View to the south, showing outcrop of Table Rock gneiss near the intersection of Ferguson Rd. and Mountain View Church Rd. in the center of the study area at waypoint SM20.

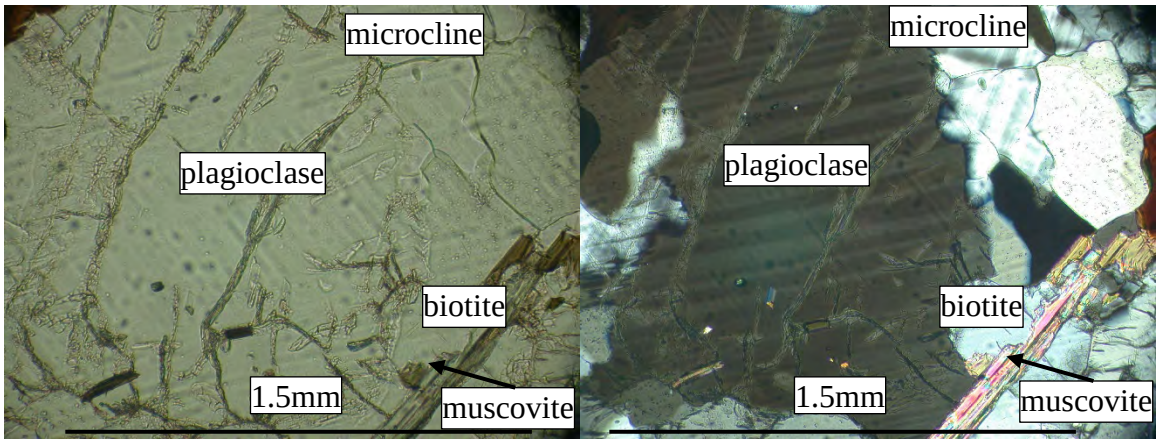

Figure 3.4: Photomicrographs of Table Rock gneiss from SM110 with plagioclase surrounded by microcline, quartz, and biotite in plane polarized (left) and cross-polarized light (right). Black or yellow bars in the rest of the chapter represent scale length in photomicrographs. Plagioclase in all micrographs (where present), represent well-developed albite twinning.

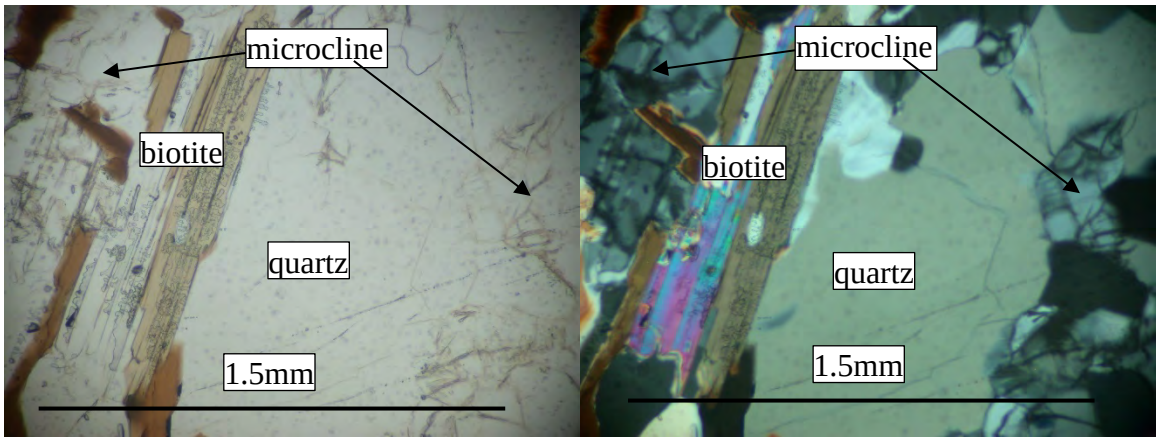

Figure 3.5: Photomicrographs of Table Rock gneiss from SM110 with quartz surrounded by biotite and microcline in plane polarized (left) and cross-polarized light (right)

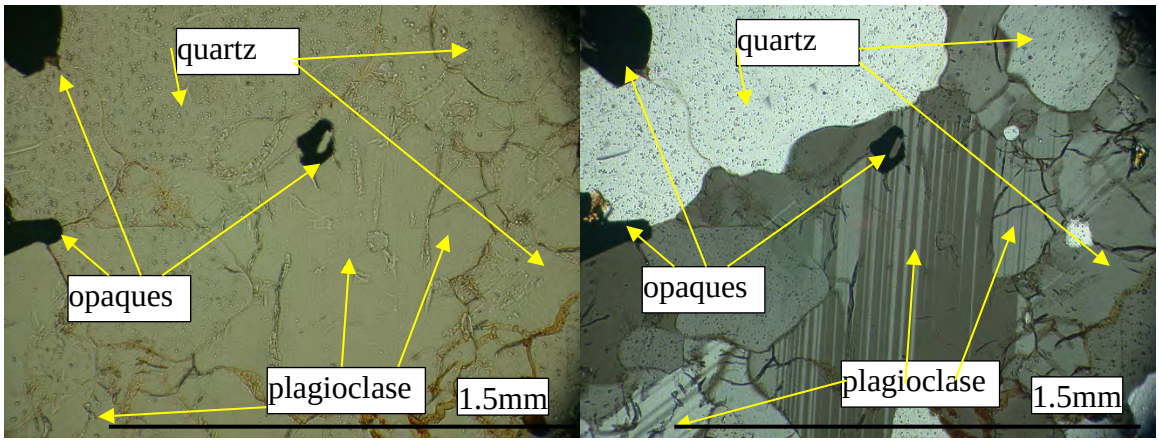

Figure 3.6: Photomicrographs of Table Rock gneiss from SM162 with plagioclase surrounded by quartz and opaques in plane polarized (left) and cross-polarized light (right)

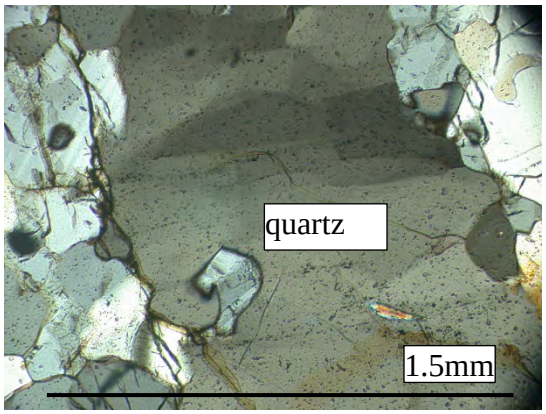

Figure 3.7: Strained quartz (undulose extincting), cross-polarized light. Table Rock gneiss, SM162.

Walhalla hornblende gneiss

An early hypothesis for the study area in this investigation was that the presence of amphibolite indicates Walhalla thrust sheet rocks. However, mapping indicated that amphibolite was too ubiquitous to use for determining placement within the Six Mile thrust sheet or the Walhalla thrust sheet. Amphibolite located near leucocratic, fine-crystalline (<1mm) Table Rock gneiss is mapped within the Walhalla hornblende gneiss (Figure 3.8-Figure 3.9). Table Rock gneiss at SM163 was found intruded into Walhalla hornblende gneiss, then later folded (Figure 3.8-Figure 3.9). This mimics what is seen at macroscopic scale in footwall rocks in study area. The Walhalla hornblende gneiss ranges in composition from a fine- to medium-foliated (1-5 mm) hornblende gneiss with relatively equal parts leucocratic and mafic compositional banding to a nonfoliated amphibolite with negligible leucocratic mineral content. A thin section from SM65 is amphibolite within Walhalla hornblende gneiss and is composed of 65% hornblende with 25% quartz and 10% plagioclase with visible banding of quartz (Figure 3.10-Figure 3.11) A thin section from SM372 is hornblende gneiss and is composed of hornblende (40%),

quartz (30%), plagioclase (20%), and microcline (10%) (Figure 3.12). Leucocratic mineral percentage is greater in SM372 (70%) than in SM65 (35%). The northwest corner of the study area is dominated by nonfoliated and foliated amphibolite with minimal leucocratic minerals. The southwest corner of the study area is dominated by biotite hornblende gneiss and hornblende biotite gneiss of varying compositions (20% leucocractic, 80% mafic minerals to 80% leucocratic, 20% mafic minerals). Footwall rocks with any hornblende were included in the Walhalla hornblende gneiss unit

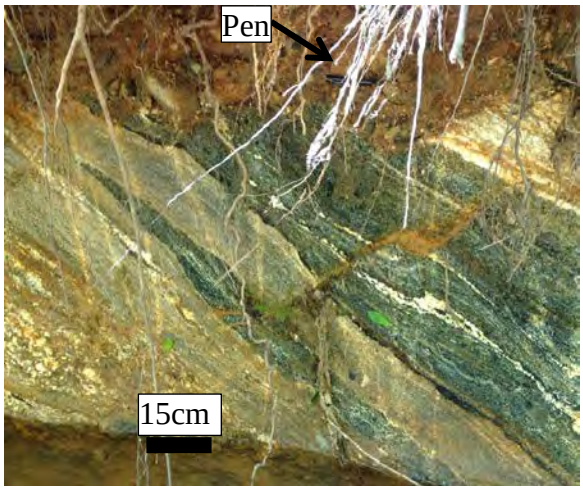

Figure 3.8: Folded Table Rock gneiss and amphibolite within Walhalla hornblende gneiss at SM163. Pen is 15cm long. View approximately to southwest.

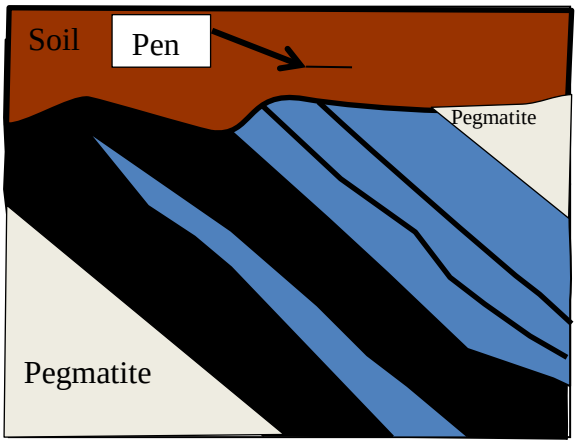

Figure 3.9: Interpretation of Figure 3.8. Folded Table Rock gneiss (black) and amphibolite within Walhalla hornblende gneiss (blue). Surrounded by concordant pegmatite. Pen is 15cm long.

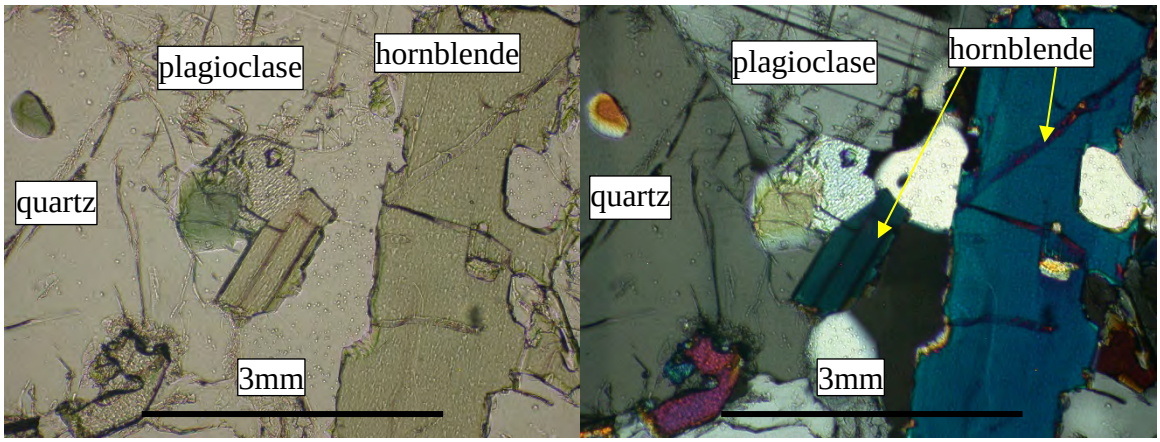

Figure 3.10: Photomicrographs of amphibolite within Walhalla hornblende gneiss from SM65 containing hornblende, plagioclase, and quartz in plane polarized (left) and cross-polarized (right) light.

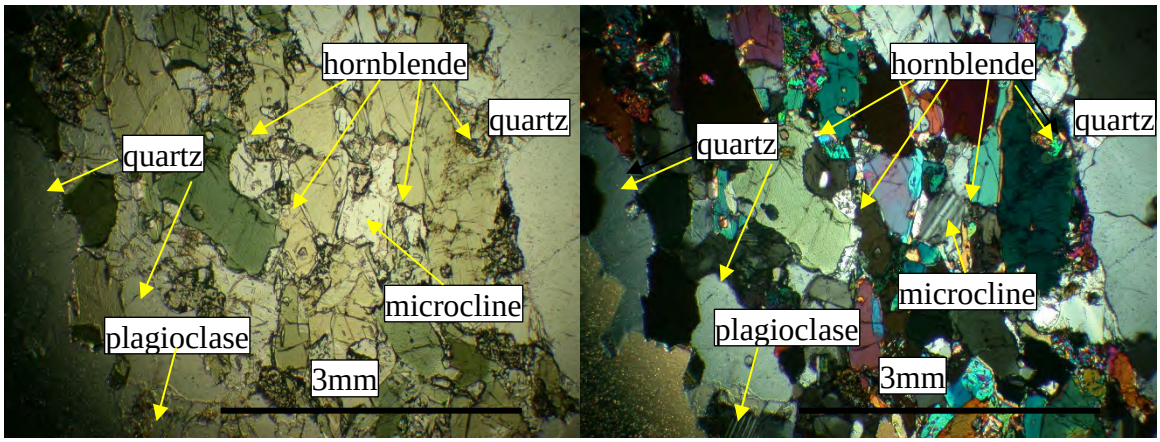

Figure 3.11: Photomicrographs of Walhalla hornblende gneiss from SM65. Green-brown pleochroic hornblende, microcline, plagioclase, and quartz in plane polarized (left) and cross-polarized (right) light. Quartz on the left and right margins is oriented in a top-to-bottom band.

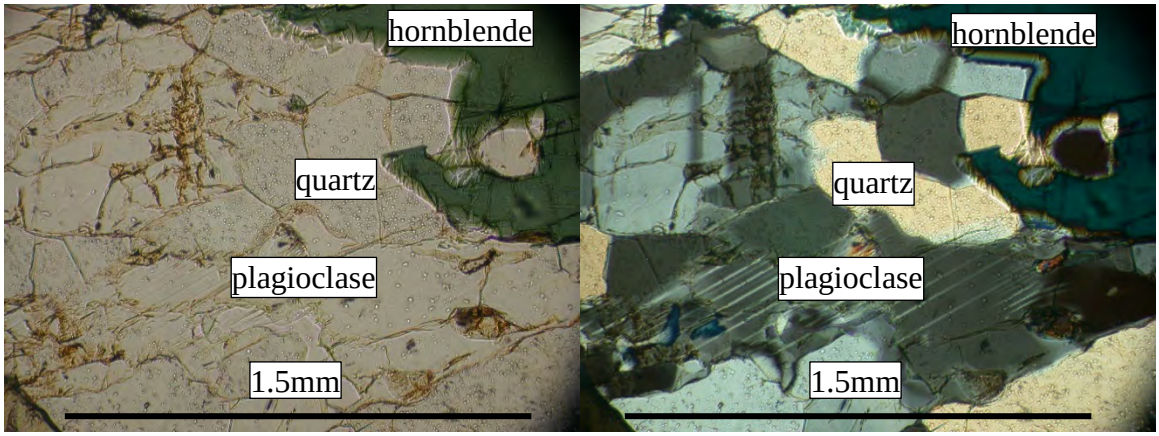

Figure 3.12: Photomicrographs of Walhalla hornblende gneiss from SM372 of plagioclase, quartz, and hornblende in plane polarized (left) and cross-polarized (right) light.

Tallulah Falls Formation

Tallulah Falls schist

A muscovite (0-80%) schist, ±biotite (0-25%), garnet (0-30%), sillimanite (0-80%) (biotite<garnet<sillimanite<muscovite in abundance) was identified in the study area and named Tallulah Falls schist, which also occurs in the Sunset quadrangle (Garihan, 2005). Tallulah Falls schist dominates the eastern portion of the study area.

Figure 3.13: View to the west showing crenulated Tallulah Falls garnet-sillimanite-muscovite-schist at waypoint SM114. Hammer head is 10cm wide.

Garnets in Tallulah Falls schist range from <2mm to 1cm. Tallulah Falls schist is locally crenulated (Figure 3.13) and weathers to red to orange, micaceous soil. A thin section from SM15 contains garnet altered along fractures to iron oxide (Figure 3.15). Sillimanite in SM15 is located proximal to the garnet, with muscovite in the matrix. A thin section from SM130 contains muscovite (55%), biotite (25%), quartz (15%), and garnet altered to iron oxide (5%) (Figure 3.15). Accessible outcrops of the Tallulah Falls schist occur at the intersection of Ferguson Rd. and Highway 183, approximately 1.2km from the intersection of Brandy Lane and Mile Creek Rd, as well as along Hillrose Dr. (Figure 2.1).

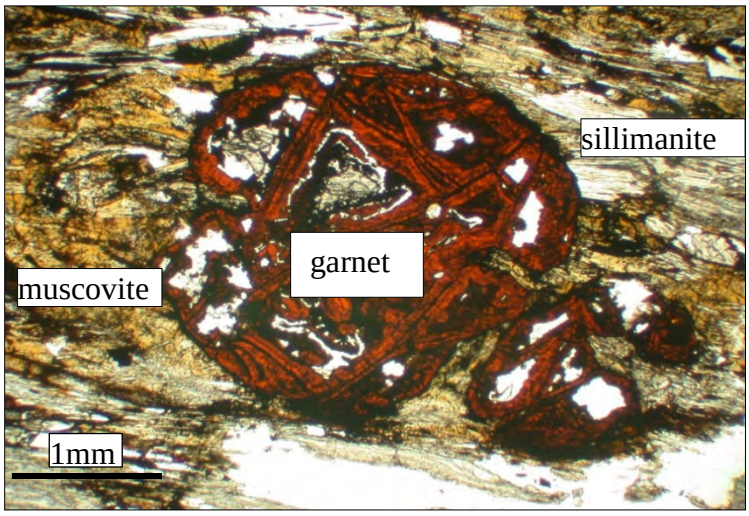

Figure 3.14: Thin section micrograph of Tallulah Falls garnet-sillimanite-muscovite-schist, SM15.

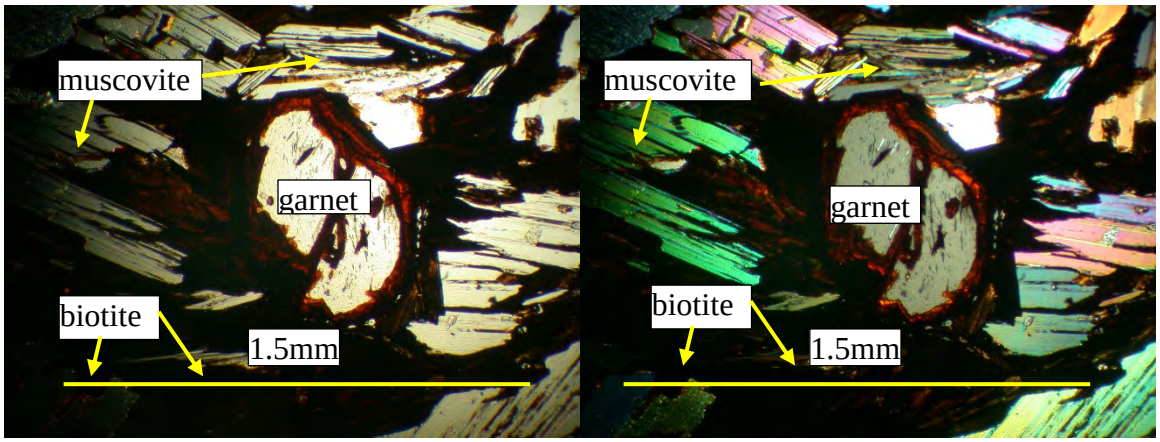

Figure 3.15: Photomicrograph of garnet, biotite, and muscovite in Tallulah Falls schist (SM130) in plane polarized (left) and cross -polarized light (right, not at 90°).

Tallulah Falls gneiss

Gray to black, fine- to medium-crystalline (1-5mm) schistose muscovite-biotite-porphyroclastic feldspathic gneiss is found proximal to Table Rock gneiss and Walhalla hornblende gneiss. Using Garihan's (2005), naming convention this lithology is identified in the current study as Tallulah Falls gneiss, which is also seen to the north in Sunset quadrangle. Tallulah Falls gneiss differs from Table

Figure 3.16: Stream exposure of Tallulah Falls gneiss, SM54. Brunton compass is 8cm wide. View approximately to the northeast.

Rock gneiss due to a higher mica content (50-60% vs. ≤20%), mica-dominated matrix, and texture (medium- to coarse-crystalline vs. fine- to medium-crystalline, respectively). A thin section from SM79 is composed of quartz (65%), biotite (20%), and plagioclase (15%) with biotite foliations interlayered with quartz (Figure 3.17-Figure 3.18). Figure 3.17 also shows triple point intersections of adjacent quartz crystals indicate quartz (here unstrained) is completely recrystallized in the rock. A thin section from SM154 is composed of plagioclase (45%), muscovite (20%), biotite (20%), and quartz (15%). Figure 3.19 and Figure 3.20 show quartz-plagioclase aggregate porphyroclasts (~6mm) surrounded by biotite, and muscovite.

Tallulah Falls gneiss appears at the leading edge of the Six Mile thrust sheet for most of its western contact with the Walhalla thrust sheet in the study area (Figure 3.27). This differs from Seneca fault contacts to the north and west that have Poor Mountain amphibolite lying directly on Table Rock gneiss in the Caesars Head-Camp Greenville area (Garihan, 2001). Hence, regionally the Seneca thrust to the north has cut upsection to higher structural levels within the metamorphic stratigraphy. Fine-crystalline,

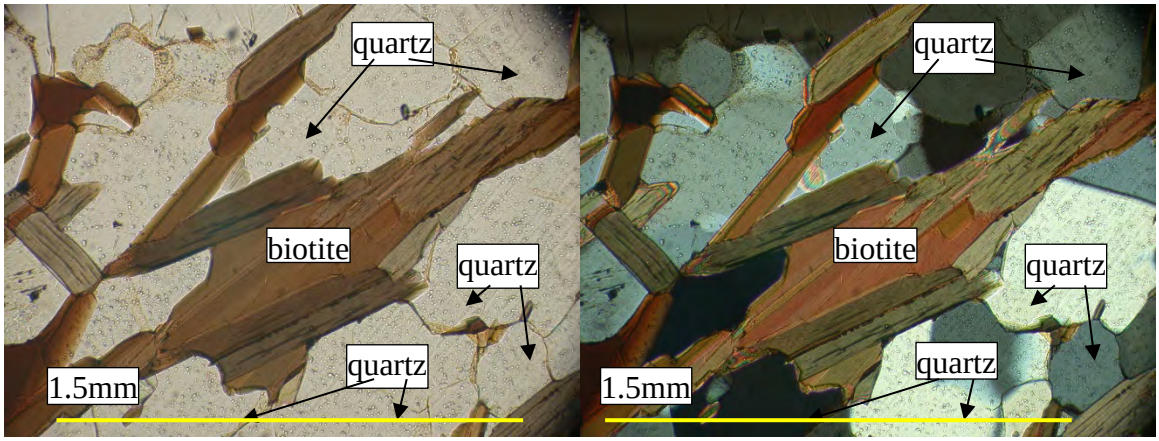

Figure 3.17: Photomicrographs of biotite and quartz from Tallulah Falls gneiss (SM79) in plane polarized (left) and cross-polarized (right) light.

equigranular, non-porphyroclastic muscovite-biotite gneiss occurs locally, which is included within the Tallulah Falls gneiss due to its proximity (1km) to other lithologies within Tallulah Falls gneiss. Tallulah Falls gneiss weathers to gray to tan, micaceous soil, and forms shoals (elevation change 1-2m) and waterfalls (2-10m) at some locations. Accessible exposures of the Tallulah Falls gneiss are located at the intersection of Highway 133 and Pearl Lane, and approximately 200m north of the intersection of Mile Creek Rd. and Woodall Mt Rd (Figure 2.1).

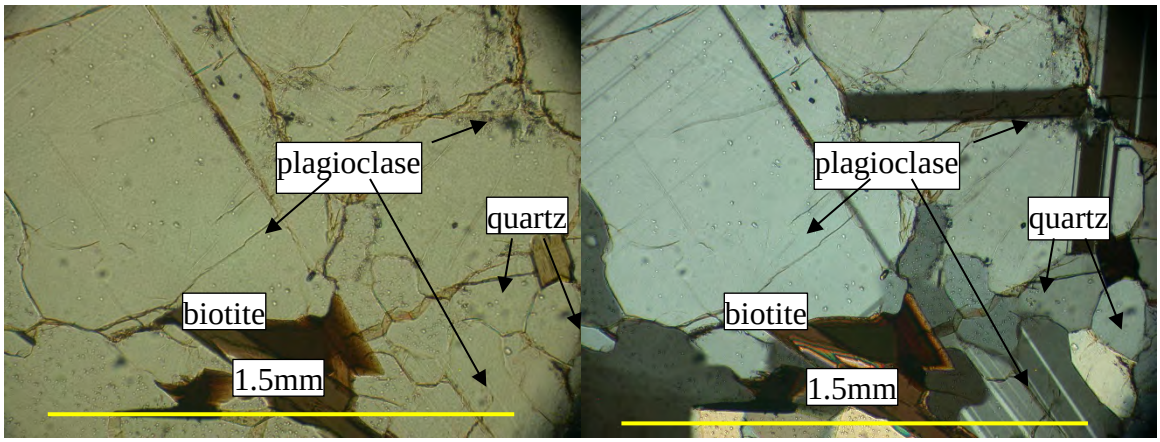

Figure 3.18: Photomicrographs of plagioclase porphyroclast surrounded by biotite and quartz in Tallulah Falls gneiss (SM79) in plane polarized (left) and cross-polarized (right) light.

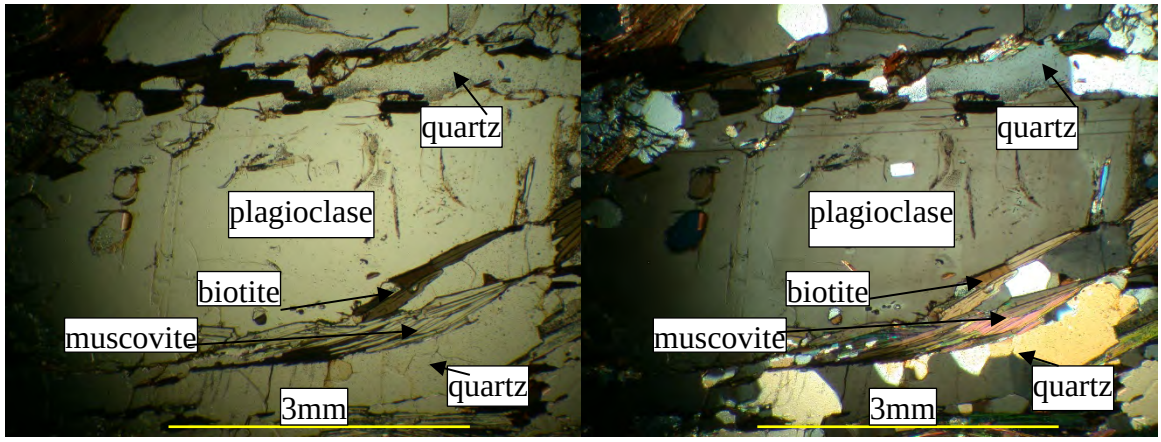

Figure 3.19: Photomicrographs of plagioclase porphyroclast surrounded by biotite and muscovite in Tallulah Falls gneiss (SM154) in plane polarized (left) and cross-polarized light.

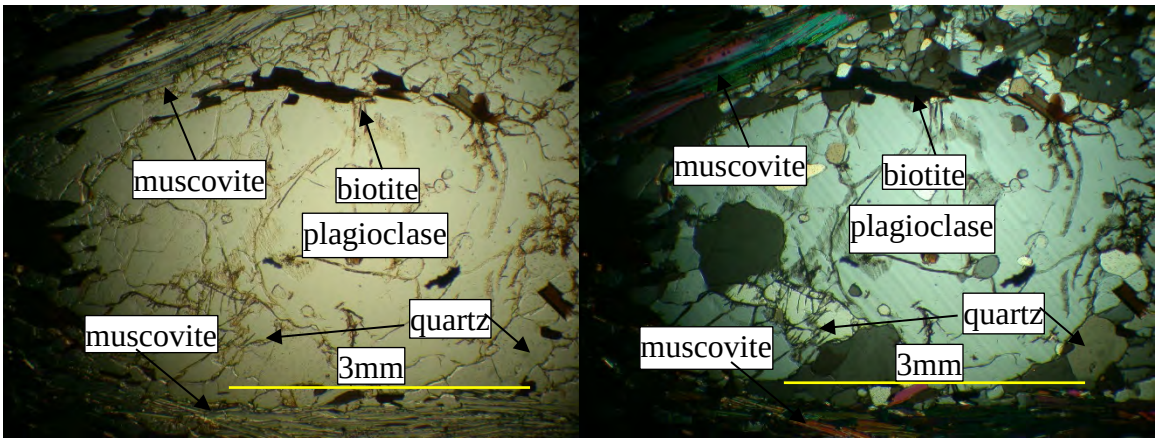

Figure 3.20: Photomicrographs of a plagioclase porphyroclast surrounded by biotite, muscovite, and quartz in plane polarized (left) and cross-polarized (right) light from Tallulah Falls gneiss from SM154.

Amphibolite within Tallulah Falls Formation

Amphibolite surrounded by porphyroclastic, medium- to coarse-crystalline, micaceous Tallulah Falls gneiss or sillimanite-garnet-muscovite Tallulah Falls schist is interpreted to be within the Tallulah Falls Formation (TFF) of the Six Mile thrust sheet (Figure 3.22-Figure 3.22). This amphibolite has less defined foliation and compositional banding and has a lower feldspar and quartz percentage than Walhalla hornblende gneiss, but is similar in composition (dominated by hornblende) and texture (fine-crystalline) to amphibolite within the Walhalla hornblende gneiss (Table 3.1). Therefore, amphibolites in the study area were differentiated by association to other footwall or hanging wall rocks. A thin section of amphibolite from SM132 is comprised of hornblende (65%), plagioclase (15%), and quartz (20%) (Figure 3.23-Figure 3.24). Amphibolite from SM52 is composed of hornblende (70%), quartz (20%), and plagioclase (10%) based on thin section examination (Figure 3.26). Percentage of leucocratic minerals was equal or lower

in amphibolite thin sections from SM132 (35%) and SM52 (30%) than in Walhalla hornblende gneiss (35%, 70% from SM65 and SM372, respectively).

Amphibolite within the Tallulah Falls Formation is often found in small pods that are 1-2m in length and, therefore, were neither mapped nor given a separate unit name in these instances (Figure 3.22). One larger area (~100,000 m^2 or 0.3mi^2) was identified in the central portion of the study area dominated by amphibolite and surrounded by Tallulah Falls gneiss and schist (Figure 3.1).

Figure 3.21: View to the south with amphibolite pod (resistant, center) surrounded by garnet-muscovite schist (reddish) in logging trail at SM320. Hammer head is 10cm wide.

Figure 3.22: View to the south with upper arrow pointing to hammer placed concordantly with amphibolite pod and lower arrow pointing to pen aligned with foliation in garnet-muscovite schist in logging trail, (SM320). Hammer is 36cm long; pen is 15cm long.

Figure 3.23: Photomicrograph of hornblende with plagioclase from amphibolite within the Tallulah Falls Formation (SM132) in plane polar (left) and polarized (right) light.

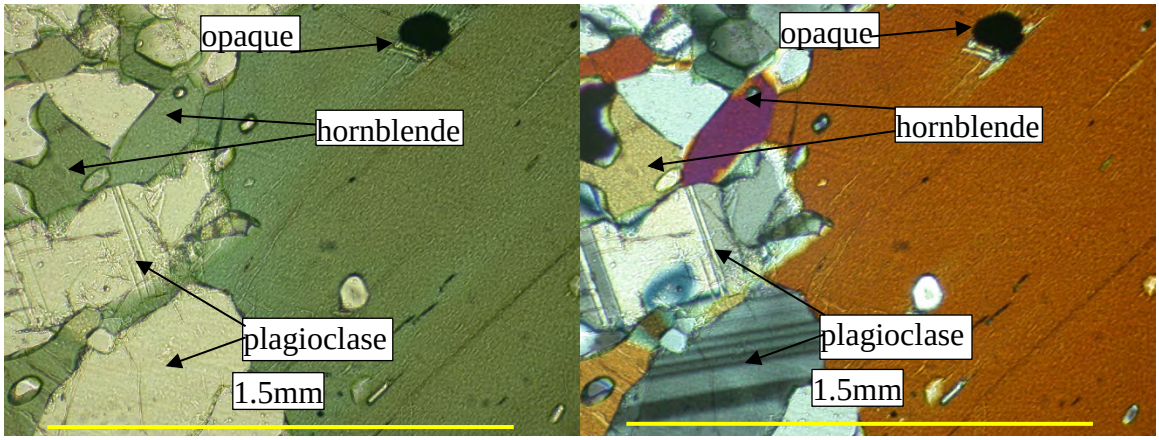

Figure 3.24: Photomicrograph of hornblende with plagioclase from amphibolite within the Tallulah Falls Formation (SM132) in plane polar (left) and polarized (right) light.

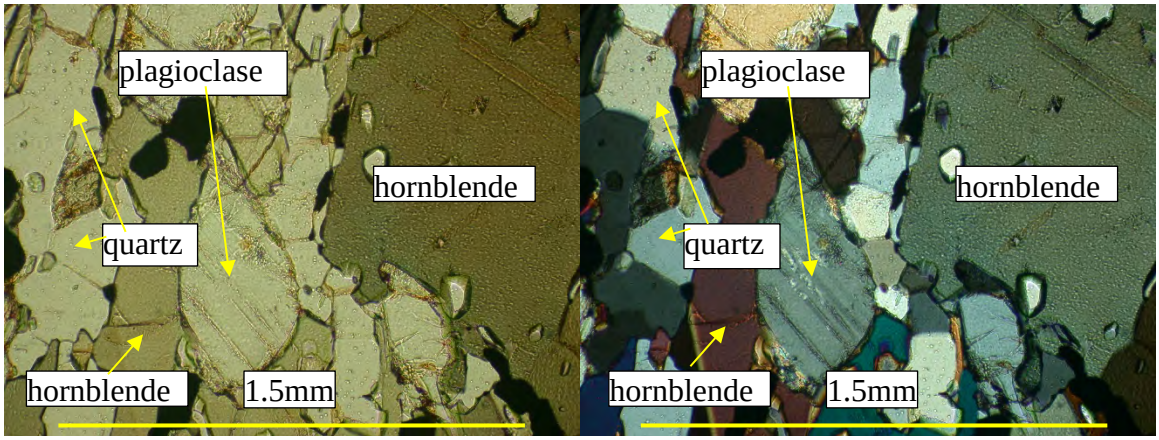

Figure 3.25: Photomicrographs of hornblende and quartz with minor plagioclase from amphibolite within the Tallulah Falls Formation (SM52) in plane polar (left) and polarized (right) light.

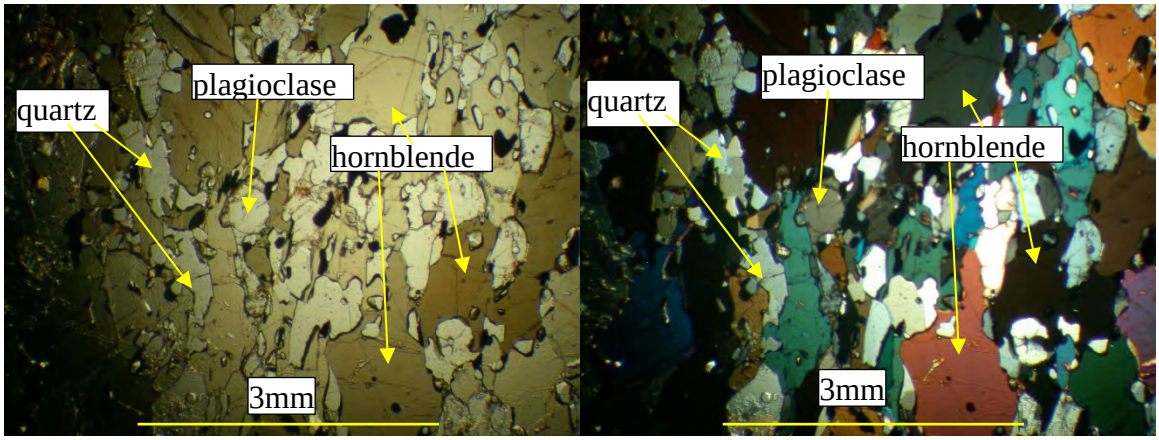

Figure 3.26: Photomicrographs of hornblende and quartz with plagioclase from amphibolite within the Tallulah Falls Formation (SM52) in plane polar (left) and polarized light (right).

Pegmatite

White, quartz-, feldspar-, and muscovite-rich, coarse-crystalline pegmatite was found as the only lithology at 17(3%) of 567 locations in the study area (Figure 3.27). In many other locations, the pegmatite was found concordant or discordant with foliation of country rock in units of both the Walhalla thrust sheet and Six Mile thrust sheet. Pegmatite was not found at a mappable scale, and the largest exposure of pegmatite was $4m^2$ at SM170 (Figure 3.27). In locations where it was found within another lithology, pegmatite was not noted because of the predominance of the other lithology.

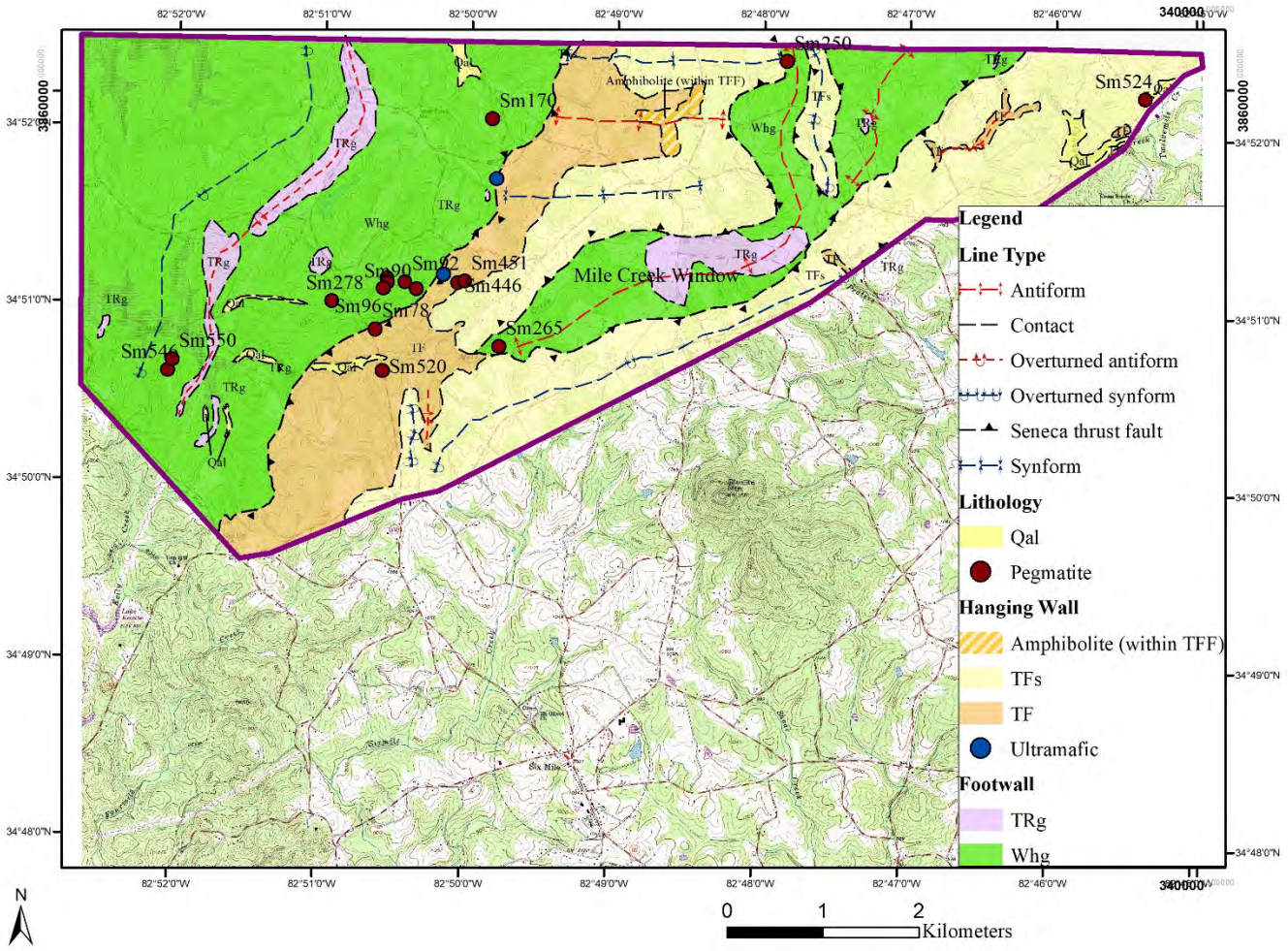

Figure 3.27: Map showing locations at which pegmatite was the only lithology observed.

Ultramafic Rocks

Two occurrences of ultramafic rocks with differing mineralogies were found within the study area (XRD locations, Figure 3.1), but not at a mappable scale. The first ultramafic occurrence was a green, schistose body ("pod", 0.5m in length) exposed in a logging trail at SM197. It contains the minerals tremolite and clinochlore, identified by XRD analysis (Figure 3.28). This pod was surrounded by amphibolite float. Ultramafic rock enveloped within amphibolite is encountered commonly in Sunset quadrangle (Garihan, 2005). While Garihan (2005) did not specifically state whether ultramafic rocks

Figure 3.28: Ultramafic pod in logging trail at SM197. Hammer head is 10cm wide. View to the southwest.

located near Seneca fault were of Walhalla or Six Mile thrust sheet origin, he suggested they are fault slices from the footwall of the thrust (Garihan, 2005).

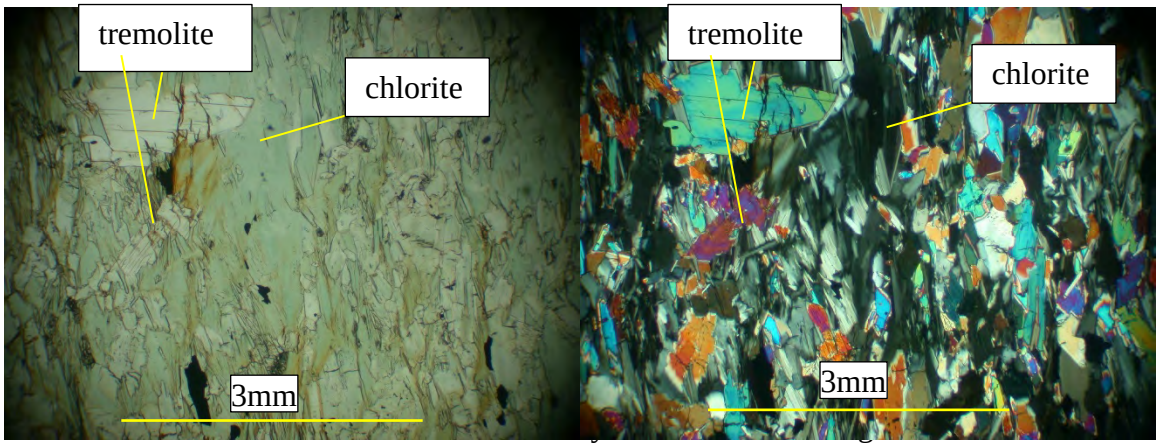

Figure 3.29: Photomicrograph of SM197, created and analyzed by M. Seigler, showing tremolite-actinolite and chlorite.

The Seneca, Walhalla, and Clemson ultramafic bodies contain chlorite, tremolite, olivine, and anthophyllite (Warner et al., 1989) similar to the clinochlore and tremolite found in SM197. Therefore, protoliths of ultramafic rocks found in the study area are probably lherzolite, or hornblende- or plagioclase-bearing peridotite (Butler, 1989).

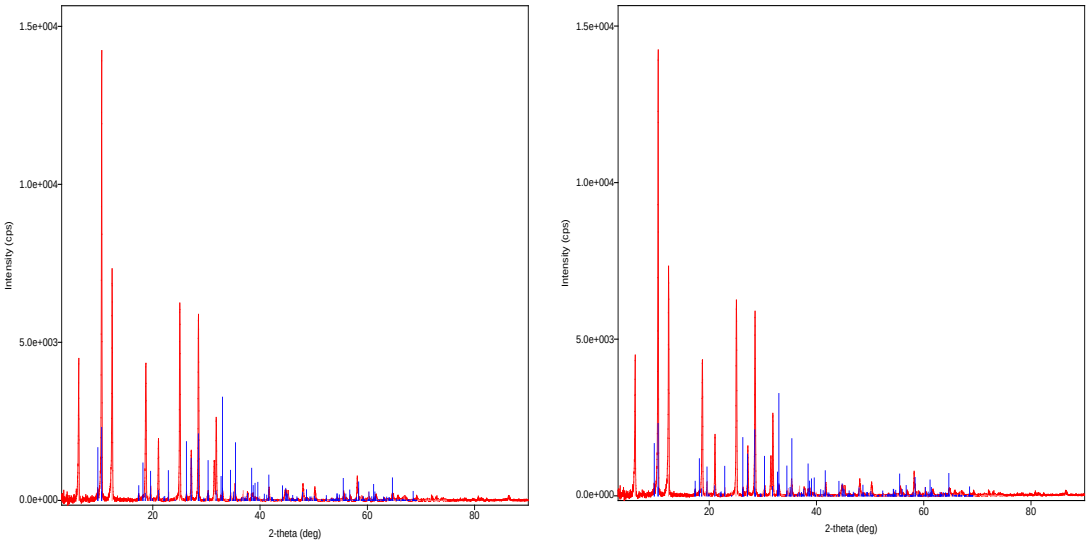

Figure 3.30: X-ray diffractograms from the ultramafic pod at SM197. Tremolite (left) and clinochlore (right), are identified based on the peaks. Diffractograms show intensity (counts per second) at diffraction angle (2Θ, degrees).

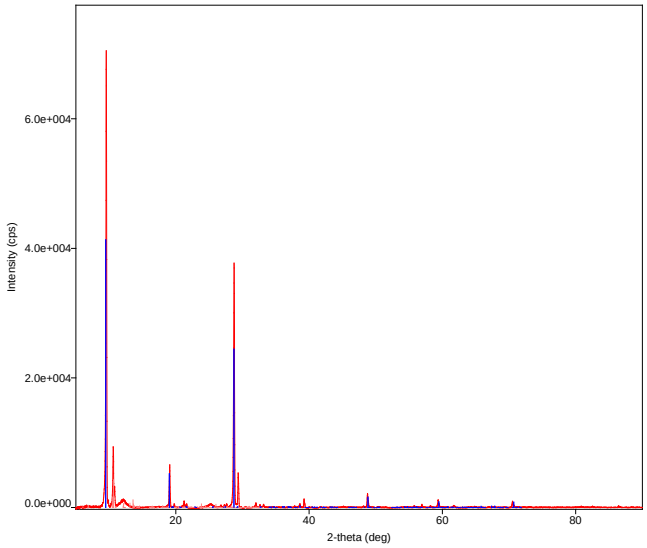

Figure 3.31: Identification of talc from X-ray diffractograms of sample from the ultramafic exposure at SM422. Peaks are intensity (counts per second) at diffraction angle (2Θ, degrees).

Table 3.1: Lithologic descriptions of rocks found in the northern third of Six Mile quadrangle and nearby areas

Thrust Sheet[a]	Formation	Unit[(d,g,h)]	Age[(b,d,e)]	Protolith[(b,c,d,e)]	Lithologic Description from Previous Studies[(b,e)]	Lithologic Description from Results of Current Study[g]	Lithologic Description Comparison between Previous [(b,e)] and Current Studies[g]
		Quaternary alluvium[g]			Gravel, sand, silt, and clay deposits of Quaternary age occur beneath flood plains and discontinuously along the stream channels of major and minor drainages of the area.[e]	Gray to tan to brown, clay to cobble-sized, alluvial deposits.	Grain size similar in both current and previous studies[(b,e)].

Walhalla thrust sheet		Table Rock gneiss[g]	Middle-Lower Ordovician[d, e]	Igneous pluton[(b,c,d,e)]	Biotite quartzo-feldspathic gneiss, locally leucocratic. The gneiss is gray to tan, fine- to medium-crystalline, and moderately well layered compositionally. Foliation is defined by aligned micas or discontinuous, lenticular aggregates of quartz and feldspar. Sheared varieties of quartzo-feldspathic gneiss contain quartz ribbons a few millimeters thick defining foliation or muscovite, owing to K-feldspar breakdown during ductile deformation. Well-developed mineral lineation occurs on foliation surfaces in many places. Unit includes medium-crystalline muscovite-	White to gray to tan, fine- to medium-crystalline, muscovite-biotite quartzo-feldspathic leucocratic gneiss. Foliation defined by aligned micas. Minor occurrences of white to gray, fine- to medium-crystalline biotite hornblende gneiss with hornblende porphyroblasts commonly ≥1cm; minor gray to black, fine- to medium-crystalline muscovite biotite schist. Unit similar in crystal size , color, and foliation to previous studies[(b,e)].	Lithologies described from both areas similar in color and crystal size. Foliation defined similarly in both current and previous studies[e,g]. Hornblende porphyroblasts not mentioned in previous study[e].

					biotite-quartz-feldspar gneiss; light-gray, medium-crystalline biotite-feldspar augen gneiss; medium-crystalline hornblende-quartz-feldspar gneiss; medium- to coarse-crystalline, poorly layered, poorly foliated biotite granitoid gneiss; and aplite, pegmatite, and quartz veins. Mafic rocks included in the map unit are amphibolite, biotite amphibolite, hornblende gneiss, and biotite schist.		
	Poor Mountain Formation	Poor Mountain quartzite[(d,h)]	Middle Ordovician[d]	Greywacke or arkose [b]	Massive to layered feldspathic micaceous quartzite and metatuff. Parallel alignment of micas defines a foliation.[b]		
		Poor Mountain	Upper Cambrian-	Mid-Ocean Rift Basalts[d]	Amphibolite and epidote amphibolite are black, fine- to		Lithologic descriptions similar for

		amphibolite[d,h]		Lower Ordovician[b]		medium-crystalline, and thinly layered rocks with fine- to coarse-crystalline leucocratic pods and layers of quartz and feldspar along foliation. The map unit also includes medium-crystalline, moderately to poorly layered hornblende gneiss; local fine-crystalline, granoblastic epidosite interlayered with amphibolite; mica schist; and minor coarse-crystalline epidote hornblendite.		amphibolite and hornblende gneiss between Garihan's (2005) and current study[e,g] in color and crystal size. Epidote (and epidosite[e]) found in both study areas. Current study[g] identified hornblende gneiss as the major lithology with minor amphibolite, in contrast to amphibolite as the major mafic lithology in Sunset quadrangle[e].
			Wallhalla hornblende gneiss[g]	Age unknown[g]	Protolith unknown[g]		Unit dominated by white to gray to black, hornblende gneiss. Foliation defined by aligned bands of hornblende and quartz-feldspar. Locally fine- to medium-crystalline amphibolite. Epidote occurs locally	

							interfoliated with hornblende. Unit adjacent to Table Rock gneiss.	
Six Mile Thrust Sheet	Tallulah Falls Formation	Upper Tallulah Falls gneiss[d,h]	Lower to Middle Cambrian[d]	Greywacke-schist-amphibolite[d]	Light- to dark-gray metagraywacke biotite-gneiss and two-mica schist unit. [b]			
		Tallulah Falls schist[g]		Aluminous schist[d]	The dominant lithologies are a dark-gray, coarse-crystalline biotite schist and a medium-crystalline, poorly layered, locally leucocratic biotite-hornblende gneiss (hornblende mode less than 50 percent). The map unit also includes various aluminous metapelite rock types, including migmatitic, medium-crystalline sillimanite-garnet-muscovite-biotite schist; medium-crystalline garnet-muscovite-biotite schist; medium- to coarse-crystalline	Tan to red to purple to black, ±garnet, ±sillimanite, ±biotite, muscovite, schist. Garnets range in size from 1mm-3cm. Schist often appears crenulated (wavelength microscopic-2cm), with axial planar cleavage forming lineations on pavement exposures of schist. Interlayered black, medium- to coarse-crystalline amphibolite found within the unit, also commonly found as float. Pods of gray to black, fine- to medium-crystalline	Amphibolite is the dominant lithology in Tallulah Falls schist in Sunset quadrangle[e], whereas schist is the dominant lithology Tallulah Falls schist in Six Mile quadrangle[g]. Garihan includes schist in his description of Tallulah Falls gneiss, as well. Amphibolite also found in current study area[f].

					sillimanite-muscovite schist; medium-crystalline graphite-garnet-mica quartzite; medium-crystalline, moderately well layered amphibolite; and hard, fine-crystalline, poorly layered hornblende gneiss.	amphibolite also found within unit.	
		Lower Tallulah Falls gneiss[g]		Greywacke-schist-amphibolite[b]	The dominant lithology is a dark-gray, fine- to medium-crystalline, schistose garnet-sillimanite-muscovite-biotite-porphyroclastic plagioclase-quartz gneiss. Muscovite is commonly medium crystalline, and biotite is fine-crystalline. Plagioclase porphyroclasts make the unit distinctive. The plagioclase porphyroclasts average approximately 1 centimeter in long dimension and are	Gray to black, medium- to coarse-crystalline schistose muscovite-biotite-porphyroclastic quartzofeldspathic gneiss. Fine-crystalline, equigranular, muscovite-biotite gneiss locally occurring. Gray to black, fine- to medium-crystalline amphibolite also found within unit.	Lithologies described in both study areas[e,g] are similar in color, crystal size, and porphyroclasts of biotite gneiss. Granoblastic calc-silicate rock not found in Tallulah Falls gneiss in current study[g].

					modified into lenticular shapes by ductile deformation. Micaceous schistosity wraps around the feldspar porphyroclasts, giving the rock a speckled appearance. The map unit also includes interlayered dark-gray, fine-crystalline muscovite-biotite gneiss; schistose sillimanite-muscovite gneiss; dark-medium-crystalline muscovite-quartz schist; medium-crystalline migmatitic sillimanite-biotite schist; and coarse-crystalline biotite gneiss. Minor lithologies include granoblastic calc-silicate rock (titanite, epidote, plagioclase, and quartz) and amphibolite.		

		Pegmatite[g]	Age unknown[g]			Light to tan, muscovite, coarse-crystalline pegmatite. Found concordant and discordant with both Six Mile Thrust Sheet and Walhalla thrust sheet rocks.	Pegmatite included in Garihan's description of Table Rock gneiss in previous study[e].
		Ultramafics[g]	Age unknown[g]		Nematoblastic clinoamphibole schist and lepidoblastic chlorite-clinoamphibole schist.	Green, fine- to medium-crystalline, schistose, tremolite-clinochlore ultramafic (SM197). White, medium-crystalline, talc ultramafic (SM422).	Previous and current studies[e,g] include clinoamphibole schist. Former study[e] does not include talc found in ultramafic rock in current study[g].

[a]As observed in field, this investigation (Sellers, 2016).
[b]Marion-South Mountains Area, North Carolina, Bier, et al. (2002)
[c]Bream (2002)
[d]Hatcher (2002)
[e]Sunset quadrangle, Garihan (2005)
[f]Northern third of Six Mile quadrangle
[g]Mapped in current study, northern third of Six Mile quadrangle.
[h]Unit mapped in nearby areas, but not observed in the northern third of Six Mile quadrangle.

Structural Data

Foliations in the study area (Figure 3.32) strike predominantly NE-SW with 66 dips to the SE (Figure 3.33), ranging from 2° to vertical (Figure 3.33; See Appendix B for full data set). Variation from the trend includes 19 NW-SE striking foliations with dips ranging from 6-88° to the NE. The compiled 103 data points had the best-fit great circle striking S46°E (136°) and dipping 80°SW (Figure 3.34). Eigenvector trend and plunges (1, 2, 3) are displayed on even-numbered figures from Figure 3.34 to Figure 3.46 and are listed in Table 3.2. Contours are displayed in 2 area-percent intervals on the even-numbered figures. According to Allmendinger (2011), the first axis (Eigenvector 1) corresponds to the greatest concentration of poles to planes, the second (Eigenvector 2) to the intermediate, and the third (Eigenvector 3) to the smallest concentration of poles to planes.

There are 45 data points from footwall units (Table Rock gneiss and Walhalla hornblende gneiss) with the best fit great circle striking S54°E (144°) and dipping 83°SW (Figure 3.35-Figure 3.36). Table Rock gneiss had 10 data points with the best-fit great circle striking S55°E (145°) and dipping 79°SW (Figure 3.37-Figure 3.38). Walhalla hornblende gneiss had 35 data points with the best-fit great circle striking S52°E (142°) and dipping 85°SW (Figure 3.39-Figure 3.40). The northwest portion of the study area is lacking in orientation data due to issues related to private property access. It is possible this area might be critical for seeing more of the relationship of Table Rock gneiss intruding into Walhalla hornblende gneiss.

There were 56 data points taken from hanging wall units (Tallulah Falls gneiss and Tallulah Falls schist), as well as 2 data points taken from foliation adjacent to purported ultramafic rocks. One such data point was taken in foliation from same outcrop as ultramafic talc at SM422, whereas the other data point was taken from foliation in an unknown lithology near ultramafic anthophyllitic float at SM78 (later excluded because of uncertainty of sample origin). The 58 measured foliations from the units had the best-fit great circle striking S56°E (146°) and dipping 78°SW (Figure 3.41-Figure 3.42). Tallulah Falls schist had 17 data points with a best-fit great circle striking S74°E (164°) and dipping 61°SW (Figure 3.43-Figure 3.44). Tallulah Falls gneiss had 39 data points with a best-fit great circle striking S47°E (137°) and dipping 81°SW (Figure 3.45-Figure 3.46).

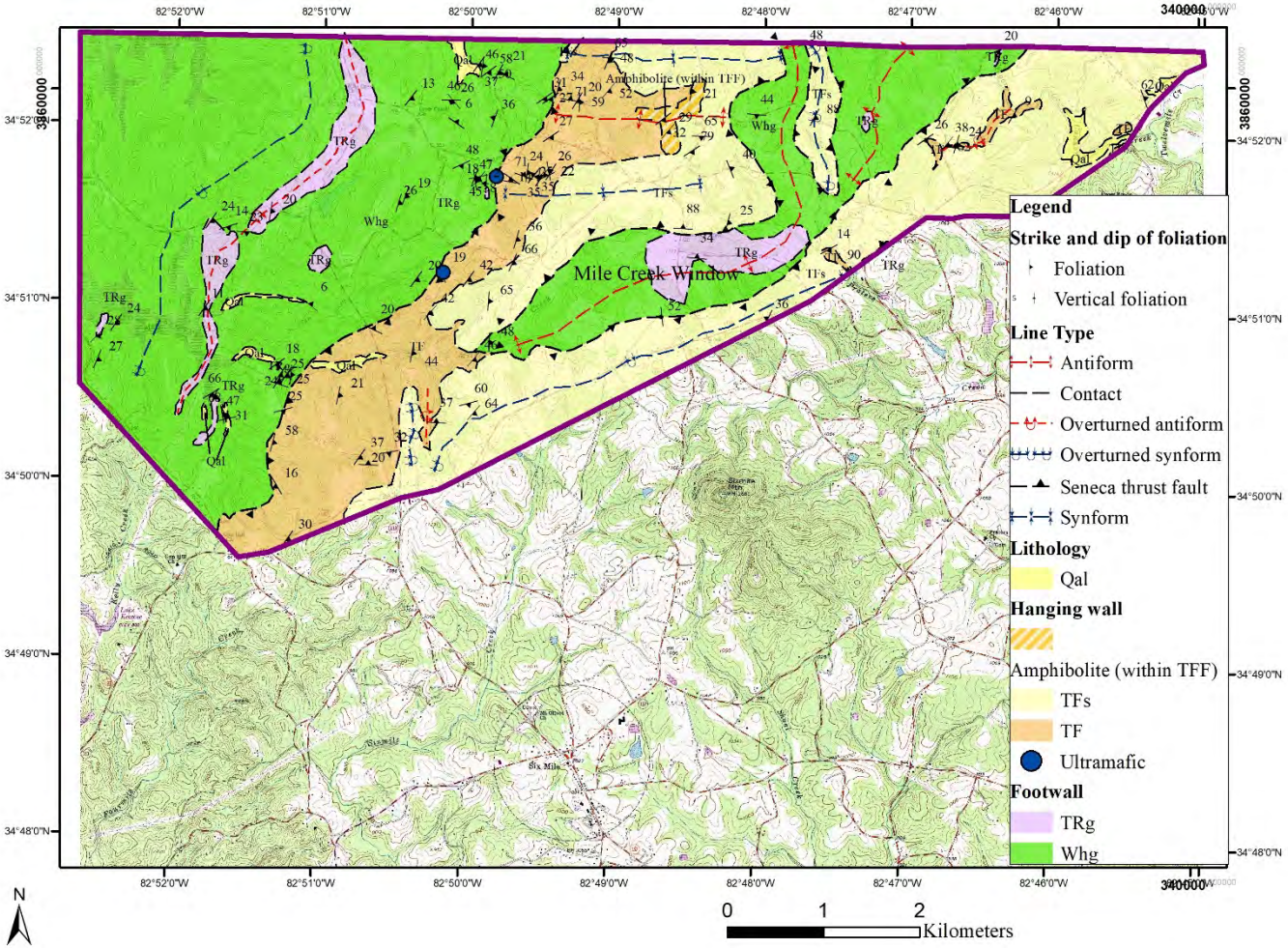

Figure 3.32: All strikes and dips in the study area.
TFs-Tallulah Falls schist; TF-Tallulah Falls gneiss.

Table 3.2: Synopsis of stereonet analyses of structural data from the study area. Strike and dip data formatted according to 'right-hand rule.' Best fit strike and dip represent strike and dip of plane that contains eigenvectors 1 and 2.

Unit	# of Data points	Best fit strike	Best fit dip	Central strike/dip from highest concentration of poles	Fisher Mean vector trend	Fisher Mean vector plunge	Eigenvector 1	Eigenvector 2	Eigenvector 3
Study area	103	146°	80°	N25°E/22°SE, 025°/22°	300°	68°	304°->66°	150°->22°	056°->10°
Footwall units	45	144°	83°	N34°E/20°SE, 034°/20°	306°	68°	308°->66°	147°->23°	054°->7°
TRg	10	145°	79°	N31°E/25°SE, 031°/25°	301°	63°	302°->63°	150°->24°	055°->11°
Whg	35	142°	85°	N36°E/21°SE, 036°/21°	308°	69°	310°->67°	144°->22°	052°->05°
Hanging wall units	58	146°	78°	N11°E/25°SE, 011°/25°	294°	68°	299°->65°	151°->22°	056°->78°
TF	39	137°	81°	N10°E/26°SE, 010°/26°	282°	72°	292°->69°	140°->18°	047°->09°
TFs	17	164°	61°	N87°W/66°NE, 273°/66°	319°	50°	326°->30°	200°->46°	074°->29°

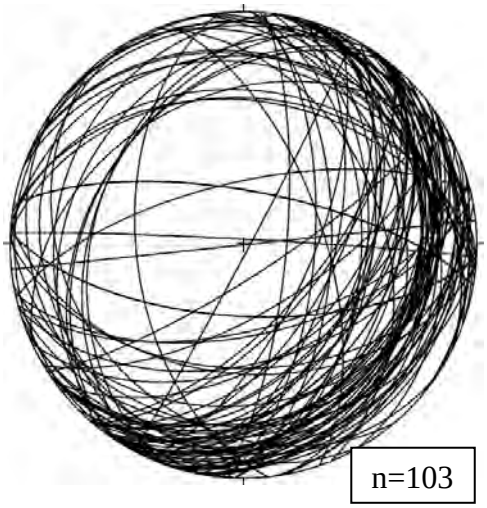

Figure 3.33: Great circles representing all foliation attitudes collected in the study area.

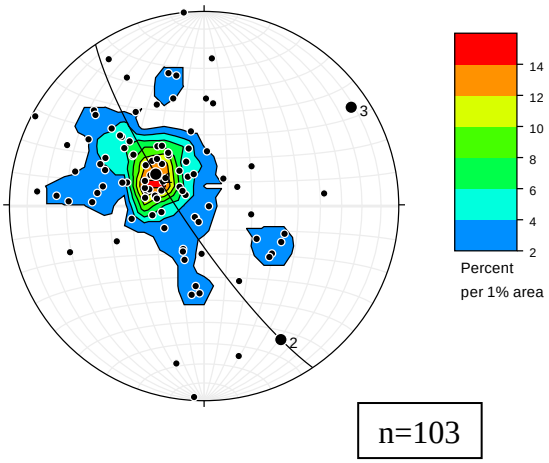

Figure 3.34: Poles to plane of foliation for all units within from the study area. Points 1-3 are eigenvalues calculated by Stereonet; see text for explanation.

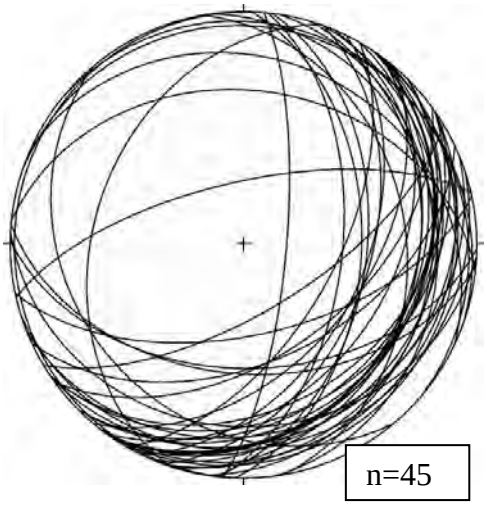

Figure 3.35: Great circles for strikes and dips of foliation measured in the study area from Table Rock gneiss and Walhalla hornblende gneiss.

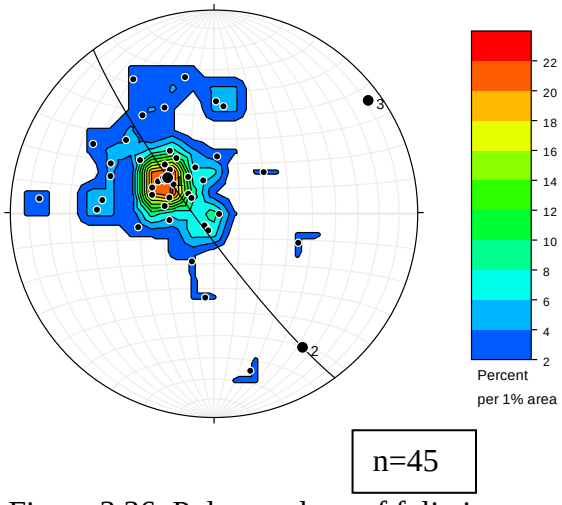

Figure 3.36: Poles to plane of foliation for the study area from Table Rock gneiss and Walhalla hornblende gneiss.

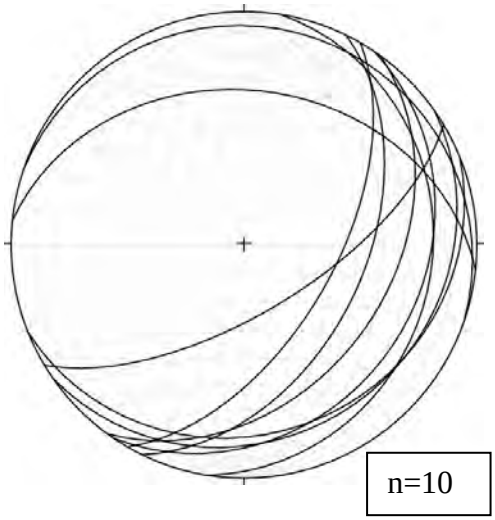

Figure 3.37: Great circles for strikes and dips of foliation measured in the study area from Table Rock gneiss.

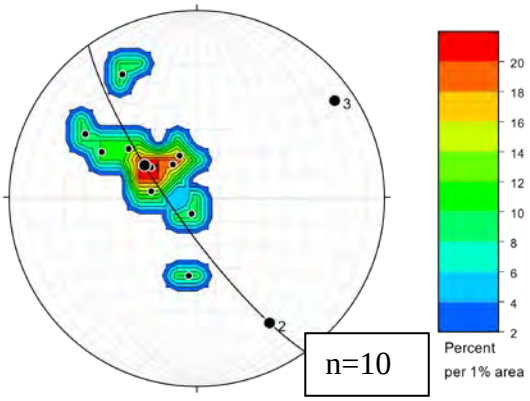

Figure 3.38: Poles to plane of foliation measured in the study area from Table Rock gneiss.

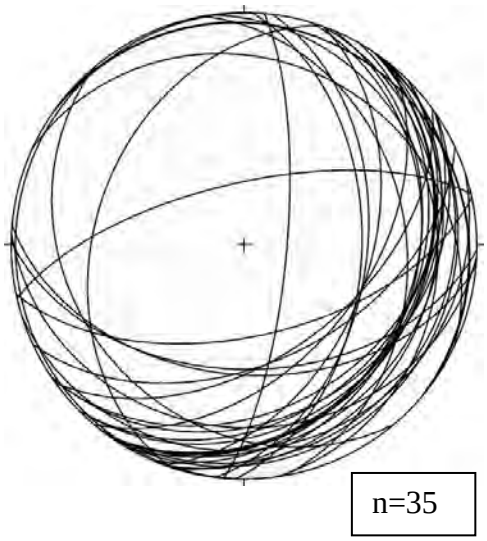

Figure 3.39: Great circles for strikes and dips of foliation measured in the study area from Walhalla hornblende gneiss.

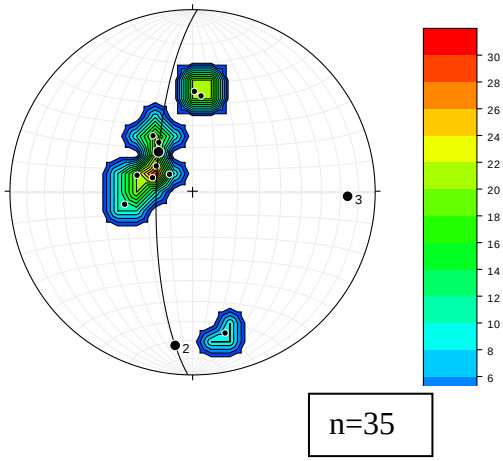

Figure 3.40: Poles to plane of foliation measured in the study area from Walhalla hornblende gneiss.

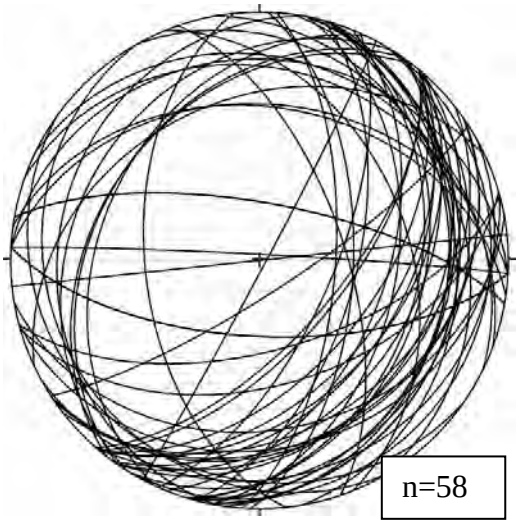

Figure 3.41: Great circles for strikes and dips of foliation measured in the study area from Tallulah Falls gneiss and Tallulah Falls schist.

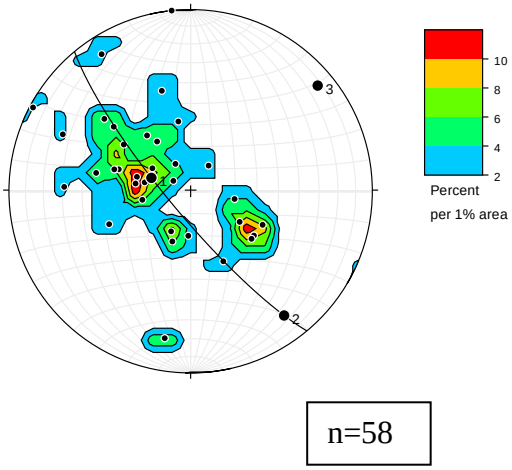

Figure 3.42: Poles to plane of foliation for the study area from Tallulah Falls gneiss and Tallulah Falls schist.

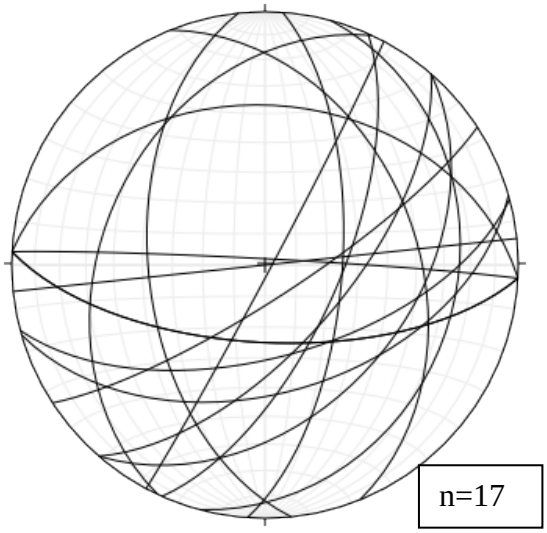

Figure 3.43: Great circles for strikes and dips of foliation measured in the study area from Tallulah Falls schist.

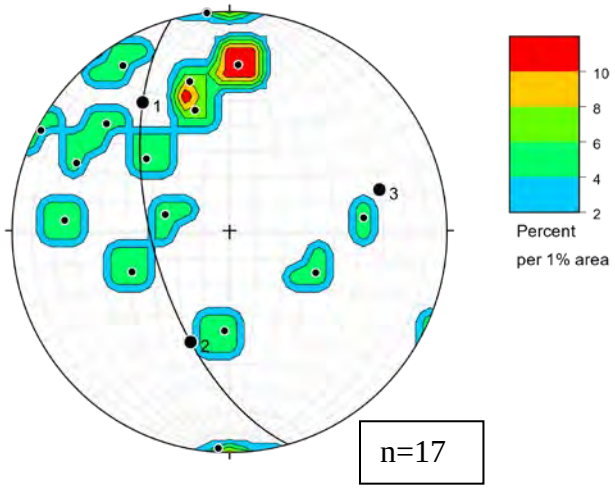

Figure 3.44: Poles to plane of foliation for the study area from Tallulah Falls schist.

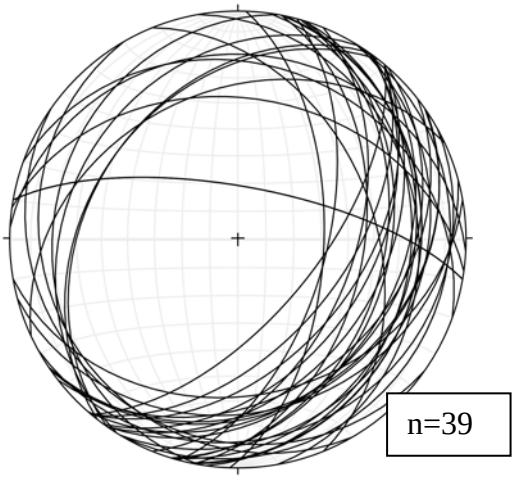

Figure 3.45: Great circles for strikes and dips of foliation measured in the study area from Tallulah Falls gneiss.

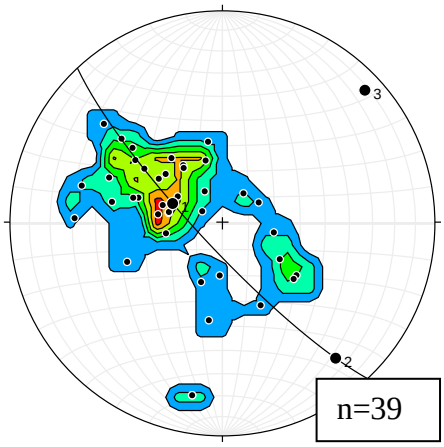

Figure 3.46: Poles to plane of foliation for the study area from Tallulah Falls gneiss.

Structural Analysis Discussion

The synoptic stereonet plot from the study area of attitude plane data (Figure 3.33) and plotted poles-to-plane diagram (Figure 3.34) indicate that the central strike and dip from highest concentration of poles (Figure 3.34) is N25°E/22°SE. The stereonet plot of attitude plane data from footwall units (Figure 3.35) indicates that the central strike and dip from highest concentration of poles is (Figure 3.36) is N34°E/20°SE. Footwall units, therefore, are striking slightly more to the east than the attitude planes from the entire study area, whereas dips remain consistent with attitudes from the study area. Attitude plane data from the Table Rock gneiss (Figure 3.37) indicates that the central strike and dip from highest concentration of poles (Figure 3.38) is N31°E/25°SE. Table Rock gneiss, therefore, has consistent strikes and dips to collective footwall data, as well as to the synoptic data set from the study area. The stereonet plot of attitude plane data (Figure 3.39) from Walhalla amphibolite indicates that the central strike and dip from

highest concentration of poles (Figure 3.40) is N36°E/21°SE. Therefore, Walhalla amphibolite strikes similarly to synoptic footwall data as well as to Table Rock gneiss attitude data with similar dip magnitudes.

The stereonet plot of attitude plane data from hanging wall units (Figure 3.41) indicates that the central strike and dip from highest concentration of poles (Figure 3.42) is N11°E/25°SE. The hanging units, therefore, are definitively striking more N-S than the synoptic footwall units, whereas dip magnitude remain similar. The stereonet plot of attitude plane data from Tallulah Falls schist (Figure 3.43) indicates that the central strike and dip from highest concentration of poles (Figure 3.44) is N87°W/66°SW. The stereonet plot of attitude plane data (Figure 3.45) indicates that the central strike and dip from highest concentration of poles (Figure 3.46) for the Tallulah Falls gneiss is N10°E/26°SE. The Tallulah Falls gneiss, therefore, is definitively striking more N-S than the synoptic footwall units with similar dip magnitude. However, Tallulah Falls schist is striking more E-W than any other subset of attitude data (including Tallulah Falls gneiss), as well as having a higher dip magnitude than any other data subset. Figure 3.42 also indicates that the hanging wall units had two central areas of poles to mean attitude data. This is likely because the central strike and dip from the highest concentration of poles of Tallulah Falls schist varies ~80° strike from Tallulah Falls gneiss. Regional trends such as those of Garihan (2002, 2005) and Garihan and Ranson (2001, 2007), as well as strikes from Tallulah Falls gneiss, are more closely aligned to N-S than strikes from Tallulah Falls schist. It is plausible that compositional layering and foliation attitudes in gneiss are different than schist because schistosity attitudes in the study area are not parallel to

compositional layering. It is also plausible that Tallulah Falls schist shows more variation in strike and dip orientations than Tallulah Falls gneiss because it is more complexly folded.

CHAPTER 4. DISCUSSION

Lithologic Re-delineation

Differentiation of Table Rock gneiss from Tallulah Falls gneiss in the study area is a major objective this investigation. Color, mineralogy, and texture of the gneisses has been crucial to differentiating the units. Table Rock gneiss in the study area is leucocratic, containing plagioclase, microcline, and quartz with minor biotite and muscovite. Tallulah Falls gneiss is mica-dominated, containing biotite and muscovite with plagioclase and quartz aggregate porphyroclasts.

Northwest Six Mile Quadrangle

As shown in Figure 4.1, Griffin (1967) mapped predominantly hornblende gneiss with biotite gneiss "stringers" in the northwest corner of Six Mile quadrangle. This investigation observed that these biotite gneiss stringers were leucocratic with minimal mica content (<15%), indicating Table Rock gneiss (TRg, purple, Figure 4.1b). The Table Rock gneiss stringers were surrounded by hornblende gneiss, interpreted in the current investigation as Walhalla hornblende gneiss and amphibolite. The expanse of Walhalla hornblende gneiss in the study area is a departure from Garihan's Sunset quadrangle map (2005) to the north that consists of predominantly Table Rock gneiss with areas of Poor Mountain amphibolite (Figure 1.3). It is hypothesized in the current study that the difference in abundance of amphibolite and hornblende gneiss between Sunset quadrangle and the area mapped in the current investigation is that Garihan (2005) included amphibolite and hornblende gneiss within the Table Rock gneiss, while a separate unit (Walhalla hornblende gneiss) was created in the current investigation

(Figure 4.2). This work defined amphibolite as containing modal hornblende >%50 and hornblende gneiss as having <50%.

Another possible explanation for the difference in amphibolite, hornblende gneiss, and Table Rock gneiss expanses between Sunset and Six Mile quadrangles is that Table Rock gneiss intruded into amphibolite and hornblende gneiss more extensively in the southern Sunset quadrangle (see Figure 3.8). The intruded Table Rock gneiss could have fingered out into hornblende gneiss in adjoining northern Six Mile quadrangle, revealing minimally intruded (except for biotite gneiss stringers) hornblende gneiss and amphibolite. The transition of dominant Table Rock gneiss to dominant hornblende gneiss and amphibolite appears to occur over a distance of a few kilometers, but the exact distance is unknown.

Upon field checking by committee members (Brame and Castle) in June 2017, leucocratic biotite gneiss, hornblende gneiss, and amphibolite were found to occur within 100m of each other in an area of Sunset Quadrangle mapped as Table Rock gneiss by Garihan (2005) (Figure 4.3; Appendix C). This can be further evidence of either difference in mapping strategies by Garihan and Sellers, or of a transition from dominant Table Rock gneiss to dominant hornblende gneiss and amphibolite.

Further, muscovite- and biotite-rich gneiss were identified east of the hornblende gneiss and amphibolite, which can be attributed to a hidden contact with Tallulah Falls gneiss. The mica-rich units indicated that the Seneca fault had been crossed, entering the Six Mile thrust sheet (orange, Figure 4.2).

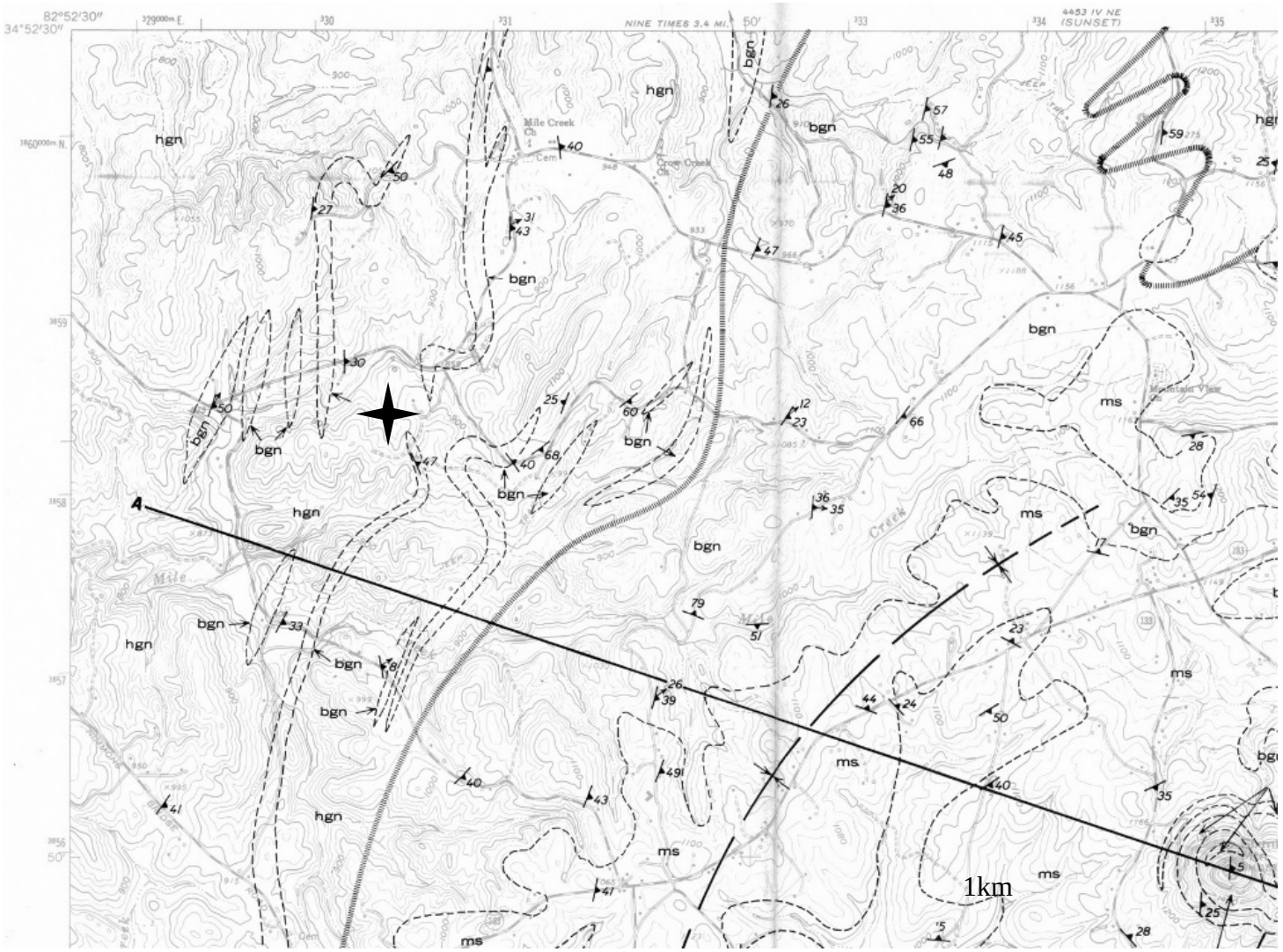

Figure 4.1: Map comparison between Griffin (1967, above) and this investigation (below) of the northwest corner of Six Mile quadrangle. Star is used for location reference. Griffin's map shows hornblende gneiss (hgn), biotite gneiss (bgn), and mica schist (ms).

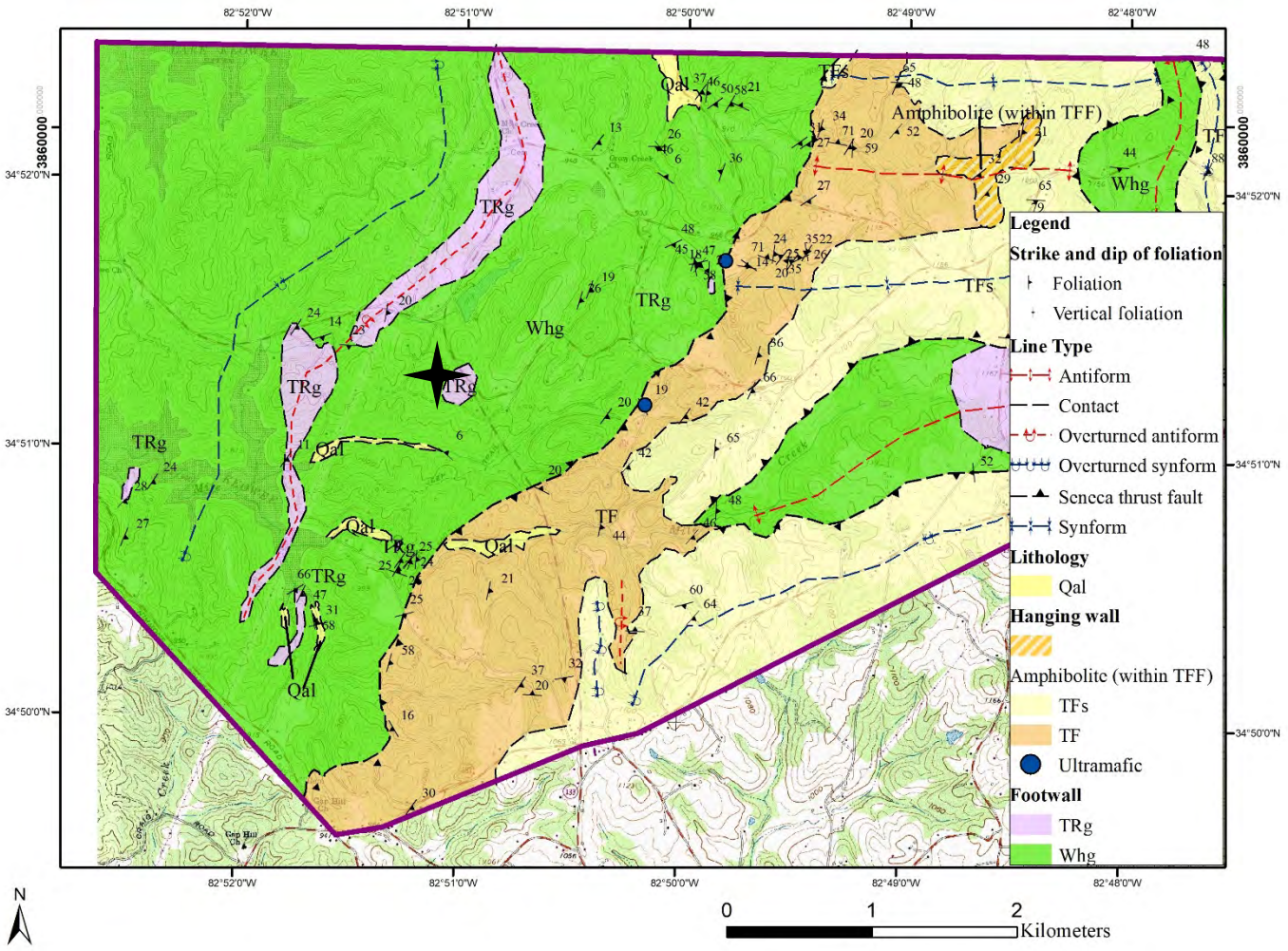

Figure 4.2: Map of northwest Six Mile quadrangle (this investigation).

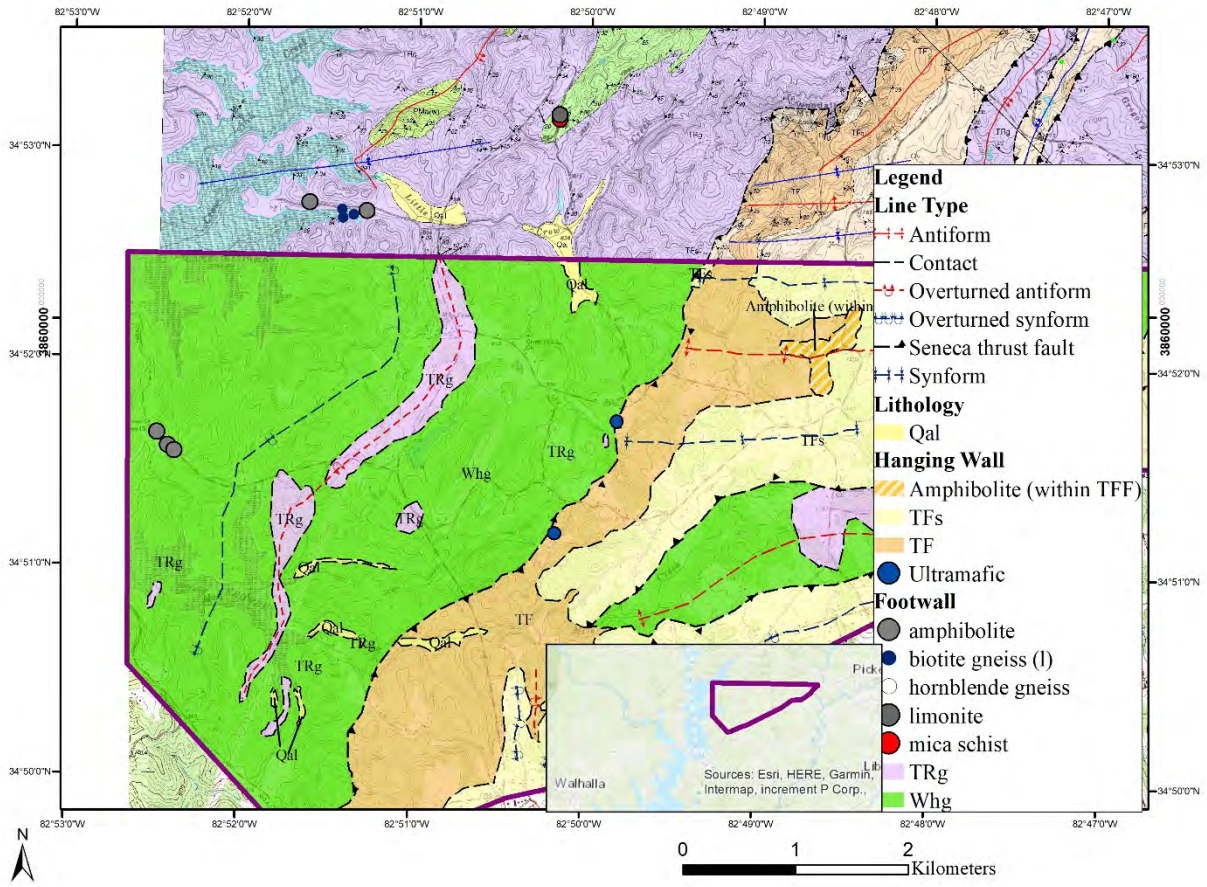

Figure 4.3: Map showing units mapped by Garihan (2005) in Sunset quadrangle near northern boundary of Six Mile quadrangle as mapped (this investigation). Inset map for reference.

North-Central Six Mile Quadrangle

Griffin mapped mica schist, biotite gneiss, as well as an area of hornblende gneiss surrounded by a gradational contact in north-central Six Mile quadrangle (Figure 4.4). Griffin (1967) did not specify what defines the gradational contact, but it can be assumed from his map that it represents a transition between hornblende gneiss (west) to biotite gneiss (east). Griffin's map patterns indicate mica schist ('ms' map unit) lies generally topographically and structurally above biotite gneiss ('bgn' map unit)-hornblende gneiss ('hgn' map unit) gradiational contact (1967; Figure 4.4). The results of this study agree with Griffin's interpretation of a gradational contact between hornblende and biotite gneisses. However, this investigation crossing the Seneca fault trace into Tallulah Falls gneiss instead of a simple gradational contact.

In this study, two types of biotite gneiss were identified. One type of biotite gneiss in the north-central portion of the quadrangle is leucocratic (80-95%), biotite-containing gneiss with biotite being the only mafic mineral observable in hand sample. This area is interpreted as a window through the Six Mile thrust sheet (purple, center, Figure 4.5). It is structurally similar to the so-called 'Clemson window' through the thrust sheet mapped by Griffin in Clemson quadrangle to the south (Griffin, 1974). Two similar windows were mapped in the Sunset quadrangle (Garihan, 2005) and merge into one window in north-central Six Mile quadrangle (Figure 4.5), henceforth named the "Mile Creek Window" (this investigation).

The other type of biotite gneiss found in the north-central portion of the quadrangle is gray to black, fine- to medium-crystalline schistose muscovite-biotite-

porphyroclastic quartzofeldspathic gneiss. Such a porphyroclastic feldspar gneiss is known regionally to lie in the lower parts of the Tallulah Falls gneiss (personal communication, Garihan, 2018). In the current study, this is identified as Tallulah Falls gneiss (orange, Figure 4.5), with mica content similar to that of Tallulah Falls gneiss in Sunset quadrangle (Garihan, 2005). Griffin (1967) mapped less extent of mica schist than mapped in the current study. Schist in the central portion of the study area (cream, Figure 4.5) containing garnet (0-30%), ±biotite (0-25%), ±sillimanite (0-80%), and ±muscovite (0-80%) was identified as Tallulah Falls schist. This lithology is also found in Sunset quadrangle (Garihan, 2005).

Mapping in the current study indicates that the central portion of northern Six Mile quadrangle contains more amphibolite (Walhalla hornblende gneiss, Figure 4.5), hornblende gneiss, and biotite hornblende gneiss than shown on Griffin's map (1967). Walhalla hornblende gneiss in the central portion of the study area was found adjacent to Table Rock gneiss.

An area of amphibolite surrounded by the Tallulah Falls Formation was identified in the central portion of the study area (Figure 4.5). This area is interpreted to represent mafic intrusions, such as dikes or mid-ocean rift basalts hypothesized by Hatcher (2002) to be the origin of the overlying Poor Mountain amphibolite. Bier et al. (2002) found pods, layers, and boudins (size not listed in reference) of amphibolite in both the upper and lower Tallulah Falls metagraywacke-biotite gneisses (referred in the current study as Tallulah Falls gneiss).

Three outcrops of sub-vertical foliation (88°NE, 79°SE, 88°SE) within Tallulah Falls schist (Figure 4.6) were observed within 400m of interpreted contacts of Table Rock gneiss and Walhalla hornblende gneiss with Tallulah Falls schist. Shallow dipping Table Rock gneiss is juxtaposed beside steeply dipping Tallulah Falls schist in the central portion of the study area (Figure 4.6). This structural relationship is interpreted to be related to the initial Seneca folded-thrust fault relationship, where the Six Mile thrust sheet was emplaced over the Walhalla thrust sheet (Griffin, 1974; Hatcher, 1978). Subsequently, secondary overturned folding of the thrust contact occurred after additional folding deformation. Overturned folds are shown on the geologic map (Figure 3.27 and Figure 3.32; Figure 4.5). E-W trending antiforms and synforms in the central portion of the study area (Figure 4.5) were inferred from opposing dip angles, as well as from alternating exposures of Tallulah Falls schist and gneiss without significant topographic relief in the same areas. Because these opposing dips do not carry into the adjacent Walhalla hornblende gneiss, the folds are assumed to have happened prior to Seneca fault thrusting. Similar E-W trending folds were encountered in southern Sunset quadrangle with apparent fault trace truncation of this easterly fold set and were interpreted as formed prior to Seneca thrusting (Garihan, 2005).

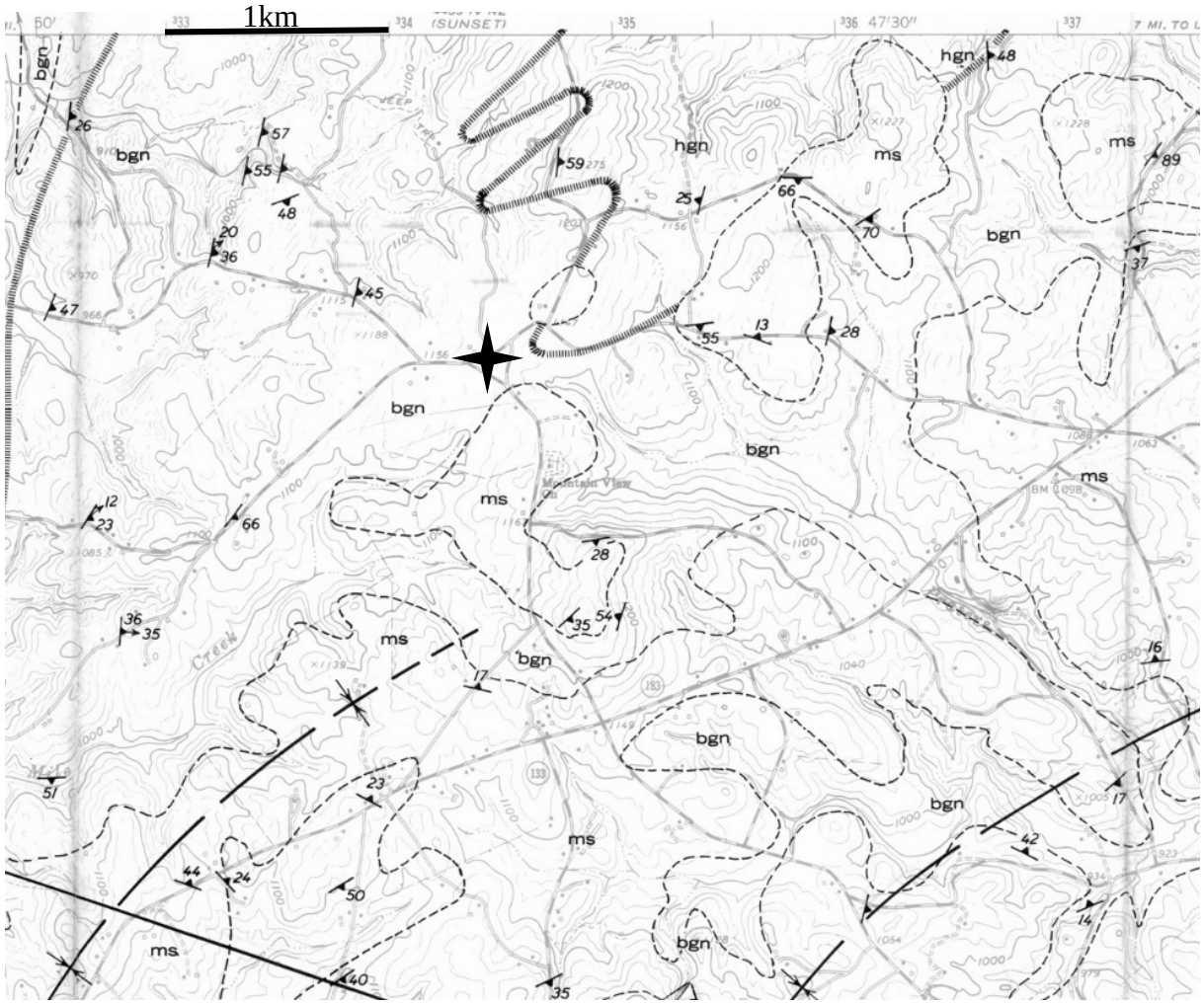

Figure 4.4: Geologic map of Griffin (1967) of the north-central portion of the Six Mile quadrangle, for comparison to Figure 4.3b, the geologic map produced in this study.

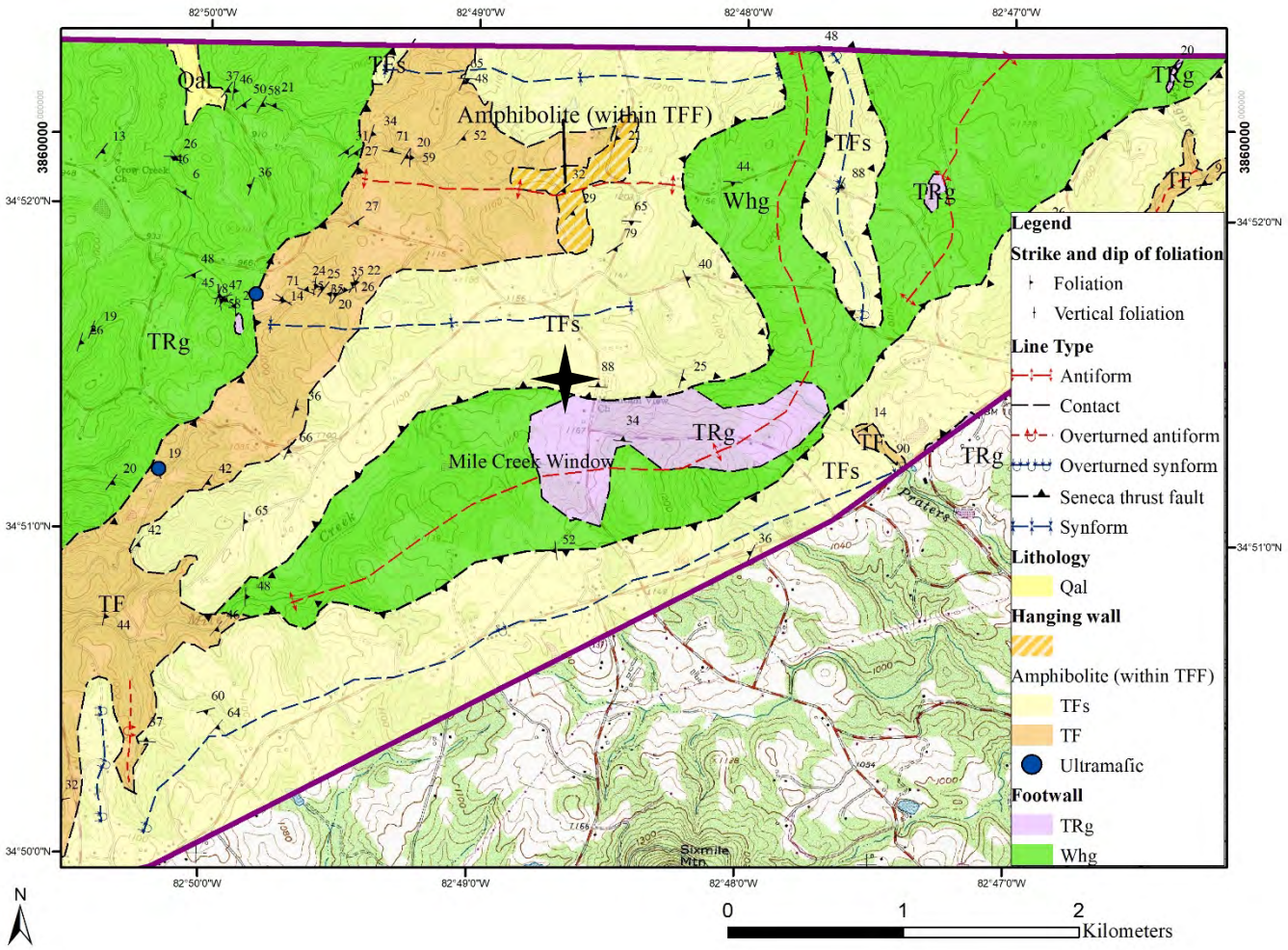

Figure 4.5: Map of north-central portion of Six Mile quadrangle (this investigation).

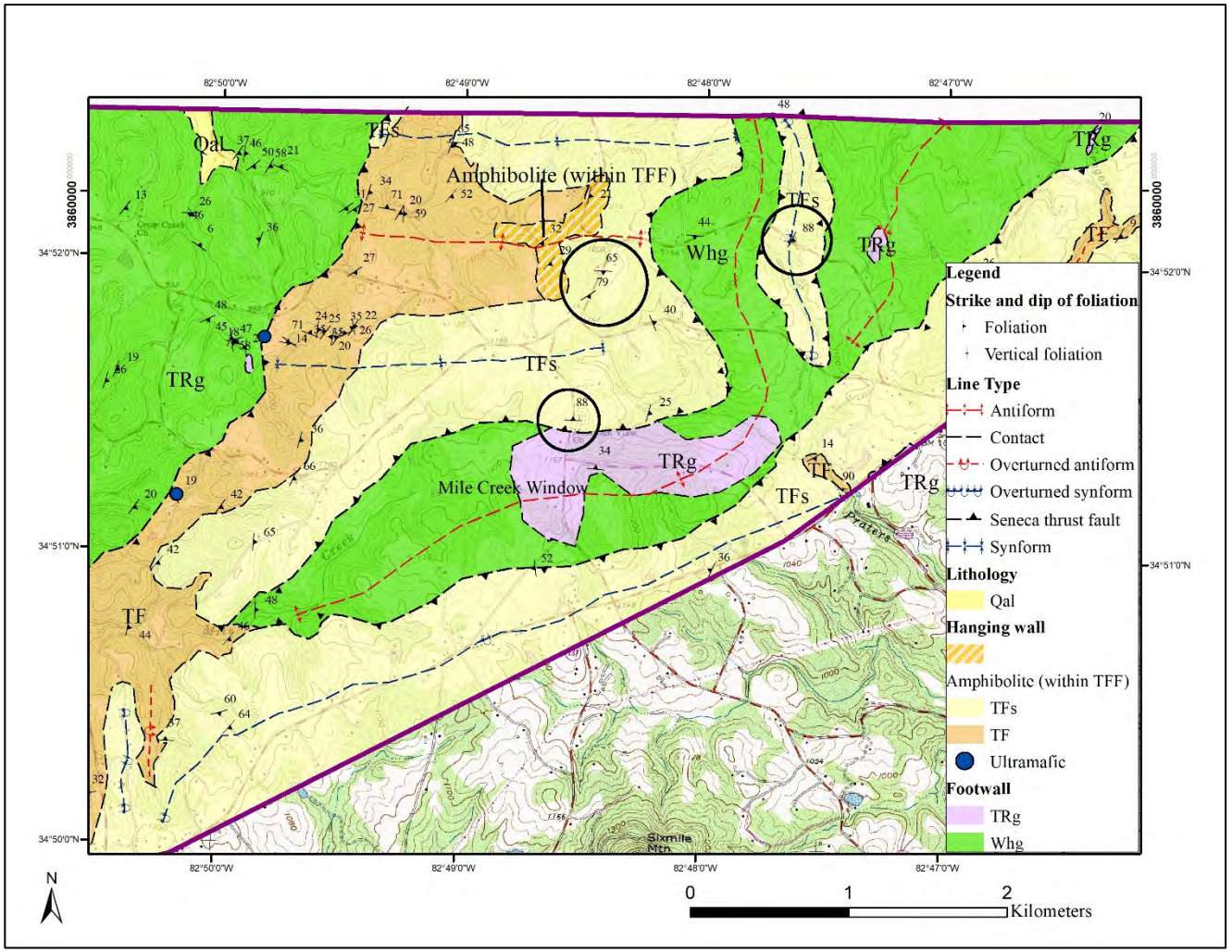

Figure 4.6: Three circled areas with near-vertical dips of foliation of Tallulah Falls schist in the north-central portion of Six Mile quadrangle. C-C' section line shown in center of the map.

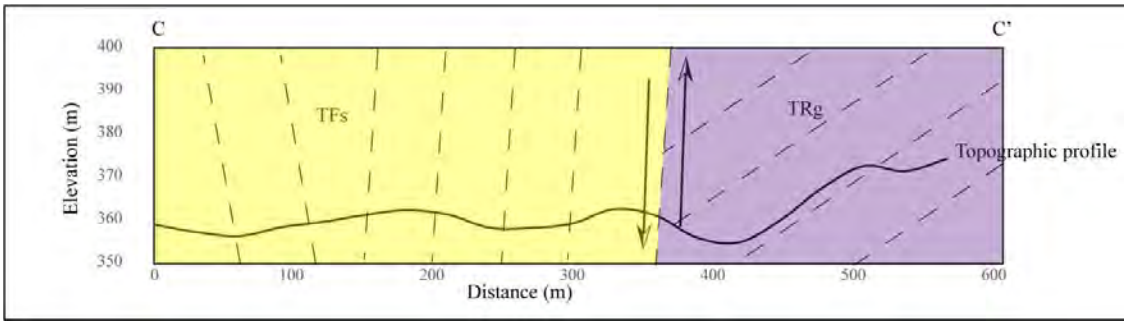

Figure 4.7: C-C' cross section of steeply dipping Tallulah Falls schist in contact with Table Rock gneiss in the central portion of the study area. Apparent normal fault in cross-section is folded Seneca thrust fault. Vertical exaggeration is 3. Section line found in Figure 4.6

Northeast Six Mile Quadrangle

The northeastern portion of Six Mile quadrangle has areas of Tallulah Falls schist with minor exposures of Tallulah Falls gneiss (Figure 4.10). The best exposures of Tallulah Falls gneiss in the northeastern corner of Six Mile quadrangle appear in shoal outcrops (Figure 4.8) in Mile Creek, as well as the upper reaches of Little Crowe Creek, Prater's Creek, and Gregory Creek. Tallulah Falls gneiss in shoal outcrops has a less porphyroclastic character than other outcrops of Tallulah Falls gneiss. Tallulah Falls gneiss is distinguishable from Table Rock gneiss because of its biotite-muscovite content (20-30%). Quaternary alluvial plains are apparent in the northeastern corner of Six Mile quadrangle, draining to Lake Keowee in the west and Twelvemile Creek to the east and concealing underlying Six Mile thrust sheet units.

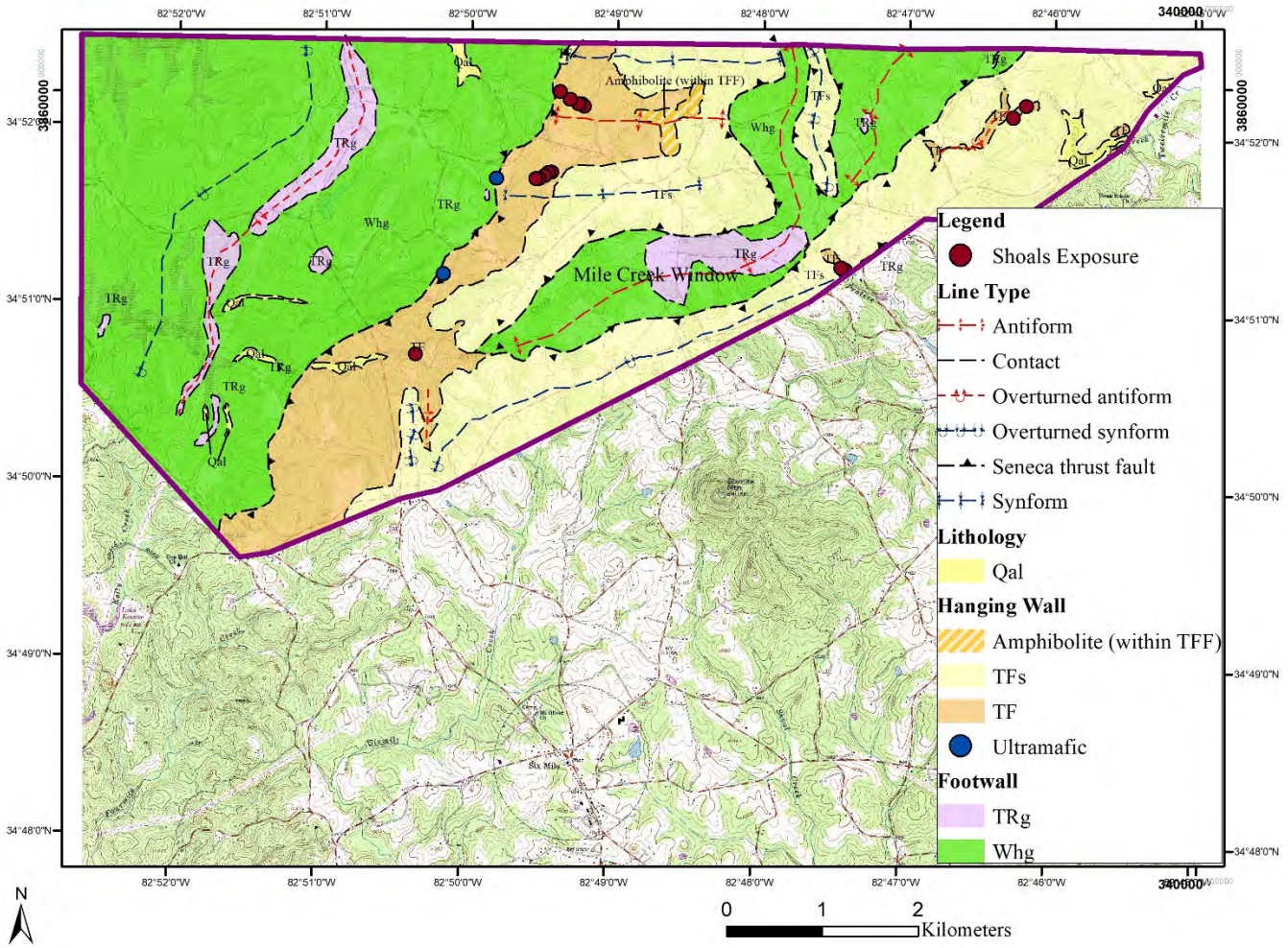

Figure 4.8: Creek shoal exposure locations of Tallulah Falls gneiss in the north-central and northeast portions of Six Mile quadrangle.

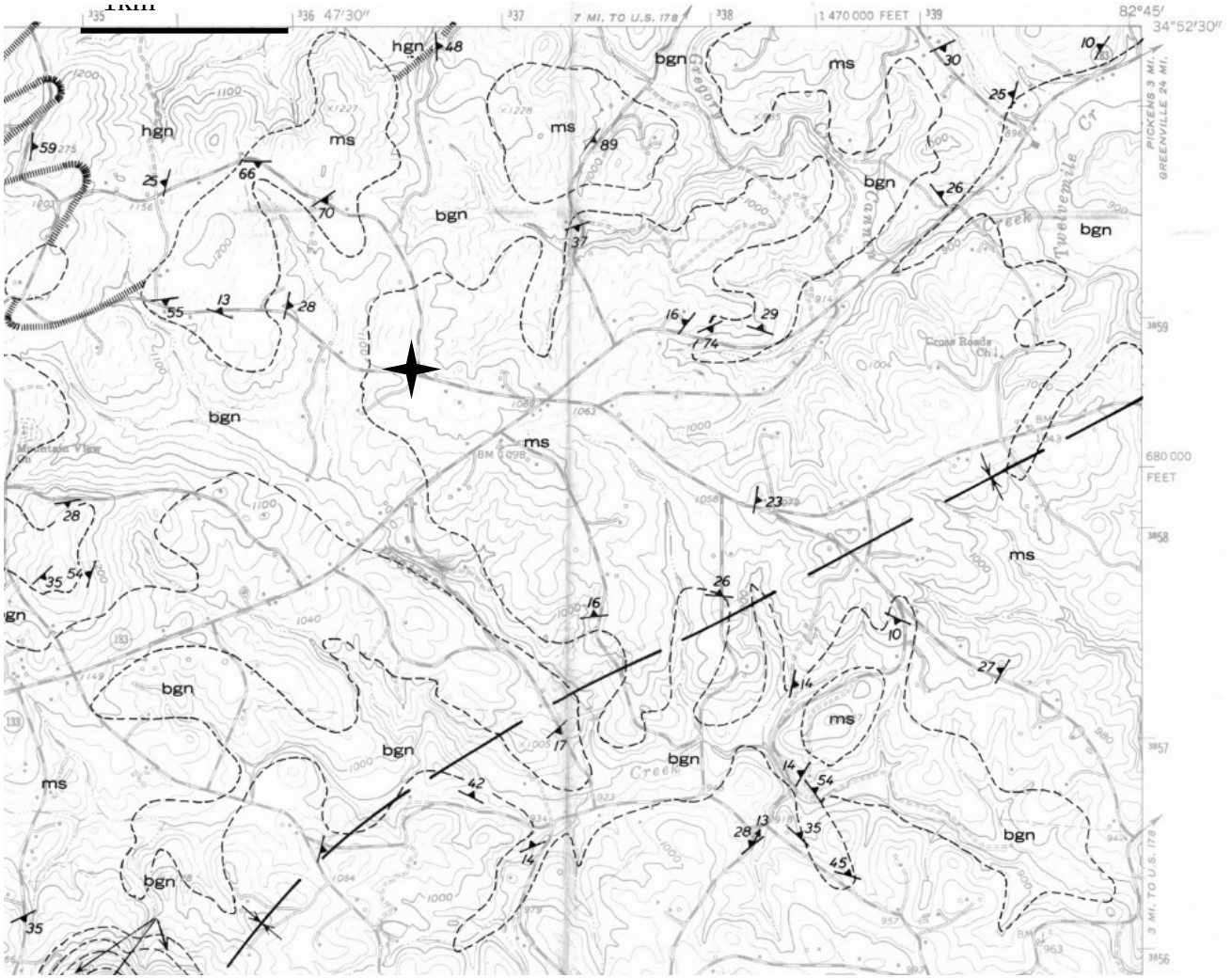

Figure 4.9: Map comparison between Griffin (1967, above) of the northeast portion of Six Mile quadrangle and Sellers (this work, below). Star used for location reference.

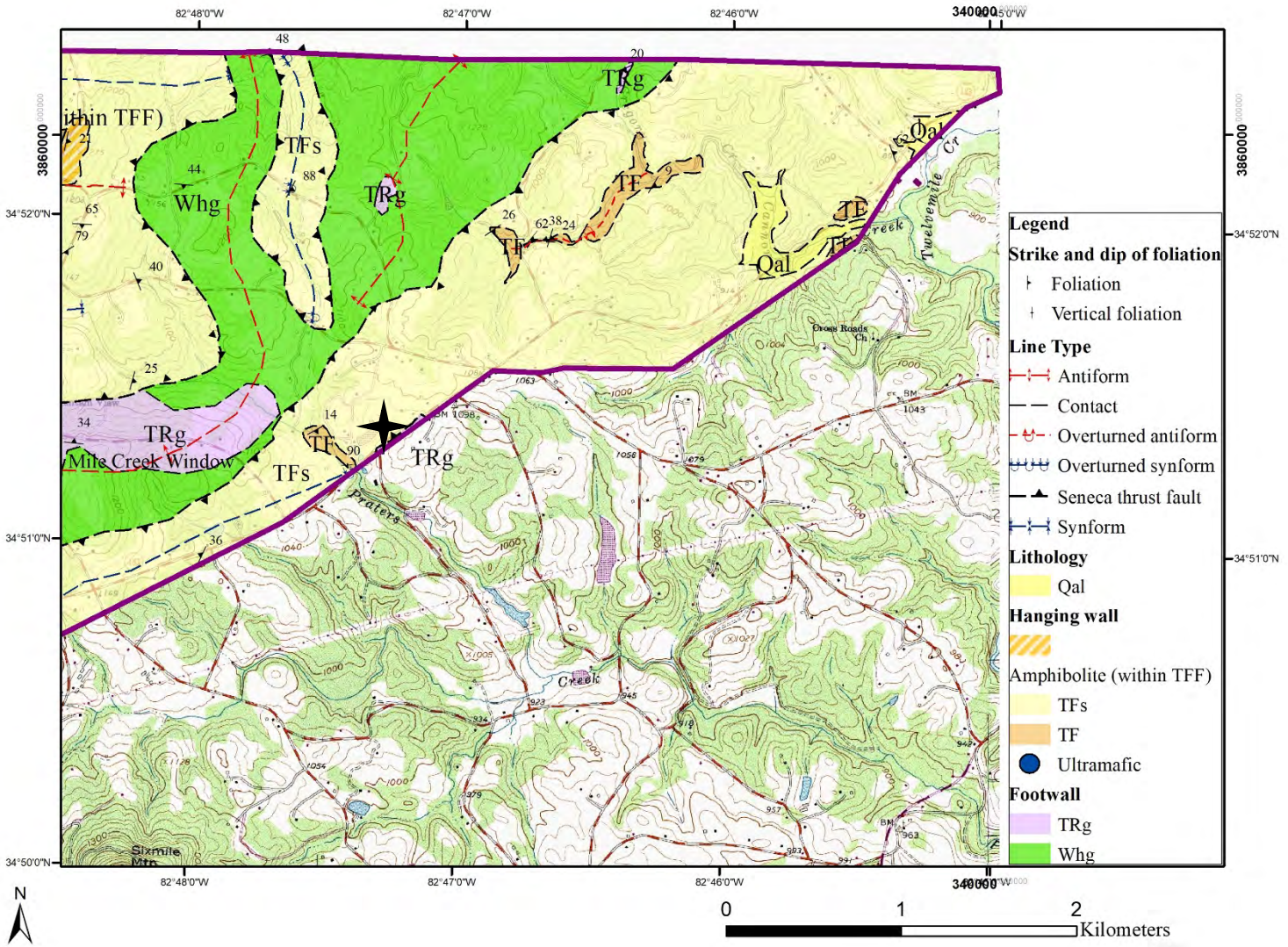

Figure 4.10: Map of northeast portion of Six Mile quadrangle by Sellers (this study).

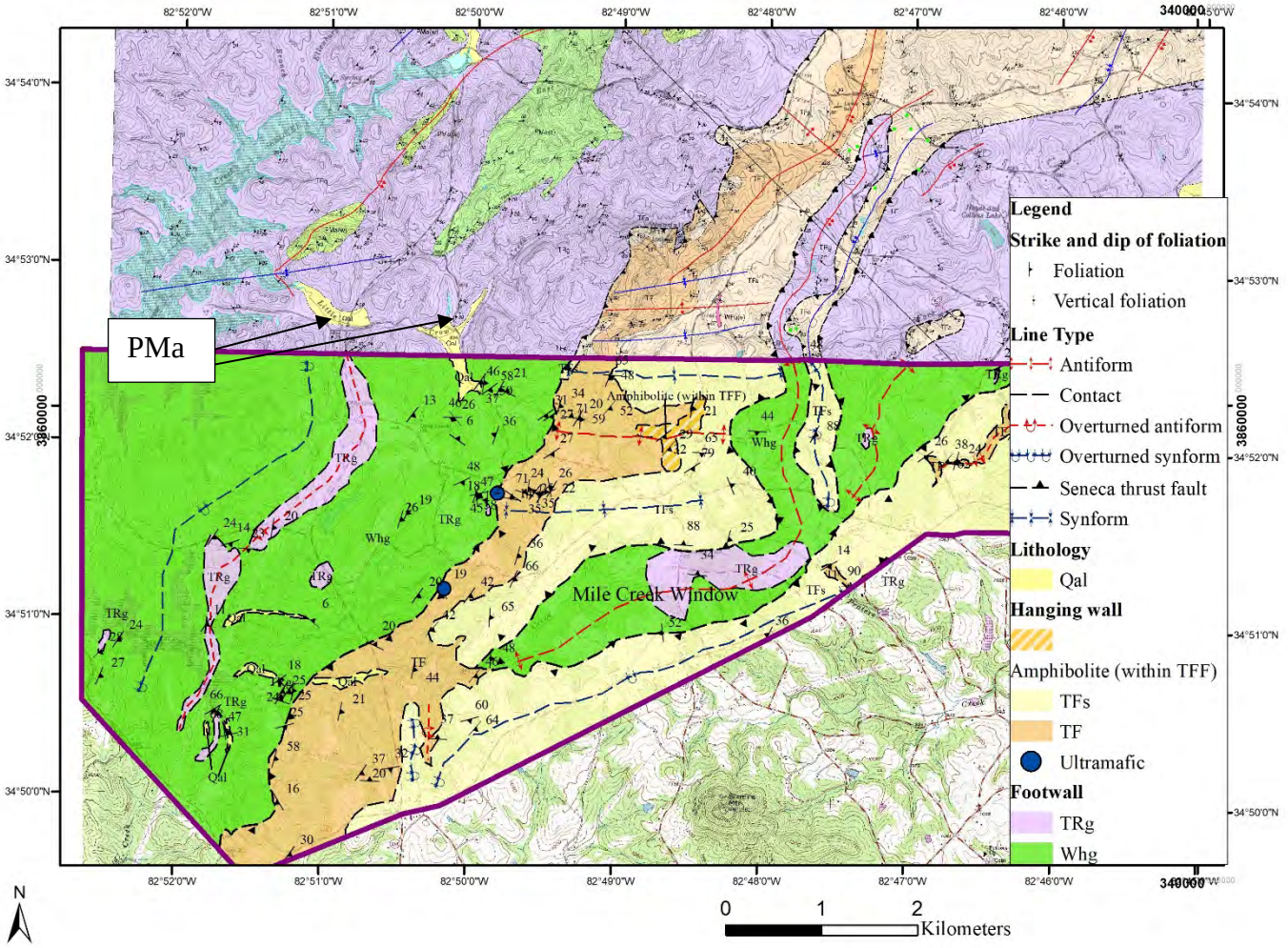

Figure 4.11: Map of Sunset quadrangle (upper; Garihan, 2005) and Six Mile quadrangle (lower; this study).

Cross-Section Discussion

The cross sections interpreted in this study show Griffin's low-dip gradient contact (Figure 4.12) between hornblende gneiss (marked hgn) and overlying biotite gneiss (marked bgn) and schist (ms) in contrast to the interpreted multi-deformed, folded surface of the Seneca fault from this study (Figure 4.13-Figure 4.14).

The structural interpretation of the rocks from the study area includes footwall Walhalla hornblende gneiss and Table Rock gneiss underlying thrusted, hanging wall Tallulah Falls gneiss and schist. The Tallulah Falls gneiss and schist is interpreted as having been folded prior to initial thrusting due to the location of outcrops seen in the central and western parts of the study area, particularly an outlying exposure of Tallulah Falls gneiss. The Tallulah Falls gneiss in the eastern part of the study area has been interpreted as a small, anticline exposure underlying Tallulah Falls schist in cross-section A-A' (Figure 4.13). Footwall and hanging wall units are interpreted as having been folded post-thrust due to the series of footwall and hanging wall units exposed from east to west, reaching the leading edge of the Seneca fault in the north-central portion of the Six Mile quadrangle.

Lithologic units in the southwest portion of the study area are interpreted as Table Rock gneiss intruded into Walhalla hornblende gneiss, underlying Six Mile thrust sheet Tallulah Falls gneiss and schist (Figure 4.14). Unlike in cross-section A-A', no extant anticlinal exposures of Tallulah Falls gneiss are seen in cross-section B-B' (Figure 4.14). Due to the discrete outcrops of Table Rock gneiss in the western part of the study area,

the Walhalla hornblende gneiss and Table Rock gneiss are interpreted as being folded post-thrust.

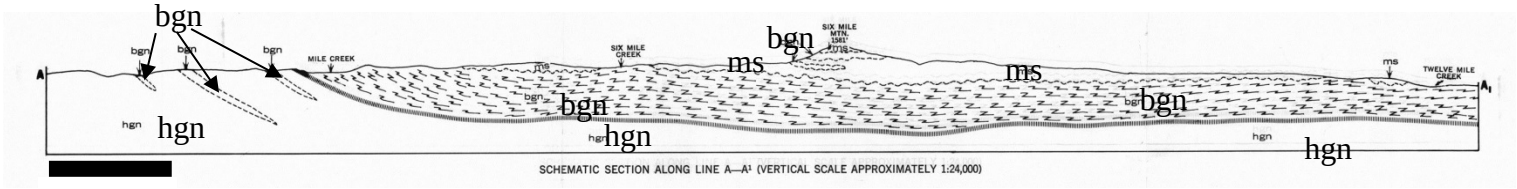

Figure 4.12: A-A' cross section created by Griffin (1967) of the Six Mile quadrangle. Section line in Figure 4.1.

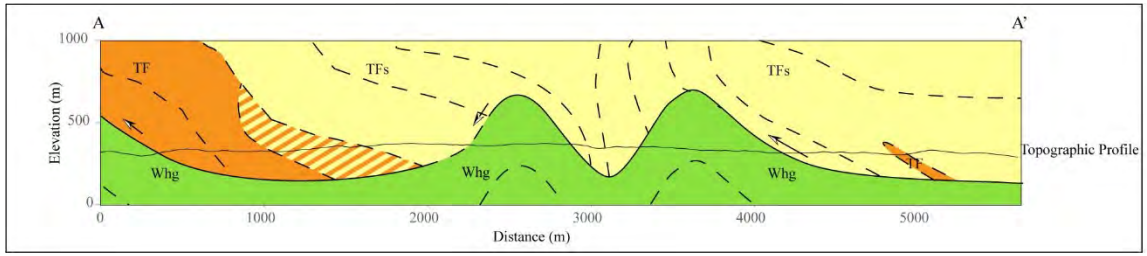

Figure 4.13: A-A' cross section created for this study of the Northern Six Mile quadrangle. Cross section created with no vertical exaggeration. Dashed lines indicate dips of local foliation. Section line shown on Figure 2.2 and on attached map.

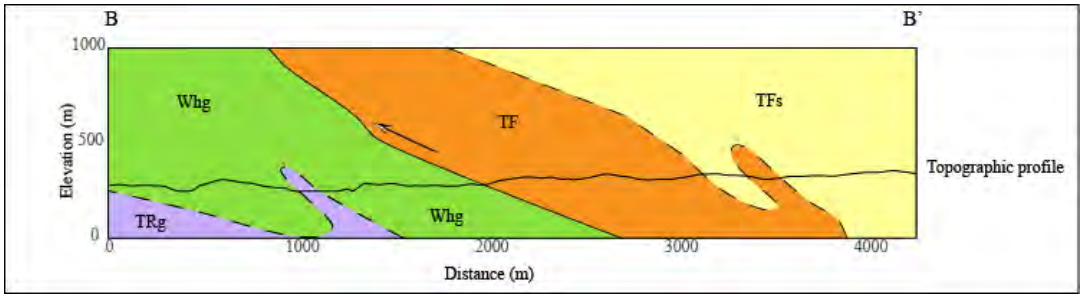

Figure 4.14: B-B' cross section created for this study of the Northern Six Mile quadrangle. Cross section created with no vertical exaggeration. Dashed lines indicate dips of local foliation. Section line shown on Figure 2.2 and on attached map.

Meso-Scale Folding

Meso-scale folding (folds seen in outcrops and hand samples) was observed in footwall and hanging wall units. Figure 4.15 shows folded saprolite in an exposure at SM563, with foliation defined by brown and leucocratic layers. The brown layers are micaceous, most likely weathered biotite in Table Rock gneiss. Two folding episodes were observed at SM563. F_1 shows an isoclinal, recumbent fold verging northwest folded by F_2, an open, inclined fold (Figure 4.15)

Meso-scale chevron folding was observed in Tallulah Falls schist (Figure 4.18) and schistose Tallulah Falls gneiss, producing a crenulation cleavage (Figure 4.19). Crenulation cleavage (F_2) was found in Tallulah Falls schist at SM132 (Figure 4.18). One

Figure 4.15: Relict folds in saprolite at SM563. Soft drink bottle behind foliage (bottom of image) is 0.2m tall. Dashed box indicates magnified area in Figure 4.16.

isoclinal fold (F_2) in Tallulah Falls gneiss at SM194 (Figure 4.19) is complexly deformed by a set of diversely oriented, inclined folds (F_3). Granitic veins (lighter) crosscutting the darker schist layers are folded. Small isoclinal fold noses visible locally. Vergence was not found at time of data collection.

Figure 4.16: Enlarged portion of Figure 4.15 to show superimposed fold geometries. Soft drink cap (yellow) is 1.5cm tall. Fold axes F_1 (blue) and F_2 (black) labeled on image. Darker brown layers are micaceous. View approximately to northwest.

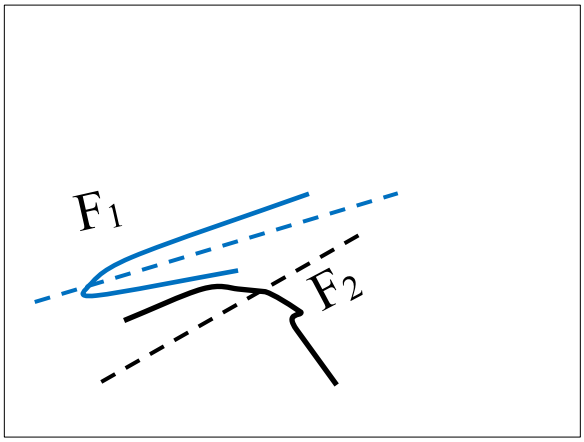

Figure 4.17: Interpretation of fold sets at SM573. Fold axes F_1 (blue) and F_2 (black) labeled on image.

Figure 4.18: Crenulated Tallulah Falls garnet muscovite sillimanite schist hand sample at SM132. View approximately to northeast.

Figure 4.19: Schistose crenulated porphyroclastic Tallulah Falls gneiss at SM194. Hammer handle for scale and space between indentions is 1cm. View approximately to southeast.

Comparison of Sunset and Six Mile Quadrangle Maps

The discussion in this section refers to detail of Figure 4.11. The southwest portion of Sunset quadrangle is dominated by Table Rock gneiss (TRg, purple) with exposures of Poor Mountain amphibolite (PMa, green). The northwest portion of Six Mile quadrangle differs from the adjoining Sunset quadrangle due to extensive amphibolite and hornblende gneiss. Table Rock gneiss in northwest Six Mile quadrangle appears as stringers located parallel to strike (~N30°E) of the Poor Mountain amphibolite found in the Sunset quadrangle, but the reason for the difference in Table Rock gneiss coverage between the quadrangles is most likely related to lithologic classification between Garihan (2005) and Sellers (this investigation) (Figure 4.11). Garihan (2005) included amphibolite, biotite amphibolite, hornblende gneiss, and biotite schist within his classification of the Table Rock gneiss (Table 3.1) whereas this investigation only classifies Table Rock gneiss as a leucocratic biotite gneiss.

The south-central portion of Sunset quadrangle has exposures of synformally folded Tallulah Falls gneiss (TF, orange) and schist (TFs, cream) with an overturned section of Tallulah Falls schist. The north-central portion of Six Mile quadrangle with contacts of Tallulah Falls schist and gneiss is similar to contacts in adjacent Sunset quadrangle. An overturned section of Tallulah Falls schist in the Sunset quadrangle continues south into the Six Mile quadrangle, as indicated by steep foliation dips in schist (88° SE on Figure 4.6) However, no evidence of overturned Walhalla hornblende gneiss was found in Six Mile quadrangle.

The northeast portion of Six Mile quadrangle has a contact between Walhalla hornblende gneiss and Tallulah Falls schist that is consistent with the location of the contact between Table Rock gneiss and Tallulah Falls schist in southeast Sunset quadrangle.

Location and Orientation of Seneca Fault

Griffin (1967) did not interpret the presence of imbricate thrust sheets in the Inner Piedmont when his Six Mile quadrangle map was published. In addition, Griffin had not differentiated biotite gneiss units in Six Mile quadrangle. Griffin's later publication (1971, Figure 4, p 1890), however, shows the Seneca fault across a broad region of the western Inner Piedmont, including Six Mile quadrangle. Garihan (2005) defined the fault in Sunset quadrangle by separating Poor Mountain amphibolite and Table Rock gneiss as footwall Walhalla thrust sheet units from Tallulah Falls Formation rocks in the hanging wall (Six Mile thrust sheet). In the current investigation, the Seneca fault was not identified in any single outcrop due to poor rock exposures in the study area. Approximate location of the Seneca fault in the study area was interpreted based on lithologic identification of either Walhalla hornblende gneiss or Table Rock gneiss (Walhalla thrust sheet, based upon lithologic identification) within close proximity (50m) of either Tallulah Falls schist or Tallulah Falls gneiss (Six Mile thrust sheet).

Two ultramafic rock bodies in the study area occur approximately 500m from the westernmost extent of the Tallulah Falls gneiss. It is unknown if the ultramafic rocks belong to the Walhalla thrust sheet or the Six Mile thrust sheet.

In the current investigation, interpretation of the position of the Seneca fault is based on steeper dips of foliation (Figure 3.13) in the Tallulah Falls gneiss and schist (dip average 41°, range 9-90°; strike average 117°, range 2-338°) than in the underlying Walhalla hornblende gneiss and Table Rock gneiss (dip average 31°, range 2-75°; strike average 98°, range 2-352°). Waterfalls were observed in multiple locations proximal to the transition from Table Rock gneiss or Walhalla hornblende gneiss to the Tallulah Falls gneiss. The waterfalls are interpreted as having greater weathering resistance of Tallulah Falls gneiss (30-40% quartz based on hand-sample visual examination) compared to other outcrops of Tallulah Falls gneiss (5-20%). A possibility for the increased quartz

Figure 4.20: Waterfall near Market Rd. in the northern Six Mile quadrangle at SM79. There is approximately 7m of drop. Height of person to the left is 1.7m. View approximately to northeast.

content at these locations could be increased sand in the parent rock of the Tallulah Falls gneiss (paragneiss). While the waterfalls were not used to define the contact between Six Mile Thrust Sheet rocks and rocks of the Walhalla thrust sheet, their proximity to the transition may be a helpful indicator for future mapping of the Seneca fault.

CHAPTER 5. SUMMARY AND CONCLUSIONS

Although outcrops in Six Mile quadrangle are weathered and locally saprolitic, six distinct lithologic units can be identified in the study area: Walhalla hornblende gneiss, Table Rock gneiss, Tallulah Falls gneiss, Tallulah Falls schist, Quaternary alluvium, and ultramafic rocks. Pegmatite was also concordant and discordant to footwall and hanging wall rocks. Walhalla hornblende gneiss and Table Rock gneiss of the Walhalla thrust sheet dominate the western portion of the study area, whereas Tallulah Falls schist and Tallulah Falls gneiss are widespread in the central and eastern portions of the study area. Table Rock gneiss and Walhalla hornblende gneiss appear in the central portion of the study area due to the folded Seneca fault contact forming a complex antiformal structural window of the overlying Six Mile thrust sheet on the Walhalla thrust sheet.

Biotite gneisses of the study area, while not previously differentiated by Griffin (1967), were divided into Table Rock gneiss of the Walhalla thrust sheet and Tallulah Falls gneiss of the overlying Six Mile thrust sheet. The major feature used to differentiate the two units is mica content. Table Rock gneiss has a maximum 15% biotite content with negligible muscovite, while Tallulah Falls gneiss frequently contains 50-60% biotite and muscovite. The gneisses are also texturally different, as Table Rock gneiss is fine- to medium-crystalline, and Tallulah Falls gneiss is medium- to coarse-crystalline with common 1-2cm porphyroclasts of quartz-feldspar aggregates in micaceous matrix.

A principal difference in footwall rocks between Sunset and Six Mile quadrangles is the dominance of Table Rock gneiss in the former and hornblende gneiss and

amphibolite in the latter. A possible cause for this difference is how different mappers lumped lithologies and how units were named. It is possible that Garihan included hornblende gneiss within the Table Rock gneiss unit and amphibolite within the Poor Mountain amphibolite unit in Sunset quadrangle, and the current investigation included hornblende gneiss and amphibolite within the Walhalla hornblende gneiss unit. This could explain the difference between the expanse of Table Rock gneiss with minor occurrences of Poor Mountain amphibolite in Sunset quadrangle, and greater Walhalla hornblende gneiss with minor occurrences of Table Rock gneiss in Six Mile quadrangle.

Alternatively, geologic mapping in the two areas indicates lithologic change of leucocratic biotite gneiss to hornblende gneiss and amphibolite over a limited distance, perhaps 1-2km, near the boundary of the quadrangles. The change may be due to the interdigitated intrusive relations of Table Rock gneiss emplaced into mafic footwall rocks near the southern margin of the Table Rock gneiss.

The Seneca fault, present in quadrangles to the north, was not observable at outcrop-scale. However, position of the fault was interpreted within approximately ±50m based on observed lithologic changes from footwall to hanging wall units. Seneca fault orientation is unknown at this time due to lack of exposed contact. Seneca fault is not commonly seen elsewhere in the western Inner Piedmont, although it is well exposed at Camp Greenville to the north of the study area (Garihan, 2001). Future investigation in Six Mile quadrangle can include delineating the known lithologic units in the remainder of Six Mile quadrangle, based on the lithologic and structural information resulting from this study.

A result of this investigation was the recognition of complex meso-scale superimposed folding in units mapped in the study area. Two generations of folding were observed in weathered Table Rock gneiss in saprolite. Three generations of Tallulah Falls gneiss and schist were observed. Table Rock gneiss exhibited a recumbent isoclinal fold later folded by an open fold. Tallulah Falls gneiss and schist both exhibited crenulated foliation (F_2) overprinting F_1 folds cut by upright to inclined folds (F_3).

A major result of this investigation is that two structural windows through the Six Mile thrust sheet exposing the Walhalla thrust sheet below, seen in southern Sunset quadrangle, continue for 1 to 2km to the south into the study area. The structural windows are separated by an overturned synform of Tallulah Falls schist, which terminates in the study area. The structural windows of footwall rocks strike N-S at the boundary with Sunset quadrangle but merge into a single window with a more E-W orientation near the center of the study area. The single structural window is named the Mile Creek window, for Mile Creek that runs through the window. The E-W orientation of the window appears to coincide with a set of E-W folds in the hanging wall. However, the E-W folds in the hanging wall are interpreted to have developed prior to Six Mile thrust sheet emplacement. A possible cause for the change in orientation of the Mile Creek window is later, post-Seneca E-W folding.

The following events are proposed to have constructed the structural geology of the study area:

1. Early-Middle Cambrian: Deposition of Tallulah Falls Formation gneiss (TF) and schist (TFs).

2. Late Ordovician: Table Rock gneiss (TRg) intruded into the Walhalla hornblende gneiss (Whg), which is of unknown age and origin.
3. Late Devonian-Mississippian: Folding of Tallulah Falls gneiss and schist.
4. Late Devonian-Mississippian: Seneca fault thrust.
5. Mississippian-Pennsylvanian: Later folding of Walhalla thrust sheet, Six Mile thrust sheet rocks, and the Seneca fault. Creation of Mile Creek Window.

APPENDICES

Appendix A: Mapping Data

Mapping Waypoint

Waypoint	Description	Latitude	Longitude	Note	Date
Sm174	amphibolite	34.85205	-82.8224		4/25/15
Sm175	limonite	34.85235	-82.8219		4/25/15
Sm176	amphibolite	34.8509	-82.8232		4/25/15
Sm177	amphibolite	34.84998	-82.8244		4/25/15
Sm178	amphibolite	34.84946	-82.8253		4/25/15
Sm155	biotite gneiss (t)	34.84408	-82.8379	porphyroclastic	4/17/15
Sm156	biotite gneiss (t)	34.84423	-82.8369	porphyroclastic	4/17/15
Sm157	biotite gneiss (t)	34.84951	-82.8404	porphyroclastic	4/17/15
Sm158	amphibolite	34.84936	-82.8415		4/17/15
Sm152	amphibolite	34.83448	-82.8356	nearly in place	4/7/15
Sm153	biotite gneiss(t)	34.8402	-82.8416	porphyroclastic, tallulah	4/7/15
Sm154	biotite gneiss(t)	34.83636	-82.8406	porphyroclastic, tallulah	4/7/15
Sm141	biotite gneiss	34.86823	-82.8531	boulder	4/1/15
Sm142	amphibolite	34.86829	-82.8538	nearly in place	4/1/15
Sm143	amphibolite	34.8686	-82.8542	epidote	4/1/15
Sm144	amphibolite	34.86805	-82.8573	float	4/1/15
Sm145	hornblende gneiss	34.86314	-82.8562	float	4/1/15
Sm146	hornblende gneiss	34.86726	-82.8608	float	4/1/15
Sm147	hornblende gneiss	34.86775	-82.8633	float	4/1/15
Sm148	amphibolite	34.86594	-82.8656	float	4/1/15
Sm149	hornblende gneiss	34.8653	-82.8695	float	4/1/15
Sm150	amphibolite	34.86326	-82.8754	float	4/1/15
Sm107	mica schist	34.8494	-82.7992	pods of leucocratic biotite gneiss visible	2/11/15
Sm108	mica schist	34.85111	-82.7941	parking available	2/11/15
Sm109	mica schist	34.8535	-82.7901	garnet abundant	2/11/15
Sm110	biotite gneiss (l)	34.8549	-82.7881		2/11/15
Sm111	amphibolite	34.86831	-82.7796	float	2/11/15
Sm112	garnet sillimanite muscovite schist	34.87046	-82.7779		2/11/15
Sm113	mica schist	34.87134	-82.7771	manganiferous quartzite/gondite	2/11/15
Sm114	garnet sillimanite muscovite schist	34.87106	-82.7761	crenulation cleavage	2/11/15
Sm115	hornblende gneiss	34.87452	-82.7744	leucocratic table rock gneiss locally	2/11/15

Sm97	garnet sillimanite muscovite schist	34.8737	-82.7601		1/28/15
Sm98	biotite gneiss (t)	34.8678	-82.759		1/28/15
Sm99	biotite gneiss(t)	34.8662	-82.7589		1/28/15
Sm100	mica schist	34.86971	-82.7656		1/28/15
Sm101	mica schist	34.86375	-82.7657		1/28/15
Sm102	muscovite schist	34.86217	-82.7744		1/28/15
Sm105	amphibolite	34.85598	-82.8264		2/10/15
Sm106	biotite gneiss(t)	34.85635	-82.8274		2/10/15
Sm103	sillimanite muscovite schist	34.86574	-82.7793		1/28/15
Sm104	biotite gneiss (l)	34.85663	-82.7857		1/28/15
Sm80	garnet sillimanite mica schist	34.86823	-82.7939		1/7/15
Sm81	amphibolite	34.86866	-82.8108		1/7/15
Sm82	amphibolite	34.86794	-82.8115		1/7/15
Sm83	amphibolite	34.86863	-82.8127		1/7/15
Sm84	amphibolite	34.86848	-82.8139		1/7/15
Sm85	biotite gneiss(t)	34.86833	-82.8168	tallulah	1/7/15
Sm93	pegmatite	34.85273	-82.8424	leucocratic	1/22/15
Sm94	pegmatite	34.85229	-82.8423	leucocratic	1/22/15
Sm95	amphibolite	34.85164	-82.8429		1/22/15
Sm96	pegmatite	34.85174	-82.8428	leucocratic	1/22/15
Sm87	hornblende gneiss	34.85272	-82.8396	float	1/20/15
sm88	hornblende gneiss	34.85232	-82.8387	in situ	1/20/15
Sm89	amphibolite	34.85225	-82.8379	float	1/20/15
Sm90	pegmatite	34.85172	-82.839	leucocratic	1/20/15
Sm91	hornblende gneiss	34.85201	-82.8402	float	1/20/15
Sm92	pegmatite	34.85237	-82.8403	leucocratic	1/20/15
Sm61	calc-silicate	34.87555	-82.8479		11/4/14
Sm60	biotite gneiss	34.8695	-82.8246		9/17/14
Sm59	biotite gneiss(t)	34.8659	-82.8239	porphyroclastic, tallulah	9/3/14
Sm4	sillimanite mica schist	34.85738	-82.8089		7/16/14
Sm1	mica schist	34.86338	-82.829		7/16/14
Sm3	mica schist	34.86552	-82.8231		7/16/14
Sm2	biotite gneiss(t)	34.86588	-82.8252	porphyroclastic, tallulah	7/16/14
Sm5	mica schist	34.86707	-82.8481		7/16/14
Sm11	schist (poorly exposed)?	34.85928	-82.8428		7/28/14
Sm15	garnet sillimanite mica schist	34.86818	-82.7938		7/29/14

Sm18	sillimanite mica schist	34.86139	-82.7774		7/29/14
Sm19	mica schist	34.85361	-82.7958		7/29/14
Sm27	mica schist	34.85956	-82.776		8/5/14
Sm51	biotite gneiss(t)	34.8697	-82.818	porphyroclastic, tallulah	8/27/14
Sm51	biotite gneiss(t)	34.87032	-82.8173	porphyroclastic, tallulah	8/27/14
Sm52	biotite gneiss(t)	34.86913	-82.8202	porphyroclastic, tallulah	9/1/14
Sm53	biotite gneiss(t)	34.86934	-82.8205	porphyroclastic, tallulah	9/1/14
Sm54	biotite gneiss(t)	34.86934	-82.8208	porphyroclastic, tallulah	9/1/14
Sm4	sillimanite mica schist	34.85738	-82.8089		7/16/14
Sm3	mica schist	34.86552	-82.8231		7/16/14
Sm5	mica schist	34.86707	-82.8481		7/16/14
Sm7	biotite gneiss (l)	34.86337	-82.8481	leucocratic	7/28/14
Sm8	biotite gneiss (l)	34.85753	-82.8622	leucocratic	7/28/14
Sm10	biotite gneiss	34.85859	-82.8554		7/28/14
Sm13	limonite	34.85392	-82.8457	weathered amphibolite?	7/28/14
Sm14	hornblende gneiss	34.86689	-82.79		7/29/14
Sm15	garnet sillimanite mica schist	34.86818	-82.7938		7/29/14
Sm16	hornblende gneiss	34.86827	-82.8005		7/29/14
Sm17	hornblende gneiss	34.87053	-82.8078		7/29/14
Sm20	biotite gneiss (l)	34.85516	-82.8072	leucocratic	7/29/14
Sm20	biotite gneiss (l)	34.8552	-82.8076	leucocratic	7/29/14
Sm21	biotite gneiss (l)	34.85143	-82.8088	leucocratic	7/29/14
Sm22	biotite gneiss(t)	34.86801	-82.8187	porphyroclastic, tallulah	7/29/14
Sm23	biotite gneiss(t)	34.8712	-82.8184	porphyroclastic, tallulah	7/29/14
Sm51	biotite gneiss(t)	34.87032	-82.8173	porphyroclastic, tallulah	8/27/14
Sm52	biotite gneiss(t)	34.86913	-82.8202	porphyroclastic, tallulah	9/1/14
Sm54	biotite gneiss(t)	34.86934	-82.8208	porphyroclastic, tallulah	9/1/14
Sm55	biotite gneiss(t)	34.86934	-82.8208	tallulah	9/1/14
Sm56	biotite gneiss(t)	34.86975	-82.8218	migmatitic, tallulah	9/1/14
Sm57	biotite gneiss(t)	34.87049	-82.823	tallulah	9/1/14
Sm58	hornblende biotite gneiss	34.86945	-82.824		9/1/14
Sm80	sillimanite garnet mica schist	34.86823	-82.794		1/7/15
Sm66	hornblende gneiss	34.85952	-82.8409		12/16/14
Sm67	hornblende gneiss	34.85972	-82.8408		12/16/14
Sm68	hornblende gneiss	34.86019	-82.8402		12/16/14

Ft01	biotite gneiss (l)	34.86693	-82.8481	leucocratic	12/31/14
Sm69	biotite gneiss	34.86661	-82.845	amphibolite also found	12/31/14
Ft02	biotite gneiss	34.86654	-82.8449	amphibolite also found	12/31/14
Sm70	hornblende gneiss	34.85921	-82.8427		12/31/14
Ft03	hornblende gneiss	34.85923	-82.8428		12/31/14
Sm71	amphibolite	34.85938	-82.8409		12/31/14
Sm72	hornblende gneiss	34.85974	-82.8409		12/31/14
Sm73	amphibolite	34.85923	-82.8427		12/31/14
Sm74	amphibolite	34.86222	-82.8354		12/31/14
Sm75	amphibolite	34.85676	-82.8414		12/31/14
Sm76	amphibolite	34.85727	-82.8431		12/31/14
Sm76	biotite gneiss (l)	34.85417	-82.8499	leucocratic	12/31/14
Sm77	hornblende gneiss	34.85078	-82.845	amphibolite also found	12/31/14
Sm78	anthophyllite	34.8479	-82.8436		12/31/14
Sm78	pegmatite	34.84792	-82.8436	green quartz-like rock found	12/31/14
Sm79	biotite gneiss(t)	34.84553	-82.839	porphyroclastic, tallulah	12/31/14
Sm65	amphibolite	34.8638	-82.8446		11/25/14
Sm62	amphibolite	34.86933	-82.8398		11/12/14
Sm63	amphibolite	34.8699	-82.8408		11/12/14
Sm64	amphibolite	34.86976	-82.8408		11/12/14
Sm117	muscovite schist	34.86039	-82.7894		2/28/15
Sm118	hornblende gneiss	34.86305	-82.7951		2/28/15
Sm119	garnet mica schist	34.86121	-82.7996		2/28/15

Sm120	garnet mica schist	34.86141	-82.8007	crenulated	2/28/15
Sm121	amphibolite	34.86345	-82.803		2/28/15
Sm122	amphibolite	34.86286	-82.8077	mica schist and black rock found	2/28/15
Sm123	amphibolite	34.86243	-82.8065		2/28/15
Sm124	garnet mica schist	34.85835	-82.8039		2/28/15
Sm125	mica schist	34.85822	-82.8034	in saprolite in creek	2/28/15
Sm126	mica schist	34.85831	-82.803	saprolite	2/28/15
Sm127	hornblende gneiss	34.86893	-82.8027		2/28/15
Sm128	garnet muscovite schist	34.87112	-82.8028		2/28/15
Sm129	mica schist	34.8727	-82.8	biotite and muscovite	2/28/15
Sm130	biotite muscovite gneiss (t)	34.87307	-82.7997		2/28/15
Sm131	garnet mica schist	34.87327	-82.7991		2/28/15
Sm132	garnet mica schist	34.87126	-82.8036		2/28/15
Sm133	hornblende gneiss	34.86827	-82.8006	porphyroclastic	2/28/15
Sm134	hornblende gneiss	34.85707	-82.8189		2/28/15
Sm135	amphibolite	34.86002	-82.8234		2/28/15
Sm136	amphibolite	34.85394	-82.8342		2/28/15
Sm137	biotite gneiss(t)	34.84733	-82.8362	porphyroclastic,tallulah	2/28/15
Sm159	amphibolite	34.86968	-82.8341		4/22/15
Sm160	amphibolite	34.87009	-82.8344	hornblende gneiss as well	4/22/15
Sm161	hornblende gneiss	34.86991	-82.8348		4/22/15
Sm162	biotite hornblende gneiss	34.86993	-82.8349		4/22/15
Sm163	amphibolite	34.86952	-82.8349		4/22/15
Sm164	amphibolite	34.86904	-82.8354	saprolite	4/22/15
Sm165	amphibolite	34.869	-82.8353	saprolite	4/22/15
Sm167	amphibolite	34.86739	-82.8347	saprolite with hornblende gneiss, pegmatite	4/22/15
Sm168	amphibolite	34.86734	-82.8341	float	4/22/15
Sm169	amphibolite	34.86774	-82.8307	float in creek	4/24/15
Sm170	pegmatite	34.86784	-82.8307		4/24/15
Sm171	biotite gneiss	34.86793	-82.8306	boulder of biotite granitoid gneiss	4/24/15
Sm172	amphibolite	34.86944	-82.8309	in place	4/24/15
Sm173	biotite gneiss (l)	34.86291	-82.8485	Table rock gneiss with interfoliated amphibolite	4/24/15
Sm179	biotite gneiss (l)	34.87255	-82.832	also hornblende gneiss	4/27/15

Sm180	hornblende gneiss	34.87251	-82.8319		4/27/15
Sm181	hornblende gneiss	34.87259	-82.8315		4/27/15
Sm182	hornblende gneiss	34.8718	-82.831		4/27/15
Sm183	hornblende gneiss	34.87176	-82.8302		4/27/15
Sm184	biotite gneiss (l)	34.87186	-82.8298	also hornblende gneiss	4/27/15
Sm185	amphibolite	34.87192	-82.8292		4/27/15
	garnetiferous quartzite	0	0		
	biotite gneiss (t)	0	0		
Sm186	amphibolite	34.86384	-82.8217	float	4/28/15
Sm188	biotite gneiss(t)	34.86368	-82.8222	porphyroclastic	4/28/15
Sm189	biotite gneiss(t)	34.86301	-82.8234	porphyroclastic	4/28/15
Sm189	biotite gneiss(t)	34.86289	-82.8238	porphyroclastic	4/28/15
Sm190	biotite gneiss(t)	34.86283	-82.8242	porphyroclastic	4/28/15
Sm191	biotite gneiss(t)	34.86253	-82.8246	porphyroclastic	4/28/15
Sm192	biotite gneiss(t)	34.86226	-82.8253	porphyroclastic	4/28/15
Sm193	biotite gneiss(t)	34.86229	-82.8253	porphyroclastic	4/28/15
Sm194	biotite gneiss(t)	34.86225	-82.8256	porphyroclastic	4/28/15
Sm195	biotite gneiss(t)	34.86259	-82.8261	porphyroclastic	4/28/15
Sm196	biotite gneiss(t)	34.86267	-82.8263	porphyroclastic	4/28/15
Sm197	ultramafic	34.86221	-82.8301		4/29/15
Sm198	amphibolite	34.86213	-82.8303	float	4/29/15
Sm199	biotite hornblende gneiss	34.86154	-82.8315		4/29/15
Sm200	biotite gneiss (l)	34.86095	-82.8311		4/29/15
Sm201	biotite gneiss (l)	34.86022	-82.8311		4/29/15
Sm202	amphibolite	34.86151	-82.8288		4/29/15
Sm203	biotite gneiss(t)	34.86184	-82.8285		4/29/15
Sm204	biotite gneiss(t)	34.862	-82.8285		4/29/15
Sm205	biotite gneiss(t)	34.86243	-82.8277		4/29/15
Sm206	biotite gneiss(t)	34.86238	-82.8277	float	4/29/15
Sm207	biotite gneiss(t)	34.86296	-82.8267		4/29/15
Sm208	biotite gneiss(t)	34.86252	-82.827		4/29/15
Sm210	biotite gneiss(t)	34.86188	-82.8282		4/29/15
Sm211	amphibolite	34.86363	-82.8351		5/5/15
Sm212	amphibolite	34.86235	-82.8352		5/5/15
Sm213	amphibolite	34.86305	-82.8348		5/5/15
Sm214	hornblende gneiss	34.86303	-82.8339	hornblende gneiss in saprolite	5/5/15
Sm215	hornblende gneiss	34.86203	-82.8323		5/5/15
Sm216	hornblende gneiss	34.86188	-82.8321	hornblende gneiss in saprolite	5/5/15

Sm217	hornblende gneiss	34.86183	-82.8322	fold	5/5/15
Sm218	hornblende gneiss	34.8618	-82.8319	hornblende gneiss in saprolite	5/5/15
Sm219	biotite gneiss(t)	34.8616	-82.8318	lots of muscovite	5/5/15
Sm220	biotite gneiss(t)	34.85415	-82.7901	lots of muscovite	5/5/15
Sm221	garnet mica schist	34.8541	-82.7903		5/5/15
Sm222	biotite gneiss(t)	34.85434	-82.7906	float	5/5/15
Sm223	garnet mica schist	34.85432	-82.7907	float	5/5/15
Sm224	biotite gneiss(t)	34.8362	-82.8406	porphyroclastic	5/5/15
Sm225	amphibolite	34.83607	-82.8405		5/5/15
Sm226	hornblende gneiss	34.83589	-82.8404		5/5/15
Sm227	hornblende gneiss	34.83606	-82.8404		5/5/15
Sm228	garnetiferous quartzite	34.83616	-82.8405		5/5/15
Sm231	biotite muscovite schist	34.8758	-82.7621		5/8/15
Sm233	muscovite schist	34.86186	-82.7918	solid chunk of muscovite	5/8/15
Sm234	biotite gneiss (l)	34.87494	-82.7729		5/12/15
Sm235	biotite gneiss (l)	34.87462	-82.7732		5/12/15
Sm236	biotite gneiss (l)	34.87347	-82.7736		5/12/15
Sm237	sillimanite garnet mica schist	34.86039	-82.7805		5/12/15
Sm238	amphibolite	34.87136	-82.8073		5/12/15
Sm240	mica schist	34.87512	-82.7945		5/16/15
Sm241	biotite gneiss (l)	34.87505	-82.7949	float	5/16/15
Sm242	mica schist	34.87502	-82.7952		5/16/15
Sm243	mica schist	34.87501	-82.7951		5/16/15
Sm244	muscovite biotite schist	34.87506	-82.7953		5/16/15
Sm245	amphibolite	34.87502	-82.7955	float	5/16/15
Sm246	biotite hornblende gneiss	34.87455	-82.7959	float	5/16/15
Sm247	amphibolite	34.87407	-82.7963	and biotite gneiss	5/16/15
Sm248	hornblende gneiss	34.87406	-82.7965		5/16/15
Sm249	hornblende gneiss	34.87377	-82.7971	lots of pegmatite	5/16/15
Sm250	pegmatite	34.87372	-82.7972	biotite schist	5/16/15
Sm251	mica schist	34.87352	-82.798		5/16/15
Sm239	garnetiferous quartzite	34.86476	-82.8077		5/14/15
Sm229	biotite gneiss(t)	34.85574	-82.7918	lots of muscovite, non-porphyroclastic	5/6/15
Sm230	biotite gneiss(t)	34.8558	-82.792		5/6/15
Sm231	biotite gneiss(t)	34.85583	-82.7928	lots of muscovite, non-porphyroclastic	5/6/15
Sm252	amphibolite	34.84768	-82.8334	float	5/18/15

Sm253	amphibolite	34.84817	-82.8337		5/18/15
Sm254	biotite gneiss(t)	34.84833	-82.8338	porphyroclastic	5/18/15
Sm255	biotite gneiss(t)	34.84835	-82.8341	porphyroclastic	5/18/15
Sm256	amphibolite	34.84692	-82.833	mica schist fragments	5/18/15
Sm257	amphibolite	34.84676	-82.8329	mica schist fragments	5/18/15
Sm258	amphibolite	34.84543	-82.8317		5/18/15
Sm259	biotite gneiss(t)	34.84516	-82.8317	porphyroclastic	5/18/15
Sm260	biotite gneiss(t)	34.84505	-82.8319	porphyroclastic	5/18/15
Sm261	biotite gneiss(t)	34.84491	-82.8321	porphyroclastic	5/18/15
Sm262	biotite gneiss(t)	34.84555	-82.8313	porphyroclastic	5/18/15
Sm263	amphibolite	34.84627	-82.8311		5/18/15
Sm264	amphibolite	34.84667	-82.8303		5/18/15
Sm265	pegmatite	34.84646	-82.8295		5/18/15
Sm266	hornblende gneiss	34.84649	-82.8292		5/18/15
Sm267	biotite gneiss (l)	34.85638	-82.8601		5/19/15
Sm268	amphibolite	34.8565	-82.8606		5/19/15
Sm269	amphibolite	34.85688	-82.8603		5/19/15
Sm271	hornblende gneiss	34.85634	-82.8592		5/19/15
Sm272	biotite hornblende gneiss	34.85638	-82.8583		5/19/15
Sm273	biotite hornblende gneiss	34.84634	-82.8619		5/19/15
Sm274	biotite hornblende gneiss	34.84934	-82.8628		5/19/15
Sm275	amphibolite	34.8491	-82.8622		5/19/15
Sm276	amphibolite	34.84919	-82.8614		5/19/15
Sm277	amphibolite	34.85096	-82.8474	float	5/20/15
Sm278	pegmatite	34.85047	-82.8487	weird	5/20/15
Sm279	amphibolite	34.85001	-82.8506		5/20/15
Sm280	amphibolite	34.85	-82.8508	saprolite	5/20/15
Sm281	amphibolite	34.8491	-82.8488		5/20/15
Sm282	biotite hornblende gneiss	34.85568	-82.7976		5/20/15
Sm283	biotite hornblende gneiss	34.8569	-82.7956		5/20/15
Sm284	biotite gneiss	34.85668	-82.7951		5/20/15
Sm285	amphibolite	34.83575	-82.8417	float	5/22/15
Sm286	biotite gneiss(t)	34.83586	-82.8417	porphyroclastic	5/22/15
Sm287	biotite gneiss(t)	34.83595	-82.8417	porphyroclastic	5/22/15
Sm288	biotite gneiss(t)	34.83706	-82.8418	porphyroclastic	5/22/15
Sm289	biotite gneiss(t)	34.83789	-82.8417	porphyroclastic	5/22/15

Sm290	biotite gneiss (l)	34.83359	-82.8425		5/26/15
Sm291	amphibolite	34.83367	-82.8428		5/26/15
Sm292	biotite gneiss(t)	34.83368	-82.8437		5/26/15
Sm293	biotite gneiss(t)	34.83469	-82.8439		5/26/15
Sm294	biotite gneiss(t)	34.83519	-82.8441		5/26/15
Sm295	amphibolite	34.83541	-82.8442		5/26/15
Sm296	biotite gneiss(t)	34.83561	-82.8449		5/26/15
Sm297	amphibolite	34.83545	-82.8458		5/26/15
Sm298	biotite gneiss(t)	34.83553	-82.8466		5/26/15
Sm299	amphibolite	34.83	-82.8603		5/26/15
Sm300	biotite gneiss(t)	34.83006	-82.8603		5/26/15
Sm301	biotite gneiss(t)	34.82833	-82.8552	porphyroclastic	5/27/15
Sm302	amphibolite	34.87354	-82.7693	float	5/27/15
Sm303	garnet biotite muscovite schist	34.87133	-82.7717		5/27/15
Sm304	biotite gneiss(t)	34.87132	-82.7723		5/27/15
Sm305	muscovite biotite schist	34.8713	-82.7726		5/27/15
Sm306	biotite quartzite	34.87055	-82.7722		5/27/15
Sm307	biotite gneiss (t)	34.87018	-82.7721	nonporphyroclastic	5/27/15
Sm308	amphibolite	34.86928	-82.7714		5/27/15
Sm309	biotite gneiss(t)	34.86875	-82.7712		5/27/15
Sm310	biotite quartzite	34.8697	-82.7705		5/27/15
Sm311	biotite gneiss(t)	34.86987	-82.7699		5/27/15
Sm312	amphibolite	34.86981	-82.7699		5/27/15
Sm313	hornblende gneiss	34.86993	-82.7688		5/27/15
Sm314	biotite gneiss(t)	34.86986	-82.7697		5/27/15
Sm315	sillimanite muscovite garnet schist	34.87093	-82.7692		5/27/15
Sm316	amphibolite	34.83865	-82.8305		5/31/15
Sm317	garnetiferous quartzite	34.8388	-82.8307		5/31/15
Sm318	amphibolite	34.83915	-82.8312		5/31/15
Sm319	amphibolite	34.83983	-82.8319		5/31/15
Sm320	garnet muscovite schist	34.83989	-82.8319		5/31/15
Sm323	mica schist	34.84065	-82.8327		5/31/15
Sm324	sillimanite muscovite schist	34.8407	-82.8336		5/31/15
Sm321	garnet muscovite schist	0	0	pods of amphibolite	5/31/15
Sm322	mica schist	0	0		5/31/15
Sm326	garnet sillimanite mica schist	34.86368	-82.7805	biotite gneiss float locally	6/1/15
Sm325	garnet mica schist	34.86313	-82.7806		6/1/15

Sm327	biotite gneiss (t)	34.86366	-82.7804	fine-crystalline, biotite and muscovite	6/1/15
Sm328	biotite gneiss (t)	34.86406	-82.78	fine-crystalline, biotite and muscovite	6/1/15
Sm329	biotite gneiss (t)	34.87323	-82.8173	porphyroclastic	6/1/15
Sm330	biotite hornblende gneiss	34.82988	-82.8597		6/2/15
Sm331	amphibolite	34.83015	-82.8592		6/2/15
Sm332	amphibolite	34.83018	-82.8587		6/2/15
Sm333	amphibolite	34.83033	-82.8579		6/2/15
Sm334	biotite gneiss (l)	34.83097	-82.8567		6/2/15
Sm335	hornblende gneiss	34.83185	-82.8563	porphyroclastic	6/2/15
Sm336	hornblende gneiss	34.83213	-82.8552	porphyroclastic	6/2/15
Sm338	biotite hornblende gneiss (t)	34.83257	-82.8545	porphyroclastic	6/2/15
Sm337	biotite gneiss (l)	34.83235	-82.855		6/2/15
Sm339	biotite gneiss(t)	34.83269	-82.8546		6/2/15
Sm340	hornblende gneiss	34.8324	-82.8574		6/2/15
Sm341	muscovite garnet amphibole schist	34.85052	-82.8305		6/5/15
Sm342	muscovite garnet schist	34.83572	-82.835		6/5/15
Sm343	biotite gneiss(t)	34.8657	-82.779	Local pegmatite	6/6/15
Sm344	muscovite biotite gneiss	34.86588	-82.7788		6/6/15
Sm345	sillimanite mica schist	34.86597	-82.7784		6/6/15
Sm346	muscovite biotite gneiss	34.86596	-82.778		6/6/15
Sm347	biotite gneiss(t)	34.86596	-82.7775		6/6/15
Sm348	biotite gneiss(t)	34.86608	-82.7767	leucocratic, porphyroclastic, muscovite-rich	6/6/15
Sm349	biotite muscovite schist	34.86593	-82.7764		6/6/15
Sm350	biotite schist	34.86587	-82.7761	Biotite schist crenulated, Locat garnet muscovite schist float	6/6/15
Sm351	biotite gneiss(t)	34.86604	-82.7757	massive boulder, leucocratic, suspect strain	6/6/15
Sm352	biotite gneiss(t)	34.86647	-82.7754		6/6/15
Sm353	sillimanite mica schist	34.86667	-82.7755		6/6/15
Sm354	biotite gneiss (t)	34.83602	-82.8432	leucocratic	6/7/15
Sm355	amphibolite	34.83816	-82.8428	float	6/7/15

Sm356	biotite gneiss (t)	34.8397	-82.8538	porphyroclastic	6/7/15
Sm357	biotite gneiss (t)	34.86624	-82.7812		6/8/15
Sm358	biotite gneiss (t)	34.86637	-82.7813	locally porphyroclastic	6/8/15
Sm359	garnet muscovite biotite schist	34.86654	-82.7813		6/8/15
Sm360	garnet muscovite sillimanite schist	34.86637	-82.7816		6/8/15
Sm361	quartz	34.86668	-82.7835		6/8/15
Sm362	Spring	34.86679	-82.7837		6/8/15
Sm363	hornblende gneiss	34.86711	-82.7837	float	6/8/15
Sm364	hornblende gneiss	34.86772	-82.7835		6/8/15
Sm365	biotite gneiss	34.8426	-82.8543		6/9/15
Sm366	hornblende gneiss	34.84264	-82.8544		6/9/15
Sm367	hornblende gneiss	34.84266	-82.8543		6/9/15
Sm368	hornblende gneiss	34.84274	-82.8542		6/9/15
Sm369	biotite hornblende gneiss	34.84299	-82.8541		6/9/15
Sm370	hornblende biotite gneiss	34.8433	-82.8528		6/9/15
Sm371	hornblende gneiss	34.84314	-82.8534	hornblende crystals ~1cm long	6/9/15
Sm372	hornblende biotite gneiss	34.84304	-82.8535		6/9/15
Sm373	hornblende gneiss	34.84309	-82.8534		6/9/15
Sm374	biotite gneiss	34.84318	-82.8538		6/9/15
Sm375	hornblende gneiss	34.8431	-82.8542		6/9/15
Sm376	hornblende gneiss	34.84319	-82.8541		6/9/15
Sm379	hornblende gneiss	34.84305	-82.8546	float	6/10/15
Sm380	hornblende gneiss	34.84391	-82.8546		6/10/15
Sm381	biotite gneiss	34.84387	-82.8545	porphyroclastic	6/10/15
Sm383	biotite gneiss	34.8441	-82.8545	porphyroclastic	6/10/15
Sm384	hornblende gneiss	34.84433	-82.8546	float, speckled	6/10/15
Sm385	hornblende gneiss	34.84444	-82.8549	float, speckled	6/10/15
Sm386	amphibolite	34.83457	-82.8344		6/18/15
Sm387	biotite muscovite schist	34.83473	-82.8346		6/18/15
Sm388	muscovite schist	34.83471	-82.835		6/18/15
Sm389	amphibolite	34.83456	-82.8351		6/18/15
Sm390	garnet muscovite schist	34.83533	-82.8348		6/19/15
Sm391	biotite muscovite schist	34.83495	-82.836		6/19/15
Sm392	muscovite schist	34.83524	-82.8365		6/19/15
Sm393	biotite muscovite schist	34.83795	-82.8371		6/19/15

Sm394	amphibolite	34.83799	-82.8371		6/19/15
Sm395	amphibolite	34.83819	-82.837		6/19/15
Sm396	biotite gneiss(t)	34.83839	-82.837		6/19/15
Sm397	amphibolite	34.83856	-82.837		6/19/15
Sm398	biotite gneiss(t)	34.83866	-82.8369		6/19/15
Sm399	muscovite biotite schist	34.83927	-82.8369		6/19/15
Sm400	muscovite biotite schist	34.83926	-82.8369	saprolite	6/19/15
Sm401	muscovite biotite schist	34.83927	-82.8364	saprolite	6/19/15
Sm402	amphibolite	34.83918	-82.8364	float	6/19/15
Sm403	biotite gneiss(t)	34.83893	-82.8364	fine-crystalline, non-porphyroclastic with garnet	6/19/15
Sm404	garnet biotite muscovite schist	34.83907	-82.8364		6/19/15
Sm405	amphibolite	34.83756	-82.8365		6/19/15
Sm406	biotite gneiss	34.87326	-82.8063		6/24/15
Sm407	garnet muscovite schist	34.87005	-82.8052		6/24/15
Sm408	amphibolite	34.86139	-82.8371		6/24/15
Sm409	biotite gneiss (l)	34.85119	-82.8087		6/24/15
Sm411	hornblende gneiss	34.82786	-82.8529		6/24/15
Sm410	garnet muscovite schist	0	0		6/24/15
Sm412	biotite gneiss (l)	34.83996	-82.8735	0.5cm	6/25/15
Sm414	biotite gneiss (l)	34.84485	-82.8757	fine-crystalline	6/25/15
Sm415	hornblende gneiss	34.84483	-82.8748	biotite hornblende gneiss locally	6/25/15
Sm416	amphibolite	34.8447	-82.8747		6/25/15
Sm417	biotite hornblende gneiss	34.84432	-82.8749		6/25/15
Sm418	hornblende gneiss	34.84416	-82.875		6/25/15
Sm419	hornblende gneiss	34.84376	-82.8754	quartz-rich	6/25/15
Sm420	hornblende biotite gneiss	34.84305	-82.8753		6/25/15
Sm421	hornblende gneiss	34.82831	-82.861		6/25/15
Sm422	ultramafic	34.85317	-82.836	anthophyllite	6/25/15
Sm423	hornblende gneiss	34.83604	-82.8694		6/27/15
Sm424	amphibolite	34.83644	-82.8698		6/27/15
Sm425	amphibolite	34.82934	-82.8543		6/27/15
Sm426	garnet muscovite schist	34.82969	-82.8545		6/27/15
Sm427	biotite hornblende gneiss	34.82985	-82.8548		6/27/15
Sm428	amphibolite	34.83002	-82.855	garnet muscovite schist	6/27/15

Sm429	amphibolite	34.83002	-82.8516		6/27/15
Sm430	garnet muscovite schist	34.83265	-82.8374		6/27/15
Sm432	garnetiferous quartzite	34.84701	-82.8757		6/29/15
Sm433	biotite gneiss	34.84674	-82.875		6/29/15
Sm434	hornblende gneiss	34.8465	-82.875		6/29/15
Sm436	biotite gneiss (l)	34.84686	-82.8748		6/29/15
Sm437	biotite hornblende gneiss	34.84794	-82.8746		6/29/15
Sm438	biotite hornblende gneiss	34.84853	-82.8741		6/29/15
Sm438	hornblende gneiss	34.8486	-82.8739		6/29/15
Sm439	hornblende gneiss	34.84806	-82.8733		6/29/15
Sm440	hornblende gneiss	34.84779	-82.8728		6/29/15
Sm441	amphibolite	34.84641	-82.8725		6/29/15
Sm442	amphibolite	34.84567	-82.8729		6/29/15
Sm443	biotite muscovite schist	34.84918	-82.8371		6/30/15
Sm444	amphibolite	34.85229	-82.8348	biotite pegmatite	6/30/15
Sm445	amphibolite	34.8524	-82.8344		6/30/15
Sm446	pegmatite	34.8524	-82.8343		6/30/15
Sm447	biotite gneiss (t)	34.85245	-82.8341	non-porphyroclastic	6/30/15
Sm448	biotite gneiss	34.85249	-82.8341		6/30/15
Sm449	amphibolite	34.85247	-82.834		6/30/15
Sm450	biotite schist	34.8524	-82.8337		6/30/15
Sm451	pegmatite	34.85253	-82.8335	also muscovite biotite gneiss, amphibolite	6/30/15
Sm452	biotite gneiss (t)	34.85242	-82.8328		6/30/15
Sm453	biotite gneiss (t)	34.85527	-82.832	porphyroclastic, waterfall	6/30/15
Sm454	biotite gneiss (l)	34.83869	-82.8468		7/1/15
Sm455	amphibolite	34.83904	-82.8474		7/1/15
Sm456	hornblende gneiss	34.83938	-82.8474		7/1/15
Sm457	amphibolite	34.83964	-82.8474	also hornblende gneiss	7/1/15
Sm458	biotite gneiss(t)	34.84006	-82.8473	porphyroclastic	7/1/15
Sm459	amphibolite	34.84187	-82.8476	also quartz	7/1/15
Sm460	biotite gneiss(t)	34.84191	-82.8476		7/1/15
Sm461	biotite gneiss(t)	34.84349	-82.8483	also amphibolite	7/1/15
Sm462	quaternary alluvial	34.84404	-82.8497		7/1/15
Sm463	biotite gneiss(t)	34.84145	-82.8473		7/1/15
Sm464	hornblende gneiss	34.83712	-82.8508		7/3/15
Sm465	biotite gneiss (l)	34.83739	-82.8533		7/3/15
Sm466	garnetiferous quartzite	34.83737	-82.8541		7/3/15

Sm467	biotite gneiss(t)	34.83713	-82.8554		7/3/15
Sm468	biotite gneiss (l)	34.83691	-82.8557		7/3/15
Sm469	biotite gneiss(t)	34.83693	-82.8555		7/3/15
Sm470	biotite gneiss(t)	34.83683	-82.8547		7/3/15
Sm471	biotite gneiss(t)	34.83723	-82.8509		7/3/15
Sm472	amphibolite	34.87347	-82.804		7/7/15
Sm473	garnetiferous quartzite	34.87358	-82.8033		7/7/15
Sm474	garnet sillimanite muscovite schist	34.87209	-82.8066		7/7/15
Sm475	manganiferous quartzite	34.87206	-82.8064		7/7/15
Sm476	amphibolite	34.86909	-82.8084	large muscovite books	7/7/15
Sm477	garnet sillimanite muscovite schist	34.87206	-82.8069		7/7/15
Sm478	garnet muscovite schist	34.86615	-82.8069		7/7/15
Sm486	hornblende gneiss	34.85019	-82.8103	leucocratic, fine-crystalline	7/8/15
Sm488	garnet muscovite sillimanite schist	34.84269	-82.8212		7/16/15
Sm489	manganiferous quartz	34.84419	-82.822		7/16/15
Sm490	garnet sillimanite muscovite schist	34.84558	-82.8244		7/16/15
Sm491	garnet sillimanite muscovite schist	34.84898	-82.8064		7/16/15
Sm492	manganiferous quartz	34.8608	-82.8149		7/16/15
Sm493	amphibolite	34.85961	-82.8155		7/16/15
Sm494	amphibolite	34.85867	-82.816		7/16/15
Sm495	garnet biotite muscovite schist	0	0		
Sm479	garnet biotite muscovite schist	34.87331	-82.8172		7/8/15
Sm480	garnet biotite muscovite schist	34.87371	-82.8167		7/8/15
Sm481	sillimanite	34.87337	-82.8174		7/8/15
Sm482	amphibolite	34.87237	-82.8162	pod of amph	7/8/15
Sm483	garnet sillimanite muscovite schist	34.87219	-82.8161		7/8/15
Sm484	biotite gneiss (t)	34.87223	-82.8159	porphyroclastic	7/8/15
Sm486	hornblende gneiss	34.85019	-82.8103	leucocratic, fine-crystalline	7/8/15
Sm485	garnet muscovite schist	34.86085	-82.8183		7/8/15

Sm487	garnet muscovite sillimanite schist	34.8493	-82.8114		7/8/15
Sm502	biotite gneiss (t)	34.87531	-82.8175		7/17/15
Sm503	biotite gneiss (t)	34.87527	-82.8178		7/17/15
Sm504	biotite gneiss (t)	34.8752	-82.8182		7/17/15
Sm505	biotite gneiss (t)	34.87548	-82.8191	local amphibolite	7/17/15
Sm506	biotite gneiss (t)	34.87556	-82.8197		7/17/15
Sm507	amphibolite	34.87557	-82.8201		7/17/15
Sm508	muscovite schist	34.87568	-82.8206		7/17/15
Sm514	amphibolite	34.86512	-82.8107		7/18/15
Sm515	amphibolite	34.86543	-82.8111		7/18/15
Sm516	amphibolite	34.86627	-82.8109		7/18/15
Sm517	biotite gneiss (t)	34.86657	-82.8104		7/18/15
Sm518	biotite gneiss (t)	34.86691	-82.8108		7/18/15
Sm519	amphibolite	34.86705	-82.8108		7/18/15
Sm520	biotite gneiss (t)	34.86723	-82.811		7/18/15
Sm520	pegmatite	34.84398	-82.8428		7/20/15
Sm521	biotite gneiss (t)	34.84393	-82.8427		7/20/15
Sm522	amphibolite	34.84358	-82.8426		7/20/15
Sm523	biotite gneiss (t)	34.84342	-82.8427		7/20/15
Sm524	pegmatite	34.8707	-82.7563	in saprolite	7/20/15
Sm525	amphibolite	34.86845	-82.8077		7/20/15
Sm526	garnet muscovite sillimanite schist	34.86824	-82.807		7/20/15
Sm527	amphibolite	34.86819	-82.8069		7/20/15
Sm528	garnet muscovite sillimanite schist	34.86802	-82.8067		7/20/15
Sm529	garnet sillimanite muscovite schist	34.83678	-82.8389		7/20/15
Sm530	garnet sillimanite muscovite schist	34.84173	-82.8391		7/20/15
Sm531	muscovite schist	34.8312	-82.8453	also limonite, amphibolite, and potential ultramafic	7/21/15
Sm532	biotite gneiss (t)	34.82923	-82.8494	porphyroclastic	7/21/15
Sm533	biotite gneiss (t)	34.86028	-82.788	non-porphyroclastic, sheared	7/21/15
Sm534	biotite gneiss (t)	34.86342	-82.8032	non-porphyroclastic, sheared	7/21/15
Sm535	garnet muscovite schist	34.86037	-82.8228		7/22/15
Sm536	garnet muscovite schist	34.86136	-82.8231		7/22/15
Sm537	amphibolite	34.86522	-82.81		7/22/15

Sm538	amphibolite	34.86549	-82.8099		7/22/15
Sm539	biotite gneiss (t)	34.86774	-82.8111		7/22/15
Sm540	biotite gneiss (t)	34.86808	-82.8109		7/22/15
Sm541	amphibolite	34.86823	-82.81		7/22/15
Sm542	amphibolite	34.85451	-82.8257	quartz	7/23/15
Sm543	garnet biotite muscovite schist	34.85414	-82.8278		7/23/15
Sm545	biotite gneiss (l)	34.8395	-82.8659	0	7/28/15
Sm546	pegmatite	34.84372	-82.8673	0	7/28/15
Sm547	amphibolite	34.8445	-82.8673	0	7/28/15
Sm548	epidote	34.84519	-82.8673	0	7/28/15
Sm549	hornblende gneiss	34.84509	-82.8671	0	7/28/15
Sm550	pegmatite	34.84475	-82.8667	0	7/28/15
Sm551	amphibolite	34.84332	-82.8657	0	7/28/15
Sm552	biotite gneiss (l)	34.84287	-82.8655	0	7/28/15
Sm553	amphibolite	34.84281	-82.8655	0	7/28/15
Sm554	amphibolite	34.84241	-82.8653	0	7/28/15
Sm555	biotite gneiss (l)	34.84215	-82.8651	0	7/28/15
Sm556	biotite gneiss (l)	34.84174	-82.8647	0	7/28/15
Sm557	amphibolite	34.84058	-82.8644	0	7/28/15
Sm558	amphibolite	34.84028	-82.8643	0	7/28/15
Sm559	amphibolite	34.83786	-82.8637	0	7/28/15
Sm560	biotite gneiss (l)	34.83688	-82.8636	0	7/28/15
Sm561	amphibolite	34.83821	-82.8628	0	7/28/15
Sm562	hornblende gneiss	34.83828	-82.8627	343	7/28/15
Sm563	fold	34.83884	-82.8626	0	7/28/15
Sm564	quaternary alluvium	34.83936	-82.8627	0	7/28/15
Sm565	biotite gneiss (l)	34.83976	-82.8633	0	7/28/15
Sm566	amphibolite	34.83978	-82.8634	0	7/28/15
Sm569	biotite gneiss (l)	34.83712	-82.863		7/30/15
Sm570	quaternary alluvium	34.83786	-82.86		7/30/15
Sm573	biotite gneiss (l)	34.84087	-82.8613		7/30/15
Sm571	amphibolite	34.83935	-82.8604		7/30/15
Sm572	amphibolite	34.83948	-82.8604		7/30/15
Sm574	biotite gneiss (l)	34.84096	-82.8614		7/30/15
Sm575	biotite gneiss (l)	34.84119	-82.862		7/30/15
Sm576	amphibolite	34.83977	-82.8623		7/30/15
Sm567	garnet muscovite schist	34.86247	-82.8063		7/29/15
Sm568	garnet muscovite schist	34.8631	-82.808		7/29/15
Sm577	hornblende gneiss	34.86075	-82.7915		8/3/15

Sm578	muscovite sillimanite schist	34.86948	-82.7938		8/3/15
Sm579	garnet muscovite schist	34.86949	-82.7933		8/3/15
Sm580	garnet muscovite sillimanite schist	34.86968	-82.792		8/3/15
Sm581	garnet sillimanite muscovite schist	34.87034	-82.7917		8/3/15
Sm582	garnet quartzite	34.87138	-82.7914		8/3/15
Sm583	garnet muscovite sillimanite schist	34.872	-82.7915		8/3/15
Sm585	garnet sillimanite muscovite schist	34.86051	-82.7887		8/3/15
Sm586	amphibolite	34.87203	-82.8489		8/3/15
Sm587	amphibolite	34.87181	-82.849		8/3/15
Sm588	amphibolite	34.87086	-82.8492	local biotite gneiss (l)	8/3/15
Sm589	amphibolite	34.87045	-82.8496		8/3/15
Sm590	amphibolite	34.86983	-82.8501		8/3/15
Sm591	hornblende biotite gneiss	34.87537	-82.7746		8/4/15
Sm592	hornblende gneiss	34.87547	-82.7748		8/4/15
Sm593	amphibolite	34.86382	-82.8083		8/4/15
Sm594	garnet sillimanite muscovite schist	34.86344	-82.8082		8/4/15
Sm595	muscovite schist	34.86337	-82.8082		8/4/15
Sm596	garnet sillimanite muscovite schist	34.86337	-82.8016		8/4/15
Sm597	quartz	34.84582	-82.8173		8/4/15
Sm598	amphibolite	34.84544	-82.817		8/4/15
Sm599	garnet sillimanite muscovite schist	34.84537	-82.8169		8/4/15
Sm600	hornblende gneiss	34.8677	-82.8012		8/5/15
Sm601	hornblende gneiss	34.86652	-82.801		8/5/15
Sm602	biotite gneiss (l)	34.86572	-82.8004		8/5/15
Sm603	amphibolite	34.86557	-82.8006		8/5/15
Sm604	biotite gneiss (l)	34.86763	-82.7883		8/5/15

Appendix B: Strikes and Dips of Foliation in Study Area

*Strikes and dips are denoted in azimuth using right-hand rule.

WP	Description	Lat	Long_	Date	Strike	Dip
Sm539	biotite gneiss (t)	34.86774	-82.8111	7/22/15	52	32
Sm543	garnet biotite muscovite schist	34.85414	-82.8278	7/23/15	24	66
Sm534	biotite gneiss (t)	34.86342	-82.8032	7/21/15	338	40
Sm15	garnet sillimanite mica schist	34.86818	-82.7938	7/29/14	28	88
Sm17	hornblende gneiss (hw)	34.87053	-82.8078	7/29/14	11	21
Sm51	biotite gneiss(t)	34.87032	-82.8173	8/27/14	40	52
Sm53	biotite gneiss(t)	34.86934	-82.8205	9/1/14	2	59
Sm55	biotite gneiss(t)	34.86934	-82.8209	9/1/14	31	20
Sm56	biotite gneiss(t)	34.86975	-82.8218	9/1/14	280	71
Sm57	biotite gneiss(t)	34.87049	-82.823	9/1/14	17	34
Sm59	biotite gneiss(t)	34.8659	-82.8239	9/3/14	56	27
Sm78	pegmatite	34.84792	-82.8436	12/31/14	296	20
Sm79	biotite gneiss(t)	34.84553	-82.839	12/31/14	11	44
Sm106	biotite gneiss(t)	34.85635	-82.8274	2/10/15	16	36
Sm107	mica schist	34.8494	-82.7992	2/11/15	205	36
Sm125	mica schist	34.85822	-82.8034	2/28/15	15	25
Sm189	biotite gneiss(t)	34.86289	-82.8238	4/28/15	350	22
Sm190	biotite gneiss(t)	34.86283	-82.8242	4/28/15	212	26
Sm191	biotite gneiss(t)	34.86253	-82.8246	4/28/15	245	35
Sm192	biotite gneiss(t)	34.86226	-82.8253	4/28/15	215	35
Sm194	biotite gneiss(t)	34.86225	-82.8256	4/28/15	190	20
Sm195	biotite gneiss(t)	34.86259	-82.8261	4/28/15	218	35
Sm196	biotite gneiss(t)	34.86267	-82.8263	4/28/15	8	25
Sm203	biotite gneiss(t)	34.86184	-82.8285	4/29/15	125	14
Sm204	biotite gneiss(t)	34.862	-82.8285	4/29/15	280	71
Sm208	biotite gneiss(t)	34.86252	-82.827	4/29/15	290	24
Sm221	garnet mica schist	34.8541	-82.7903	5/5/15	84	90
Sm230	biotite gneiss(t)	34.8558	-82.792	5/6/15	61	14
Sm239	garnetiferous quartzite	34.86476	-82.8077	5/14/15	57	79
Sm244	muscovite biotite schist	34.87506	-82.7953	5/16/15	74	48

Sm261	biotite gneiss(t)	34.84491	-82.8321	5/18/15	40	46
Sm287	biotite gneiss(t)	34.83595	-82.8417	5/22/15	80	32
Sm294	biotite gneiss(t)	34.83519	-82.8441	5/26/15	273	20
Sm296	biotite gneiss(t)	34.83561	-82.8449	5/26/15	35	37
Sm309	biotite gneiss(t)	34.86875	-82.7712	5/27/15	31	9
Sm320	garnet muscovite schist	34.83989	-82.8319	5/31/15	41	64
Sm323	mica schist	34.84065	-82.8327	5/31/15	75	60
Sm329	biotite gneiss (t)	34.87323	-82.8173	6/1/15	22	48
Sm339	biotite gneiss(t)	34.83269	-82.8546	6/2/15	150	16
Sm341	muscovite garnet amphibole schist	34.85052	-82.8305	6/5/15	4	65
Sm344	muscovite biotite gneiss	34.86588	-82.7788	6/6/15	40	62
Sm346	muscovite biotite gneiss	34.86596	-82.778	6/6/15	278	38
Sm347	biotite gneiss(t)	34.86596	-82.7775	6/6/15	17	24
Sm356	biotite gneiss (t)	34.8397	-82.8538	6/7/15	75	25
Sm357	biotite gneiss (t)	34.86624	-82.7812	6/8/15	55	26
Sm401	muscovite biotite schist	34.83927	-82.8364	6/19/15	273	37
Sm411	hornblende gneiss	34.82786	-82.8529	6/24/15	35	30
Sm443	biotite muscovite schist	34.84918	-82.8371	6/30/15	41	42
Sm452	biotite gneiss (t)	34.85242	-82.8328	6/30/15	36	42
Sm463	biotite gneiss(t)	34.84145	-82.8473	7/1/15	12	21
Sm470	biotite gneiss(t)	34.83683	-82.8547	7/3/15	15	58
Sm478	garnet muscovite schist	34.86615	-82.8069	7/7/15	93	65
Sm479	garnet biotite muscovite schist	34.87332	-82.8172	7/8/15	93	65
Sm487	garnet muscovite sillimanite schist	34.8493	-82.8114	7/8/15	174	52
Sm517	biotite gneiss (t)	34.86657	-82.8104	7/18/15	41	29
Sm5	garnet muscovite schist	334637.2	3858565	12/30/1899 0:00:00	273	88
Sm571	amphibolite	34.83935	-82.8604	7/30/15	257	68
Sm572	amphibolite	34.83948	-82.8604	7/30/15	350	31
Sm574	biotite gneiss (l)	34.84096	-82.8614	7/30/15	26	47

Sm575	biotite gneiss (l)	34.84119	-82.862	7/30/15	59	66
Sm8	biotite gneiss (l)	34.85754	-82.8622	7/28/14	34	24
Sm10	biotite gneiss	34.85859	-82.8554	7/28/14	9	20
Sm20	biotite gneiss (l)	34.85516	-82.8072	7/29/14	276	34
Sm58	hornblende biotite gneiss	34.86945	-82.824	9/1/14	56	27
Sm60	biotite gneiss	34.8695	-82.8246	9/17/14	55	31
Sm62	amphibolite	34.86933	-82.8398	11/12/14	38	13
Sm66	hornblende gneiss	34.85952	-82.8409	12/16/14	17	26
Sm68	hornblende gneiss	34.86019	-82.8402	12/16/14	20	19
Sm88	hornblende gneiss	34.85232	-82.8387	1/20/15	36	20
Sm133	hornblende gneiss	34.86827	-82.8006	2/28/15	95	44
Sm164	amphibolite	34.86904	-82.8354	4/22/15	91	46
Sm165	amphibolite	34.869	-82.8353	4/22/15	140	26
Sm167	amphibolite	34.86739	-82.8347	4/22/15	305	6
Sm169	amphibolite	34.86774	-82.8307	4/24/15	199	36
Sm179	biotite gneiss (l)	34.87255	-82.832	4/27/15	36	37
Sm181	hornblende gneiss	34.87259	-82.8315	4/27/15	7	46
Sm182	hornblende gneiss	34.8718	-82.831	4/27/15	54	50
Sm184	biotite gneiss (l)	34.87186	-82.8298	4/27/15	30	58
Sm185	amphibolite	34.87192	-82.8292	4/27/15	295	21
Sm199	biotite hornblende gneiss	34.86154	-82.8315	4/29/15	182	2
Sm214	hornblende gneiss	34.86303	-82.8339	5/5/15	65	48
Sm215	hornblende gneiss	34.86203	-82.8323	5/5/15	20	45
Sm216	hornblende gneiss	34.86188	-82.8321	5/5/15	78	58
Sm217	hornblende gneiss	34.86184	-82.8322	5/5/15	352	18
Sm218	hornblende gneiss	34.8618	-82.8319	5/5/15	40	47
Sm235	biotite gneiss (l)	34.87462	-82.7732	5/12/15	68	20
Sm264	amphibolite	34.84667	-82.8303	5/18/15	2	48

Sm269	amphibolite	34.85688	-82.8603	5/19/15	72	14
Sm272	biotite hornblende gneiss	34.85638	-82.8583	5/19/15	93	23
Sm274	biotite hornblende gneiss	34.84934	-82.8628	5/19/15	35	11
Sm280	amphibolite	34.85	-82.8508	5/20/15	310	6
Sm365	biotite gneiss	34.84261	-82.8543	6/9/15	289	7
Sm367	hornblende gneiss	34.84266	-82.8543	6/9/15	30	26
Sm370	hornblende biotite gneiss	34.8433	-82.8528	6/9/15	5	75
Sm371	hornblende gneiss	34.84314	-82.8534	6/9/15	35	24
Sm373	hornblende gneiss	34.84309	-82.8534	6/9/15	45	25
Sm376	hornblende gneiss	34.84319	-82.8541	6/9/15	35	25
Sm383	biotite gneiss	34.8441	-82.8545	6/10/15	55	18
Sm417	biotite hornblende gneiss	34.84433	-82.8749	6/25/15	23	27
Sm434	hornblende gneiss	34.8465	-82.875	6/29/15	45	28
Sm440	hornblende gneiss	34.84779	-82.8728	6/29/15	34	24

Appendix C: Sunset quadrangle excursion 6/20/2017

OBJECTID	Description	Latitude	Longitude
1	biotite gneiss (l)	330261.9	3860963
2	biotite gneiss (l)	330364.2	3860917
3	hornblende gneiss	330468.2	3860937
4	amphibolite	330482.3	3860950
5	biotite gneiss (l)	330268.9	3860888
6	hornblende gneiss	329963.8	3861014
7	amphibolite	329975.2	3861029
8	amphibolite	328823.4	3859058
9	amphibolite	328881.6	3858984
10	amphibolite	328976.9	3858884
11	mica schist	332191.5	3861761
12	limonite	332191.5	3861800

REFERENCES

Allmendinger, R., 2011, Stereonet 7 for Windows:, http://www.geo.cornell.edu/geology/faculty/RWA/programs/stereonet.html.

Bier, S.E., Bream, B., and Giorgis, S.D., 2002, Inner Piedmont stratigraphy, metamorphism, and deformation in the Marion-South Mountains area, North Carolina, *in* Inner Piedmont geology in the South Mountains-Blue Ridge Foothills and the southwestern Brushy Mountains, central-western North Carolina, Annual Field Trip Guidebook, Carolina Geological Society, p. 65–99.

Bream, B., 2002, The southern Appalachian Inner Piedmont: New perspectives based on recent detailed geologic mapping, Nd isotopic evidence, and zircon geochronology, *in* Inner Piedmont geology in the South Mountains-Blue Ridge Foothills and the southwestern Brushy Mountains, central-western North Carolina, Annual Field Trip Guidebook, Carolina Geological Society, p. 45–63.

Butler, J.R., 1989, Review and classification of ultramafic bodies in the Piedmont of the Carolinas: Geological Society of America Special Paper, v. 231, p. 19–32.

Davis, G.H., and Reynolds, S.J., 1996, Structural Geology of Rocks and Regions, *in* Structural Geology of Rocks and Regions. 2nd Edition, Wiley.

Edelman, S.H., Liu, A., and Hatcher, R.D., 1987, The Brevard Zone in South Carolina and Adjacent Areas: An Alleghanian Orogen-Scale Dextral Shear Zone Reactivated as a Thrust Fault: The Journal of Geology, v. 95, p. 793–806.

Fossen, H., 2010, Structural geology: Cambridge University Press.

Garihan, J.M., 2001, Observations of the Seneca fault and their implications for thrust sheet emplacement in the Inner Piedmont of the Carolinas: South Carolina Geology, v. 43, p. 1-13.

Garihan, J.M., 2002, Geology of Standingstone Mountain quadrangle, Western Inner Piedmont, North and South Carolina, *in* Inner Piedmont geology in the South Mountains-Blue Ridge Foothills and the southwestern Brushy Mountains, central-western North Carolina, Annual Field Trip Guidebook, Carolina Geological Society, p. 19–32.

Garihan, J.M., 2005, Geologic Map of the Sunset 7.5-minute quadrangle, Pickens County, South Carolina: South Carolina Department of Natural Resources Geologic Quadrangle Map GQM-28, scale 1:24000.

Garihan, J.M., 2007, Geologic Map of the Cleveland 7.5-minute quadrangle, Greenville and Pickens Counties, South Carolina: Geologic Quadrangle Map GQM-33,.scale 1:24000.

Garihan, John M., 2012, Sequencing brittle faulting in the Inner Piedmont, South Carolina: South Carolina Geology, v. 48, p. 37-49.

Garihan, J.M., and Ranson, W.A., 2001a, Geologic Map of the Table Rock 7.5-minute quadrangle, Greenville and Pickens Counties, South Carolina, and Transylvania County, North Carolina: Geologic Quadrangle Map GQM-9, scale 1:24000.

Garihan, J.M., and Ranson, W.A., 2001b, Geologic Transect Across the Table Rock and Eastatoe Gap 7.5-Minute quadrangles, Western Inner Piedmont, Greenville and Pickens Counties, SC-NC, *in* Southeastern Section, Geological Society of America Abstracts with Programs. v. 33, no. 2.

Garihan, J.M., and Ranson, W.A., 2007, Geologic map of the Standingstone Mountain 7.5-minute quadrangle, Greenville County, South Carolina and Transylvania and Henderson Counties, North Carolina: Geologic Quadrangle Map GQM-35, scale 1:24000.

Gober, M., and Ranson, W., 2005, Petrology of the Nine Times Amphibolite-Ultramafic Body from the Sunset 7.5-Minute Quadrangle, Western Inner Piedmont of South Carolina, Geological Society of America Abstracts with Programs, v. 37, no. 2, p. 46.

Griffin, V.S., 1967, Geology of the Six Mile quadrangle: South Carolina Division of Geology Map Series MS-14, scale 1:24000.

Griffin, V.S., 1971, The Inner Piedmont belt of the southern crystalline Appalachians: Geological Society of America Bulletin, v. 82, p. 1885–1898.

Griffin, V.S., 1974, Analysis of the Piedmont in northwest South Carolina: Geological Society of America Bulletin, v. 85, p. 1123–1138.

Hatcher, R.D., 1978, Tectonics of the western Piedmont and Blue Ridge, Southern Appalachians; review and speculation: American Journal of Science, v. 278, p. 276–304.

Hatcher, R.D., 2002, An inner Piedmont primer, *in* Annual Field Trip Guidebook, Raleigh, NC, Carolina Geological Society, p. 1–18.

Hopson, J.L., and Hatcher, R.D., 1988, Structural and stratigraphic setting of the Alto allochthon, northeast Georgia.: Geological Society of America Bulletin, v. 100, p. 339–350.

Merschat, A.J., Jr, R.D.H., and Davis, T.L., 2005, The northern Inner Piedmont, southern Appalachians, USA: kinematics of transpression and SW-directed mid-crustal flow: Journal of Structural Geology, v. 27, p. 1252–1281.

Nelson, A.E., 1988, Stacked crystalline thrust sheets and episodes of regional metamorphism in northeastern Georgia and northwestern South Carolina; a reinterpretation: USGS Numbered Series Bulletin 1822.

Overstreet, W.C., and Bell, H., 1965, The crystalline rocks of South Carolina: relation of rock units in the geologic belts of the Piedmont and Blue Ridge provinces of South Carolina.: USGS Numbered Series Bulletin 1183.

Ranson, W. A., Williams, I. S., and Garihan, J.M., 1999, Shrimp zircon U-Pb ages of granitoids from the Inner Piedmont of South Carolina: Evidence for Ordovician magmatism involving mid to late Proterozoic crust: Geological Society of America, Abstracts with Programs, v. 31, n. 7, p. A-167.

Warner, R.D., Griffin, V.S., Steiner, J.C., Schmitt, R.A., and Bryan, J.G., 1989, Ultramafic chlorite-tremolite-olivine schists: three bodies from the Inner Piedmont belt, South Carolina: Geological Society of America Special Papers, v. 231, p. 63–74.